THESIS REPORT
Master's Degree
Institute for Systems Research

An Optical Area-Scattering Based Approach for the Measurement of Surface Roughness Formed during Machining

by D.L. DeVoe
Advisor: G.M. Zhang

The Institute for Systems Research is supported by the National Science Foundation Engineering Research Center Program (NSFD CD 8803012), Industry and the University

M.S. 93-11

Abstract

Title of thesis:	An Optical Area-Scattering Based Approach for the Measurement of Surface Roughness Formed During Machining
Name of degree candidate:	Don L. DeVoe
Degree and year:	Master of Science, 1993
Thesis directed by:	Assistant Professor Guangming Zhang

The measurement of surface roughness during a machining process is critical for the automatic control of surface quality in a computer-integrated manufacturing (CIM) system. In this work, a method of surface roughness assessment is investigated which is particularly applicable for in-process roughness measurement. The measurement system employs a novel application of light-scattering theory, which has been used in a number of commercially available optical surface roughness measurement techniques.

The need for such a measurement system is discussed, and a review of several systems currently available for this purpose is provided. The theory upon which many of these optical systems is based is introduced, and the theory is extended for application to the measurement system introduced in this work. The differences and advantages of the developed vision system, compared to other optical systems, are investigated. Particular attention is paid to the area-based nature of the new technique. The performance of a prototype vision system is considered, and the results of a factorial design are interpreted to determine the sensitivity of the system to six environmental and system configuration factors. A calibration curve, which relates the surface roughness of fifty aluminum workpieces to an optical roughness parameter, is developed to provide a method of determining surface roughness directly from optical

measurements. A prototype of a second optical system is constructed to attach directly to a CNC milling machine, and the suitability of this system for use in a machining environment is investigated.

There are three stages of this work. In the first stage, a preliminary experimental study is performed to investigate some of the basic attributes of the vision system. While this study is fairly simple, it demonstrates the potential usefulness of the proposed system. In the second stage, a prototype vision system is designed and constructed, and a detailed factorial design is undertaken to develop an empirical model of the system output as a function of six factors related to the system configuration and environmental conditions. Several calibration curves are produced for relating the system output to a range of known surface roughnesses. In the third stage, a prototype system is integrated with a Computer Numerically Controlled (CNC) milling machine to investigate the feasibility of using the system in a true machining environment. The results indicate some of the advantages and limitations of the proposed system.

An Optical Area-Scattering Based Approach for the Measurement of Surface Roughness Formed During Machining

by

Don L. DeVoe

Thesis submitted to the Faculty of the Graduate School
of The University of Maryland in partial fulfillment
of the requirements for the degree of
Master of Science
1993

Advisory Committee:

Assistant Professor Guangming Zhang, Chairman/Advisor
Professor Lung-Wen Tsai
Assistant Professor Ioannis Minis

Acknowledgments

The author wishes to express his sincere gratitude to Dr. Guangming Zhang, who has provided consistent technical and moral support throughout the many stages of progress of this work. The author thanks Drs. L. Ives and S. Jahanmir, and Mr. J. Song of the National Institute of Standards and Technology for the use of facilities in the Ceramics and Metrology Divisions. The author acknowledges the support of the University General Research Board during the preliminary experimental study, and the Institute for Systems Research at the University of Maryland at College Park under Engineering Research Centers Program: NSFD CDF 8803012.

Table of Contents

Subject Page

List of Tables v

List of Figures vi

List of Equations viii

Chapter 1 Introduction

1.1. Background 1

1.2. Problem Definition 5

1.3. Survey of Current Optical Systems 7

1.4. A Preliminary Description of Vision System Operation 11

Chapter 2 Literature Review

2.1. Terminology and Definitions 13

2.2. Surface Categorization 15

2.2.1. Periodic vs. Random Surfaces 15

2.2.2. Roughness Criteria 15

2.2.3. One- vs. Two-Dimensional Surfaces 18

2.3. Scattering Theories of Electromagnetic waves 18

2.3.1. Beckmann's Scattering Model 18

2.3.2. Surface Facet Model 22

Chapter 3 Vision System Description, Theory, and Operation

3.1. Fundamentals of Operation and System Components 24

3.2. Application of Scattering Theory to Vision System Operation 28

3.3. Phenomena Affecting Vision System Performance 34

Chapter 4 Experimental Procedure and Results

4.1. Preliminary Study 37

4.4.1. Sample Preparation and Measurement Apparatus 37

4.1.2. Logarithmic Regression Analysis 44

4.2. Specimen Preparation 46

4.3. Vision System Measurements 47

4.3.1. Histogram Variation 47

4.3.2. Incident Angle 49

4.3.3. Baseline Calibration 51

4.3.4. Roughness Correlation 52

4.4. Sensitivity Analysis 53

4.4.1. Parameters Affecting Systems Performance 54

4.4.2. Factorial Design 55

4.4.3. Significance of Effects 58

4.5. Comparison of Alternate Optical Parameters 64

Chapter 5 Integration of Vision System and CNC Machine

5.1. Design Considerations 67

5.2. Calibration of Integrated Vision System 73

5.3. System Performance Under Motion 78

5.4. System Performance During Machining Operation 86

Chapter 6 Conclusions and Recommendations

Appendix A – Experimental Data 95

Appendix B – Surface Roughness Characterization Parameters 99

Appendix C – Hardware Specifications 102

References 104

Index 106

List of Tables

Table	Page
Table 4.1 - Optical and Stylus Parameters	40
Table 4.2 – Optical measurements at various incident angles	50
Table 4.3 — Factorial design levels	55
Table 4.4 — Factorial Design Grid	57
Table 4.5 — Calculation of natural variation for factorial design	58
Table 5.1 – Vision system settings used for integrated system	73
Table 5.2 — Calculation of natural variation for $\Omega_2 = \sigma * \mu / 1000$	79
Table 5.3 – Settings used during machining operation	86
Table 5.4 – Roughness measurements during milling process	87
Table A1 – Stylus measurement results for experimental samples	95
Table A2 – Optical data from integrated system calibration experiment	96
Table A3 – Optical data for feed rate experiment using integrated vision system	98

List of Figures

Figure	Page
Figure 1.1 – Traditional off-line output control	2
Figure 1.2 – Integrated active control of machining process	4
Figure 1.3 – Schematic diagram of the TIS (from Detrio et al.)	9
Figure 1.4 – Schematic diagram of infrared surface roughness probe	11
Figure 1.5 – Schematic diagram of vision system operation	12
Figure 2.1 – Raleigh criterion	16
Figure 2.2 – Definition of scattering geometry	19
Figure 2.3 – Transition from purely specular reflection to diffuse scattering	21
Figure 2.4 – Comparison between scattering model and surface facet reflection model	23
Figure 3.1 – Depiction of vision system operation	25
Figure 3.2 – Photograph of prototype vision system	26
Figure 3.3 – Typical gray-level histogram of illuminated rough surface	26
Figure 3.4 – Projected light intensity gradient from a quarter-circle	29
Figure 3.5 – two-dimensional reflection under combined scattering/facet model	31
Figure 3.6 – Shadowing effects	35
Figure 3.7 – Multiple scattering	36
Figure 4.1 – Machining parameter settings used to produce preliminary samples	39
Figure 4.2 – Lighting system	40
Figure 4.3 – Images of aluminum samples	41
Figure 4.4 – Surface profiles of each sample	42
Figure 4.5 – 3-dimensional reconstructions of surface topography	42

Figure 4.6 – 3-dimensional reconstruction of surface topography using stylus instrument at the National Institute of Standards and Technology 43

Figure 4.7(a, b, c) - relationship between values of arithmetic average deviation determined using optical inspection method and average roughness values determined using Perthometer stylus device at the National Institute of Standards and Technology 45

Figure 4.8 – Variation of gray-level histogram with increasing surface roughness 48

Figure 4.9 – Effect of incident angle on system sensitivity 50

Figure 4.10 – Optical calibration curve for aluminum 52

Figure 4.11 – Optical calibration curve using $\Omega_2 = \mu * \sigma / 1000$ 65

Figure 5.1 – Schematic of vision apparatus used with CNC milling machine 70

Figure 5.2 – Photograph of vision apparatus mounted onto Matsuura 510 Milling Center 70

Figure 5.3 – Photograph of vision apparatus indicating proximity to cutting tool and workpiece 72

Figure 5.4 – Secondary light reflection from camera lens 74

Figure 5.5 – Effect of eliminating glare on histogram 75

Figure 5.6 – Optical calibration curve for integrated system 76

Figure 5.7 – Dependence of Ω_2 on feed rate 78

Figure 5.8 – Surface images captured under four different feed rates 84

Figure 5.9 – Distortion of surface reconstructions due to feed rates 85

Figure 5.10 – Proposed technique for repelling coolant from lens 88

Figure B1 – Graphical comparison of texture components 100

List of Equations

Equation	Page
Equation 2.1 – Phase difference due to step height	16
Equation 2.2 – Raleigh criterion	17
Equation 2.3 – Determination of effective roughness	17
Equation 2.4 – Beckmann's scattering equation	20
Equation 3.1 – Histogram mean and standard deviation	27
Equation 3.2 – Gamma distribution parameters	27
Equations 3.3 and 3.4 – Spectral contribution: $C(\lambda)$	32
Equation 3.5 – Scattered power equation	32
Equation 4.1 – Mean histogram level	38
Equation 4.2 – Standard deviation of brightness levels in histogram	38
Equation 4.3 – Root mean squared value of brightness levels in histogram	38
Equation 4.4 – Arithmatic average deviation of brightness levels in histogram	39
Equation 4.5 – Optical roughness parameter (Ω_1)	47
Equation 4.6 – Brightness coefficient	49
Equation 4.7 – Roughness calibration curve (using Ω_1)	53
Equation 4.8 – Empirical model of system performance	59
Equation 4.9 – Optical roughness parameter (Ω_2)	64
Equation 4.10 – Roughness calibration curve (using Ω_2)	65
Equation 5.1 – Roughness calibration curve for integrated system	77
Equation B1 – Average roughness (R_a) definition	101

Nomenclature

A	Surface area illuminated by incident light ($A = X_S Y_S$)
b_i	i^{th} brightness level ($0 \leq i \leq 255$)
$C(\lambda)$	Ratio of spectral power contribution of wavelength λ to total incident power
g	Scattering equation parameters (used for simplification)
h	Step height difference between two surfaces
L	Trace length of stylus measurement
F_i	Frequency count of all pixels in an image
N	Number of data points used to digitize trace length
n	Number of pixels in an image
$P(\lambda)$	Spectral power contribution for wavelength λ
q	Surface height (deviation from mean level)
q_i	Surface height of ith data point along trace
R_a	Average roughness
R^2	Correlation Coefficient
s	Distance along trace length
T	Statistical correlation distance between peaks on the surface, as defined by Beckmann (1963)
V_x, V_y, V_{xy}	Scattering equation parameters (used for simplification)
X, Y, Z	Global coordinates (relative to overall surface)
X_S, Y_S	x, y dimensions of a surface area A illuminated by the incident radiation
x, y, z	Local coordinates (relative to a surface facet)
x_i	brightness level of the ith pixel ($0 \leq i \leq n$)
α	Horizontal orientation of light source with respect to machining direction

Δs	Path difference between two light rays
$\Delta\theta$	Phase difference between two light rays
ε	Brightness coefficient
η	Surface slope
Γ	Gamma parameter from gamma distribution
γ	Angle of incidence (global)
λ	Wavelength of incident radiation
λ_{min}	Lower wavelength limit of sensitivity for optical receiver
λ_{max}	Upper wavelength limit of sensitivity for optical receiver
μ	Mean histogram level
Ω	General optical roughness parameter
Ω_1	Optical roughness parameter, Type I: $\Omega_1 = \mu/\sigma$
Ω_2	Optical roughness parameter, Type II: $\Omega_2 = \mu\sigma/1000$
Φ	Surface slope
σ	Standard deviation of histogram
σ_c	Standard deviation of measurements for confidence testing
σ_h	Standard deviation of surface height
θ_1	Angle of incidence (local)
θ_2	Vertical angle of observation (local)
θ_3	Horizontal angle of observation (local)
Ψ	Mean scattered power

CHAPTER 1
INTRODUCTION

1.1. Background

Surface roughness, or texture, is the 'fingerprint' left on a machined workpiece after a manufacturing process. The texture produced by the tool feed marks used in the process, and the smaller surface deviations which occur within the tool marks, are referred to as the primary roughness, while longer wavelength surface irregularities caused by other factors are referred to as the secondary roughness, or waviness. Surface texture is vital to the performance and basic function of a broad range of industrial products. In order to ensure that machined parts have been manufactured with the desired surface roughness, a sample of the parts is typically examined after machining. The primary disadvantage of this post-machining inspection process is that it does not allow for corrections to be made during machining. Additionally, it becomes tedious to sort defective parts, since each part must be examined individually after being machined for the implementation of a 100% inspection plan. The need for improved flexibility, productivity, and product quality in a modern manufacturing environment points to the need for high-speed in-process surface roughness measurement systems. Inspection of surface roughness during a machining process can provide a quality control check on the process, indicating if the surface finish of the machined part is within some specified tolerance, without disrupting the production process.

Traditional methods for controlling the output quality of machining processes involve off-line techniques. For instance, Figure 1.1 outlines an off-line methodology for maintaining output quality in a milling operation. A database is consulted to

determine appropriate initial machine tool settings based on the type of part and material being machined. The part is machined, and a sample of the finished workpieces are examined to check the surface finish and dimensional accuracy of the parts. If the quality of the parts in the sample is acceptable, as determined from statistical quality control methods, then the process is continued. If the sample of parts is of unacceptable quality, then the cause of the failure is determined, and the machining parameters are adjusted accordingly in order to achieve the desired quality level.

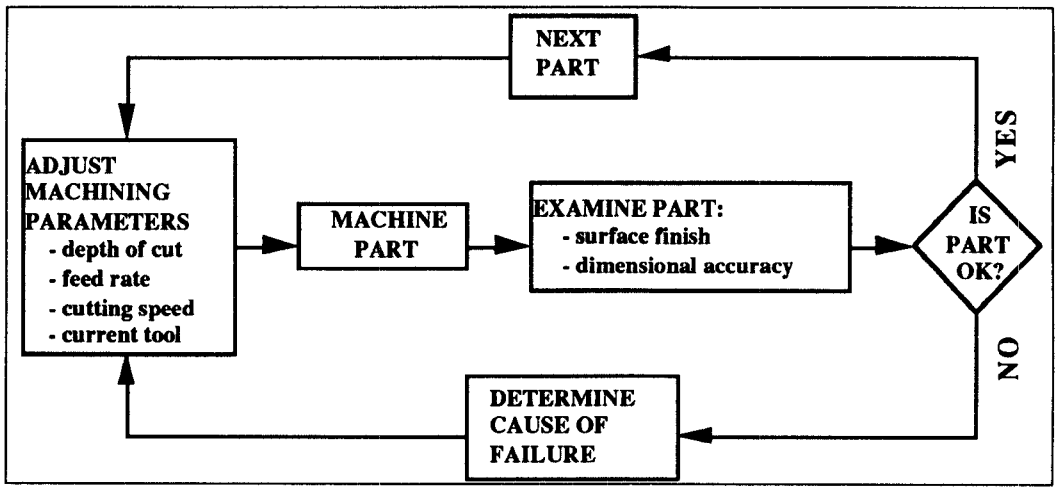

Figure 1.1 – Traditional off-line output control

This passive method of quality control has a number of disadvantages:

- A technician is required to operate the profilometer, resulting in additional manufacturing costs and potential human error in measurement accuracy.
- Measured roughness data must be manually entered into a quality control system.

- Since only a sample of machined parts are typically examined, many out-of-specification parts may pass undetected, or parts within specifications may fail.
- Machining parameters must be manually adjusted to maintain surface quality.

A better alternative to the passive control methodology is the active control methodology. Under this scheme, sensors attached to the machining process provide a continuous flow of information regarding the current status of the process output, and a control system uses this information to adjust the machining parameters, ensuring that the process output is at an acceptable level. Figure 1.2 shows an ideal active control system. Here, sensors attached to the process measure such variables as cutting force and tool temperature. The measured process variables are used to determine tool wear, surface finish, dimensional accuracy, and/or any other parameter which is to be controlled. A control system examines these parameters, and provides feedback to the process by adjusting the machining parameters, changing the current cutting tool (if significant tool wear has occurred), or adjusting actuators integrated into the process.

The measurement of surface finish on the shop floor has been an important element of many quality control programs. The traditional methods of surface roughness assessment employed in these quality control programs have proven successful for the task of off-line surface measurement. However, there is a need for high-speed in-process measurement devices applicable to CIM systems which can measure the surface roughness during a machining process. Such a system should provide appropriate feedback to the process to ensure that the machined surface finish

remains within desired tolerances. In-process inspection systems are necessary for the automatic control of surface quality in a sensor-based manufacturing environment.

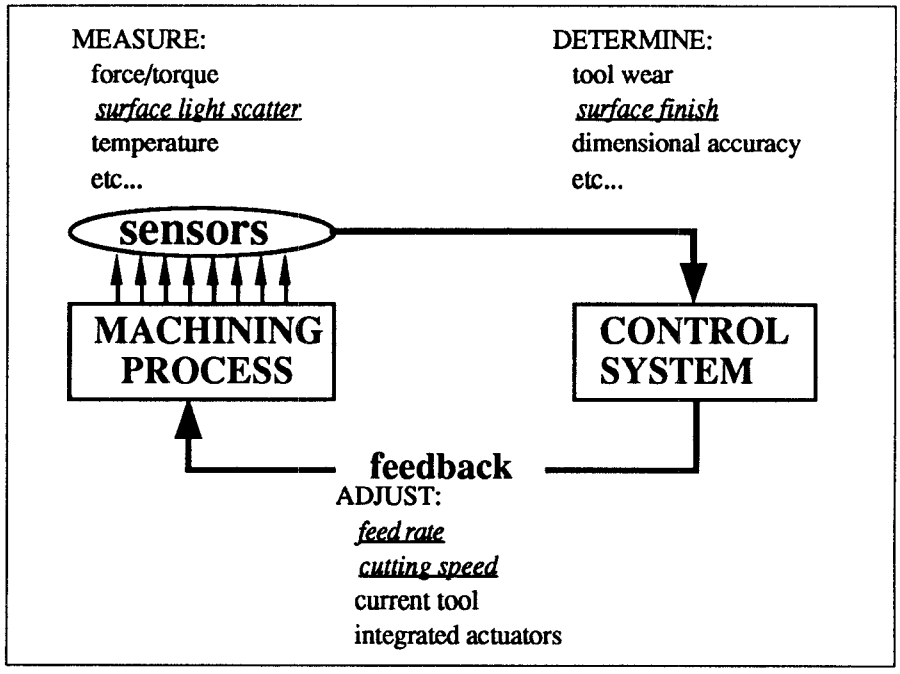

Figure 1.2 – Integrated active control of machining process

Currently available methods of surface measurement suffer from a number of disadvantages which limit their application to in-process measurement schemes. Traditional methods of profilometry, such as stylus devices, require direct contact with the surface, thus limiting measurement speed, requiring navigation around surface discontinuities, and allowing environmental vibration to introduce significant noise into the measurements. Several non-contact measurement methods have been proposed to avoid the problems associated with stylus devices, such as laser-based profilometry devices and linear diode arrays, which can achieve much faster measurement speeds than stylus profilometers (Jansson 1984). However, these optical methods perform their measurement over a very limited area of the surface (either a point or line), and thus they require multiple measurements to accurately characterize a region of the

surface large enough to provide adequate information regarding the overall surface topography. Such systems can be said to measure local surface roughness, as opposed to area-based systems which are capable of measuring the global surface roughness. In the case of many laser-based profilometry systems, multiple measurements over a range of incident and observation angles are required to determine the local roughness from a single point on the surface . The optical method proposed in this work employs an extension of the same theoretical framework used in these other optical systems, but it avoids many of the disadvantages associated with stylus devices, and it is capable of yielding roughness information from a large region of the surface in a single measurement, thus obviating the need for multiple single-point or line measurements across the surface as required with other optical measurement techniques.

1.2. Problem Definition

Traditional methods of surface roughness assessment have the disadvantage of requiring direct contact with the surface, as is the case with the common stylus-type devices. Such contact-based techniques are less than ideal for in-process inspection of surface roughness for several reasons:

- the measurement speed is limited due to the need for physical contact with the surface.
- non-continuous surfaces are extremely difficult to inspect, as the stylus tip must be navigated around any discontinuities in the surface.
- surface damage may occur due to wear between the stylus tip and the surface under inspection.

- the apparatus must be carefully isolated from vibrations, which can become difficult in a machining environment.
- roughness values are determined using a limited number of single-line traces, which may not be representative the entire surface.
- the surface must be free of oil, dirt, and other contaminants — in an actual machining environment, the surface must be cleaned, measured, and re-lubricated, which is expensive to implement as a high speed in-line process.

Recent research efforts in the manufacturing community have been focused on the development of improved, high precision machines, equipment and processes through advances in dimensional measurement techniques, sensors to monitor and control precision machines, and physical models of precision machining processes. The use of in-process surface roughness assessment represents one such area of interest. Several non-contact methods have been suggested as alternative surface roughness measurement techniques more suited for in-process inspection than traditional methods. Examples include laser-based systems, ultrasonic techniques, capacitance methods, and fiber-optic methods (Spurgeon 1974).

Laser-based profilometry systems and linear diode arrays have been shown to be capable of achieving faster measurement speeds than stylus methods by measuring the intensity of light scattered from a surface (Jansson 1984), but these methods suffer from an inability to characterize the entire surface topography. Additionally, many optically-based systems, such as the Total Integrated Scatter device (Detrio 1985), are cumbersome to impliment and so are not suitable for on line measurement. Ultrasonic methods have been succesfully used to measure surface finish to a reasonable degree of accuracy (Blessing 1988). As with optical methods, ultrasonic techniques are limited to

the measurement of roughness from a relatively small region of the surface. Capacitance methods have been succesfully employed for on line surface finish measurement (Garbini 1992) by measuring the electric fringe-field between a thin metalic strip and the surface under observation. This technique provides average roughness information, as well as higher order statistical surface information by determining the surface profile and performing measurements directly on this profile. Fringe-field assessment of surface roughness is limited to the measurement of one-dimensional traces across a surface. Unlike the fringe-field capacitive technique, area-based capacitive methods have been used to determine the average surface finish from a large region of a surface (Lieberman 1988), but these area-based techniques are unable to provide information regarding higher order surface statistics.

The ideal measurement system should combine the speed of laser-based systems, the accuracy of contact profiling techniques, the capability of measuring higher order surface statistics (e.g. waviness, surface slope, kurtosis, peak-to-peak level, etc.) from traces of the surface found in fringe-field capacitive systems, and the ability to characterize a large two-dimensional region of the surface found in area-based capacitive methods. This last point is especially pertinent in milling operations, where the roughness can vary significantly over a single milled path, so that the ability to gather roughness data from a large area of the machined surface is important.

1.3. Survey of Current Optical Systems

There are presently a number of commercially available roughness assessment systems which employ an optical measurement method. In fact, there is a fairly diverse

selection of such systems, ranging from desktop systems designed for individual sample measurements to laser-array systems designed for production line quality control. Nearly all of these systems employ a coherent light source (e.g. laser) to illuminate a small point of the surface under consideration, and an array (linear or grid) of light sensors to examine the reflected light intensity at different points around the surface. Several of these system will be discussed here to provide a sense of the current level of advancement in this area.

All optical techniques may be divided into two categories: profiling techniques, and area techniques. Optical profiling techniques may be further divided into three sub-categories: optical sectioning, interferometry, and focus detection (Vorburger 1989). These profiling techniques have limited use due to their inability to perform area-based measurements, and they will not be discussed here. Area-based optical techniques invariably utilize light scattering theory. Various versions of scattering theory have been employed to examine the relationship between the roughness of a surface and the angular distribution of light reflected from the surface. This relationship has been developed either through empirical observation (Huynh 1990, Luk 1989), or by appealing directly to a scattering theory (Church 1979).

There is a wide variety of instruments which make use of the light scattering phenomena (note the plural here, since there are several effects caused by light scattering which can provide information about the surface roughness). For example, a technique called Total Integrated Scatter (TIS) has been standardized by the ASTM for measuring the roughness of optical surfaces (Detrio 1985). TIS uses the apparatus shown in Figure 1.3. Here, a laser beam is directed through a hole in a hemisphere which houses the specimen being measured. The light strikes the surface, and the specular component

of the incident light (see Chapter 2) is reflected back through the hole and is not measured. The diffuse component of the scattered light, however, is reflected onto the hemisphere, which directs all incoming radiation onto a detector located at the hemisphere's conjugate point. The TIS has been very successful for measuring extremely smooth optical surfaces, but the theory on which it is based fails for rougher surfaces (Vorburger 1989)

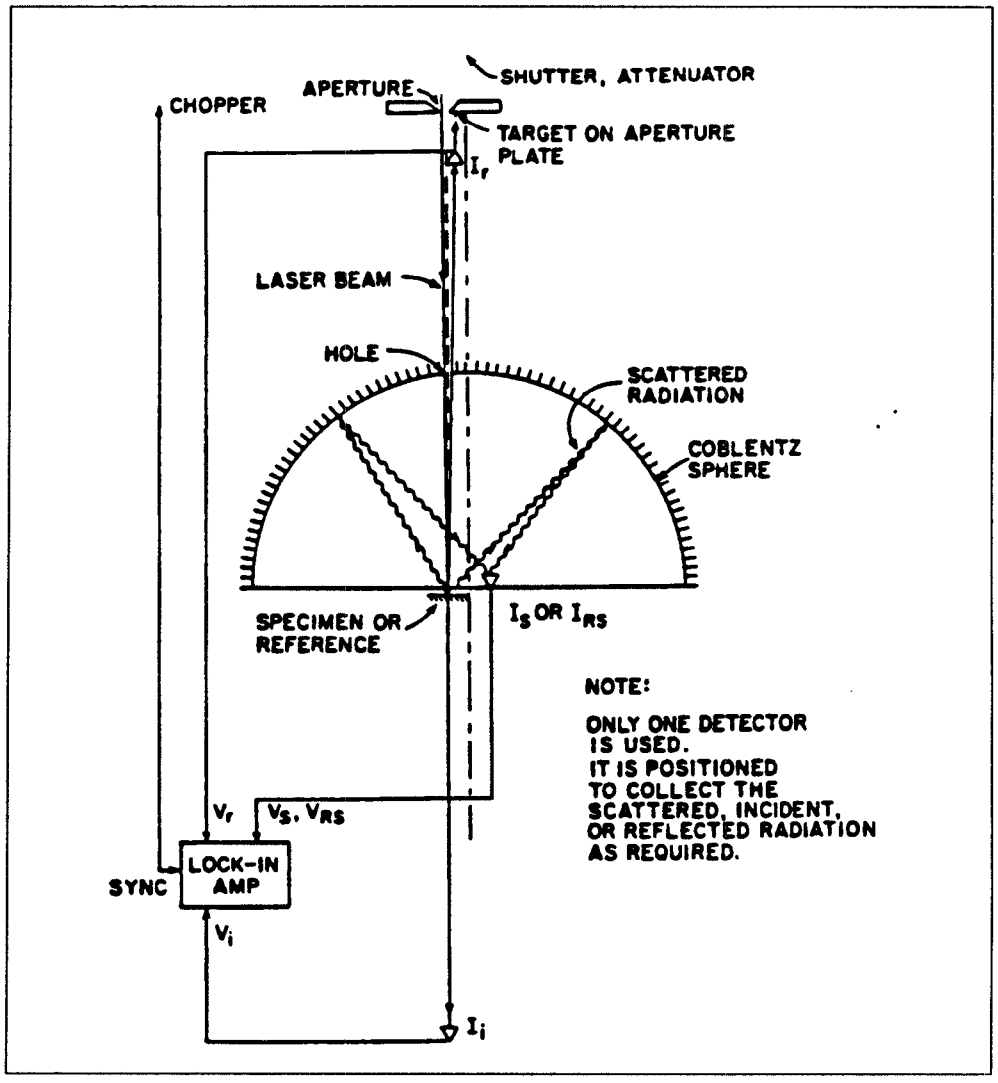

Figure 1.3 – Schematic diagram of the TIS (from Detrio et al.)

Another device which employs optical scattering is the 'detector array for laser light angular scattering,' or DALLAS, developed by the National Institute for Standards and Technology (NIST). The basic function of this device is similar to that of the TIS, but it is capable of measuring much rougher surfaces. A laser light source is directed down onto the surface, and the scattered light is reflected onto a semicircular yoke (rather than a hemisphere in the case of the TIS). An series of lenses in the yoke direct the scattered light onto an array of photodetectors, which can be sampled to yield the scattered intensity as a function of the angular displacement from the incident light direction. A stepper motor is used to rotate the yoke through 180° to provide a full map of the scattered radiation over the entire hemisphere. Workers at NIST have expressed the intention of extending the DALLAS technology for in-process roughness inspection.

A commercially available device which uses the light scattering approach is depicted in Figure 1.4. An infrared LED light source illuminates a collimating lens to a convex measurement lens, which directs the light onto a 1.8 mm point on the surface. The scattered light is collected by an array of photodiodes sensitive to UV radiation. If the surface is smooth, the reflected light beam will be essentially the same width as the incident beam. As the surface becomes rougher, the width of the beam will increase according to scattering theory. An optical parameter is calculated based on the width of the scattered light pattern, and an empirically-derived correlation curve is consulted to determine the roughness of the surface. While this device has the advantages of being compact (compared to the TIS and DALLAS) and commercially available, it suffers from limited sensitivity (Zimmerman 1989).

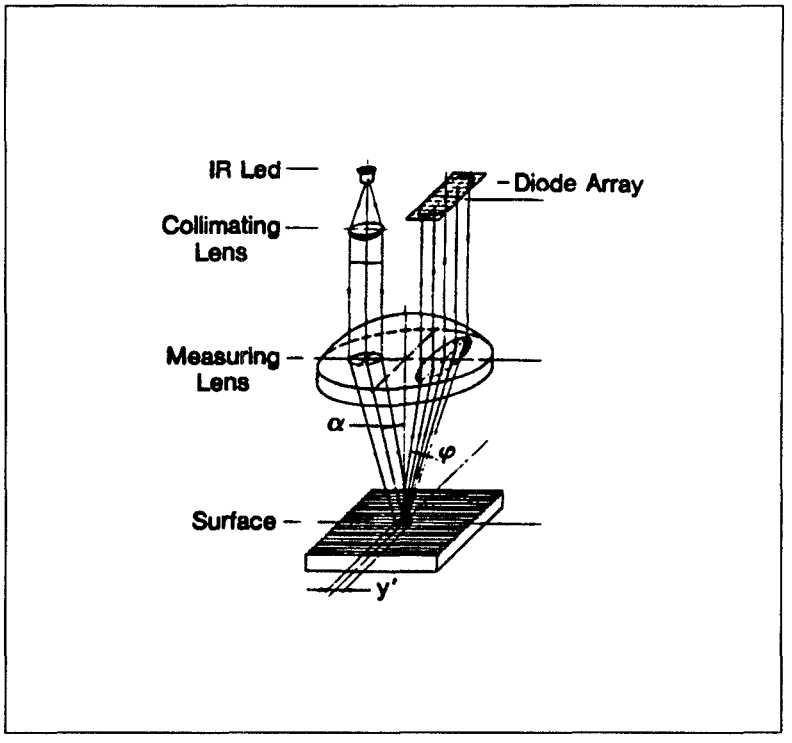

Figure 1.4 – Schematic diagram of infrared surface roughness probe (from Brodman et al.)

1.4. A Preliminary Description of Vision System Operation

Before discussing the theory upon which the vision system presented in this work is based, a preliminary description of the system will be presented here. The purpose of this description is to provide a brief overview of the system's operation which will bring to light some of the primary differences of the system compared to the other optical system presented in Section 1.3.

While the other optical systems discussed have been concerned with the measurement of reflected light intensity over a full range of reflection angles, or studying the width of the scattered field in the case of the infrared roughness probe, the vision system examines the brightness levels from a digitized image of the surface.

Figure 1.5 shows the basic operation of the system. A light source illuminates the surface at a given incident angle, and a lens focuses the light scattered from the surface into a CCD array. A digitizer then captures the image from the CCD array, and a computer is used to perform the appropriate processing to determine the surface roughness directly from the digitized image of the surface. This vision system also differs from the aforementioned systems by the fact that it gathers data from a fairly large area of the surface, while the other techniques perform their measurements on relatively small areas.

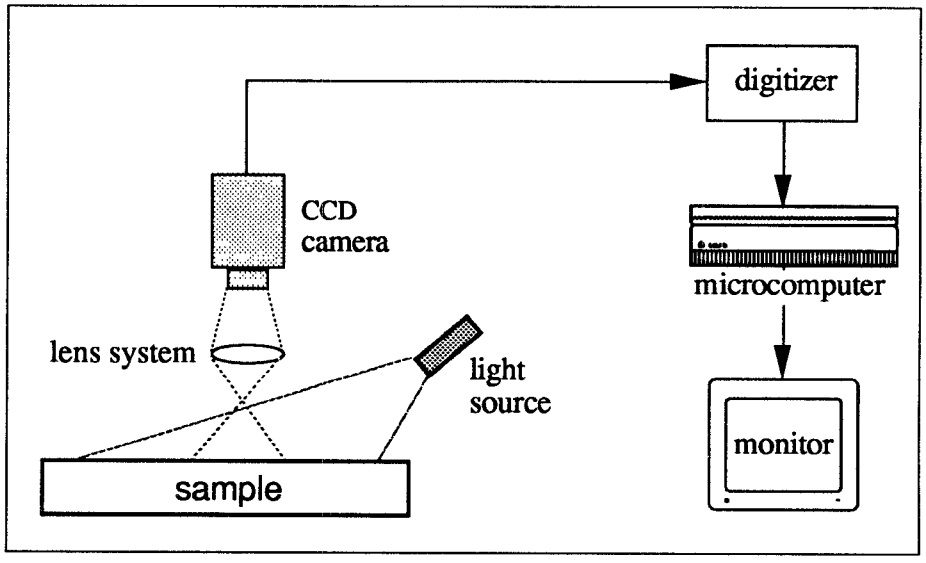

Figure 1.5 – Schematic diagram of vision system operation

The scattering theories which are used to provide a basis for the system operation will be investigated in Chapter 2. Chapter 3 applies the theory to the vision system at hand, and Chapter 4 considers the performance of the system under a variety of conditions. finally, Chapter 5 discusses the integration of the vision system with a CNC milling machine tool to investigate the potential for using the system in a machining environment.

CHAPTER 2
LITERATURE REVIEW

2.1. Terminology and Definitions

The theory surrounding optical methods of surface roughness measurement, such as the DALLAS, TIS, and infrared surface roughness probe presented in Chapter 1, involves an understanding of the interaction of electromagnetic waves with the surface under consideration. In particular, the manner in which light is reflected from a rough surface is of paramount interest. In a monograph by Beckmann [1963], one element of this interaction, called scattering, has been approached in a rigorous manner, and the material from this monograph provides an excellent basis for understanding this problem. While much of the basic research in electromagnetic wave scattering was motivated by the study of radar signal interference due to irregularities in the ground, the results are equally applicable to radiation in the visible spectrum as applied in this work. Beckmann's scattering theory is combined with a geometric interpretation of reflection to provide the theoretical basis of the system described in this work. Before this theory is presented, some basic terms related to electromagnetic reflection needs to be presented.

The terms 'specular reflection' and 'diffuse reflection' are used to describe two extremes of the manner in which electromagnetic radiation reflects from the surface of a material. Specular reflection occurs as a result of constructive interference between multiple scattered and re-radiated waves. Light exhibits purely specular reflection from a given material when the entire light energy is reflected away from the material at an

angle equal to the incident angle (the specular direction), as measured from the material's surface. The phase of specular reflection is coherent. In contrast, light exhibits diffuse reflection when the specular direction is not favored over other directions for the reflected energy. The phase of diffuse reflection is incoherent. There is a continuous transition from diffuse to specular reflection. In reflection from any real engineering material, a combination of both types of reflection will be present. This fact is fundamental to the operation of the vision system described in this work.

Since the phase of specular reflection is coherent, the total power density of light waves from specular reflection is determined from the vector sum of the individual waves. In contrast, the incoherent nature of diffuse reflection allows the mean power density of light waves from diffuse reflection to be calculated from the algebraic sum of the individual mean power densities. This is true since the phase of coherent waves is constant, while incoherent waves have a random phase. As with specular and diffuse reflection, there is a continuous transition between coherent and incoherent light.

An important term which needs to be introduced is 'scattering'. Scattering refers to reflection which is diffuse (incoherent). Scattering occurs for any surface which is rough, and it will be shown later that the amount and nature of the scattering is a function of the roughness of the reflecting material. Note that, as stated earlier, reflected light typically consists of two components: specular reflection and diffuse scattering. In addition, diffuse scattering is composed of two components: scattering due to surface waviness much larger than the wavelength of incident light, and scattering due to surface roughness in the same range as the wavelength of incident light. The former component of diffuse scattering is highly directional, while the latter component is essentially isotropic in its scattering.

2.2. Surface Categorization

The treatment of Beckmann's scattering theory to roughness measurement of engineering materials depends largely on three factors: the periodicity, effective roughness, and dimensionality of a given surface.

2.2.1. Periodic vs. Random Surfaces

The theoretical treatment of scatter from surfaces with periodic roughness is substantially simpler than that for random surfaces. Unfortunately, most surfaces created via engineering processes, such as grinding and milling, are essentially random in nature. Of particular interest are random surfaces whose height distribution is Gaussian, as such surfaces can be conveniently described by their mean level, standard deviation, and correlation function. For this work, the theory which is presented and developed is based on the presumption that the surface under consideration is essentially Gaussian (note that for some machining processes, this assumption is not entirely valid).

2.2.2. Roughness Criteria

A surface can be considered optically rough or smooth on the basis of the Raleigh criterion, which uses a simple light ray model to describe the relationship between the wavelength of the incident light (λ), the angle of incidence (γ), and the surface roughness (h). Consider two light rays incident on a surface with a step

discontinuity of height h as shown in Figure 2.1. The light ray striking the lower step experiences a path difference of $\Delta S = 2h\sin\gamma$ compared to the second light ray which strikes the upper step. Assuming the incident rays are initially in phase, the path difference between the rays results in a reflected phase difference dictated by Equation 2.1.

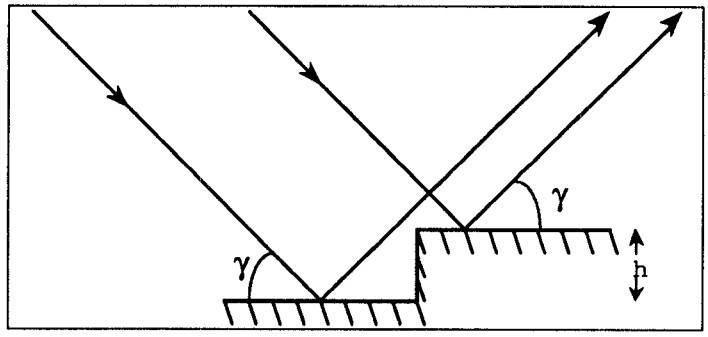

Figure 2.1 – Rayleigh criterion

$$\Delta\phi = \frac{2\pi}{\lambda}\Delta S = \frac{4\pi h}{\lambda}\sin\gamma \qquad (2.1)$$

If there is no phase difference between the reflected rays, then the total reflected energy is simply the algebraic sum of the incident rays, directed entirely in the specular direction. Under this condition, the surface is smooth (h = 0). As the step height increases and the phase difference approaches π, then the energy reflected in the specular direction approaches zero, due to the phase cancellation between the rays. If the incident energy is not reflected in the specular direction, then it must have been redirected in some other direction, and hence scattering has occurred and the surface is rough. Somewhere between these two extremes is a point just beyond which a surface may be considered effectively rough. An appropriate value for this point has been suggested as $\Delta\phi = \pi/8$ (Kerr, 1951). Applying this value, the Rayleigh Criterion states that a surface may be considered effectively rough for

$$h > \frac{\lambda}{32 \sin \gamma} \tag{2.2}$$

Another way of considering this criterion is that a surface becomes effectively smooth as $h/\lambda \rightarrow 0$ or $\gamma \rightarrow 0$. That is, as either of these two parameters tends towards zero, the dominant reflection mechanism for the surface is specular reflection, while diffuse reflection plays a less important role. See Figure 2.3 for a description of how specular reflection gives way to diffuse scattering as the dominant reflection mechanism as the surface roughness increases.

For an analysis of the light field scattered from a surface to yield information about the surface roughness, diffuse scattering must first occur. Thus, the surface must be optically rough, as dictated by the Raleigh Criterion, for the given wavelengths of light incident on the surface. Since the CCD receiver used in the vision system is sensitive to virtually the full spectrum of visible light, we are concerned only with incident wavelengths in the range of 4000 Å < λ < 7000 Å. Noting that the vision system is intended to operate for roughnesses in the range of 0.05μm < R_a < 0.7μm, the Raleigh Criterion can be applied to determine if this range is sufficiently rough for incident radiation in the visible spectrum. Assuming a incident angle of 15° (see Chapter 4 for a discussion of the effects of changes in incident angles on system performance), the Raleigh Criterion dictates that any surface rougher than about

$$h > \frac{\lambda}{32 \sin \gamma} = \frac{4000(10^{-10})}{32 \sin(15°)} = 0.048 \mu m \tag{2.3}$$

will be effectively rough for the given system. Since a surface with step heights of 0.048 μm will be effectively rough, it is reasonable to expect the system to operate for surface with R_a > 0.048/2 μm = 0.024 μm.

2.2.3. One- vs. Two-Dimensional Surfaces

A surface can be considered one-dimensionally rough in a particular direction if the correlation distance in that direction is much smaller than the correlation distance in the perpendicular direction. A surface which is two-dimensionally rough has perpendicular correlation distances in a similar range. The theoretical treatment of light reflection for these two types of surfaces differs somewhat, since the scattered waves from a one-dimensionally rough surface tends to reflect cylindrical waves, while two-dimensionally rough surfaces reflect spherical waves. That is, one-dimensionally rough surfaces scatter light in a manner similar to radiation emitted from a length of wire, while two-dimensionally rough surfaces scatter light in a manner similar to radiation emitted from a point source. Since most engineering surfaces are two-dimensionally rough, only the two-dimensional case of scattering will be discussed here.

2.3. Scattering Theories of Electromagnetic waves

2.3.1. Beckmann's Scattering Model

A number of models have been advanced to describe the scattering of electromagnetic radiation from rough surfaces (Twersky 1957, Rice 1951). Some of these models are concerned with very specific applications, while others have led to the development of very general mathematical descriptions of the scattering problem, without providing explicit results which can be used in a practical manner. One theory put forward by P. Beckmann in a 1963 monograph provides a general formulation of the scattering problem, while also yielding concrete mathematical relationships between

surface parameters and scattering directions and intensities. This theory has found popular application in several different point- and line-based surface roughness measurement systems, as noted in Section 1.3. Some of the results from Beckmann's theory can be conveniently applied to the area-based measurement system in this work with some basic conceptual extensions which will be discussed in Section 3.2. The fundamental results of Beckmann's theory which are of interest here are provided in this section, along with the definition of the scattering geometry used by Beckmann.

Consider a light ray incident on a flat but optically rough surface, with an incident angle of θ_1 as measured from the surface normal (which coincides with the z-axis in figure 2.2). Due to the roughness of the surface, some of the incident light is scattered away from the specular direction. We could choose some arbitrary observation angle from which to measure the scattered radiation, define by angles θ_2 and θ_3, where θ_2 is measured from the surface normal and θ_3 is the horizontal angle between the projection of the incident light on the surface and the projection of the observation vector on the surface.

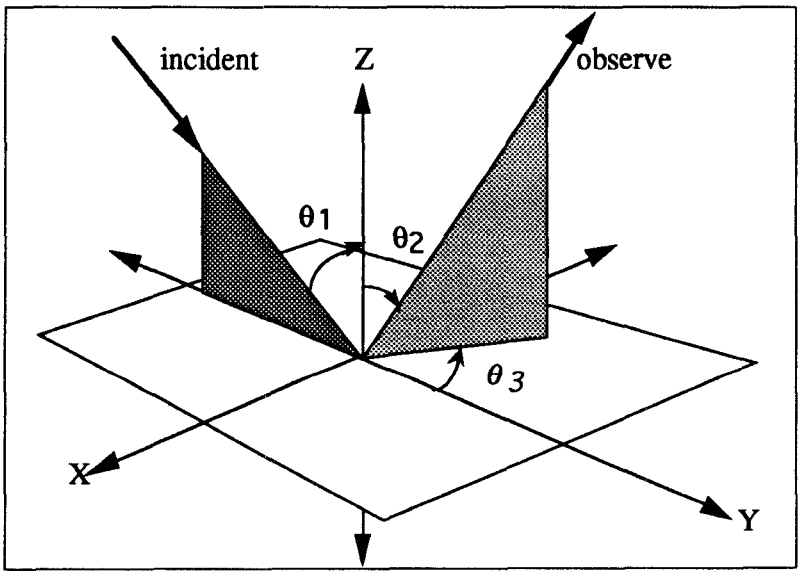

Figure 2.2 – Definition of scattering geometry

According to Beckmann's theory, the mean scattered power (Ψ) of incident light is a function of surface roughness, incident wavelength, incident angle, observation angles, correlation distance between the hills or valleys in the surface, and planar dimensions of the illuminated surface. The equation describing this relationship is given by Beckmann as

$$\Psi = e^{-g}\left[\rho_0^2 + \frac{\pi FT^2}{A}\sum_{m=1}^{\infty}\frac{g^m}{m!m}\exp\left(\frac{-v_{xy}^2 T^2}{4m}\right)\right] \tag{2.4}$$

where

$$\rho_0 = \frac{\sin(v_x X_s)\sin(v_y Y_s)}{(v_x X_s)(v_y Y_s)}$$

$$F = \frac{1+\cos\theta_1\cos\theta_2 - \sin\theta_1\sin\theta_2\cos\theta_3}{\cos\theta_1(\cos\theta_1+\cos\theta_2)}$$

$$g = \frac{2\pi\sigma_h}{\lambda}(\cos\theta_1+\cos\theta_2)$$

$$v_x = \frac{2\pi}{\lambda}(\sin\theta_1 - \sin\theta_2\cos\theta_3), \quad v_y = \frac{2\pi}{\lambda}\sin\theta_2\sin\theta, \quad v_{xy} = \sqrt{v_x^2+v_y^2}$$

As shown in Beckmann's work, Equation 2.4 dictates the intensity of scattered radiation in a given observation direction based solely on the local roughness of the surface (over a relatively small area), assuming a constant incident angle. This relationship has been successfully applied to several point and line profilometry devices by examining the mean scattered power from a concentrated, coherent light source over a range of incident and observation angles. Such systems provide information regarding the local surface roughness, since the scattered light is measured from a

relatively small area of the surface (Vorburger 1990). The theory can be extended to the area-based measurement system at hand as discussed in Section 3.2.

Figure 2.3 shows a typical transition from specular to diffuse reflection as the surface roughness increases, as dictated by Eqn. 2.4. In the smooth surface of case (1), the incident light is reflected entirely in the specular direction. In the slightly rough surface of case (2), the scattered radiation exhibits a strong spike in the specular direction, with side lobes of smaller intensity around the specular direction. In case (3), a moderately rough surface, the incident radiation is scattered diffusely, but still with a tendency towards the specular direction. In the very rough surface of case (4), the diffuse light has lost the preference for scattering in the specular direction.

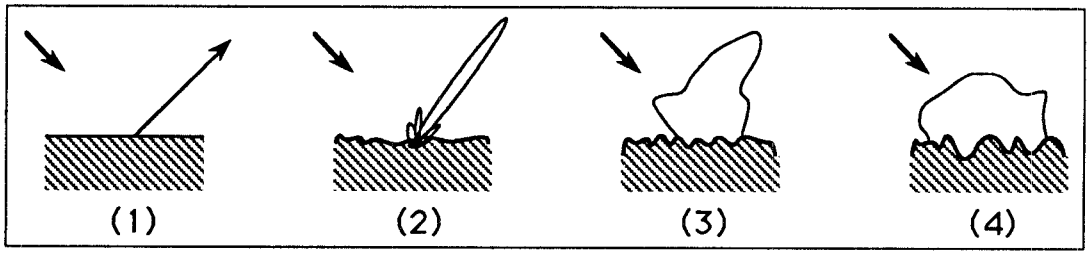

Figure 2.3 – Transition from purely specular reflection to diffuse scattering

In this work, Beckman's treatment of the light scattering problem and it's application to the measurement of local roughness is accepted. Furthermore, Beckmann's scattering theory is extended for application to the area-based measurement system at hand, which is capable of measuring the global surface roughness.

2.3.2. Surface Facet Model

While Beckmann's light scattering theory considers the statistical properties of the surface under investigation to determine the nature of light reflected from the surface, a much simpler discussion of reflection can be presented by modeling the surface as a net of interconnected flat facets reflect light in a purely specular fashion. In this model, the incident light is considered to act as a collection of simple light rays with different phases. The light rays are reflected from the surface based purely on the geometric orientation of each individual facet of the surface, such that the angle of reflection is equal to the angle of incidence (with opposite sense as measured from the surface normal of each facet). The resultant field reflected in this manner is the vector sum with respect to the phases of all rays in a given direction . A two-dimensional example of this model is depicted in Figure 2.4, which shows the modeling of a continuous surface as a series of connected surface facets, and the reflection of several light rays from these facets. Note that the scattering model predicts a diffuse scattered field due to the local roughness of the surface, with the predominant direction of energy reflection coinciding with the specular direction, while the surface facet model says little regarding the scattered field other than predicting the direction of specular reflection for each individual light ray incident on the facets. Thus, the surface facet model is a geometric rather than statistical model of scattering.

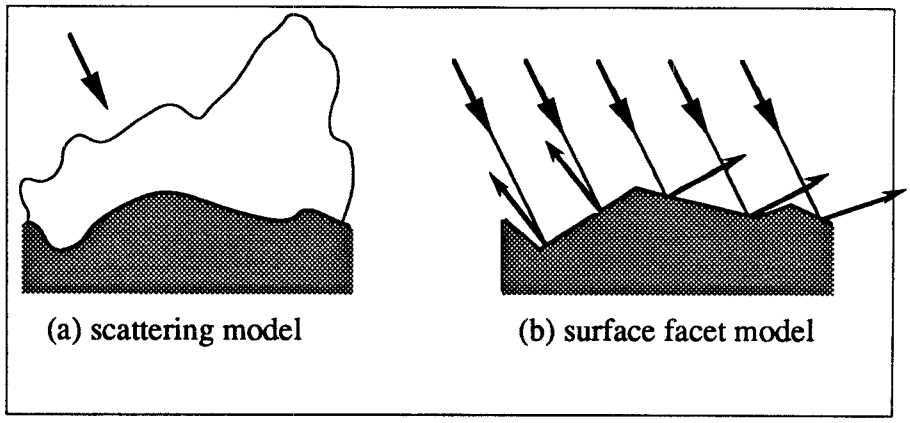

Figure 2.4 – Comparison between scattering model and surface facet reflection model

Clearly, the surface facet model of light reflection is very simplistic, and cannot account for many of the phenomena of light scattering. However, the model does provide a starting point for describing some of the basic aspects of light reflection. In fact, the surface facet approach has been applied to scattering problems by describing a surface made up of facets as a Markov chain, and determining the field scattered by the realization of the chain using a statistical approach (Beckmann 1963). The surface facet model will be considered in conjunction with the scattering model in Section 3.2 in order to provide a theoretical basis for the behavior of the vision system.

CHAPTER 3
VISION SYSTEM DESCRIPTION, THEORY, AND OPERATION

Using the fundamental light scattering theory presented in Chapter 2, the operation of the vision system presented in this research can be discussed from an analytical viewpoint. In this chapter, the basic operation of the system is discussed, and light scattering theory is used to develop a relationship between surface roughness and the image received by the vision system. Several phenomena which affect the performance of the vision system are also investigated.

3.1. Fundamentals of Operation and System Components

The photo-optical measurement method proposed here uses the apparatus shown in Figure 3.1. Here a sample is illuminated by a light source directed through a fiber optic cable, and a CCD camera using a high magnification lens system provides a video signal which a frame grabber converts into an 8-bit gray scale digital image at a rate of 30 frames per second. This image is then sent to a microcomputer for processing. The computer examines the scattered light pattern in the image, and calculates an optical roughness parameter, designated by Ω, from statistical properties of the image's gray-level histogram. The R_a value for the surface is then determined through the use of a correlation curve which uniquely relates a given value of Ω to a range of R_a values. The resulting R_a value is either displayed on a video monitor for observation or used as feedback to the machining process.

To implement the proposed optical measurement method, a prototype vision system was designed and constructed. As shown in Figure 3.2, a test stand (lower right) holds an aluminum sample being measured. A fiber optic cable leads from a variable intensity lighting box (lower center) to the machined surface, where an adjustable fixture is used to orient the light onto the surface as required. The CCD camera at the top of the test stand sends a signal to a frame grabber within the microcomputer. Image processing software running on the computer is used to display the image and yield the optical roughness parameter for the surface on a monitor.

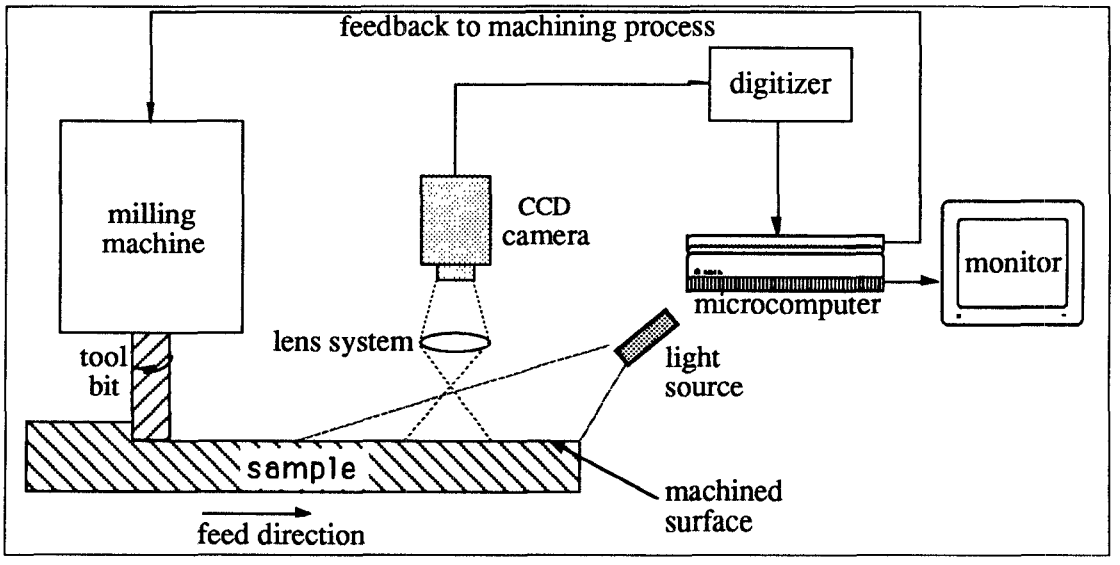

Figure 3.1 – Depiction of vision system operation

The frame grabber used in the prototype system acquires a 510x490 pixel image which reflects the activation levels of the CCD elements in the camera. This 256 gray-level image captured by the frame grabber is sent to an image processing software package for analysis. A histogram-based approach is taken to examine the image. In this approach, the gray-level of each of the pixels in the image is determined, and a frequency table for each distinct gray level (0-255) is constructed. It provides a

histogram which reflects the distribution of the gray-levels in the image. A typical histogram is depicted in Figure 3.3.

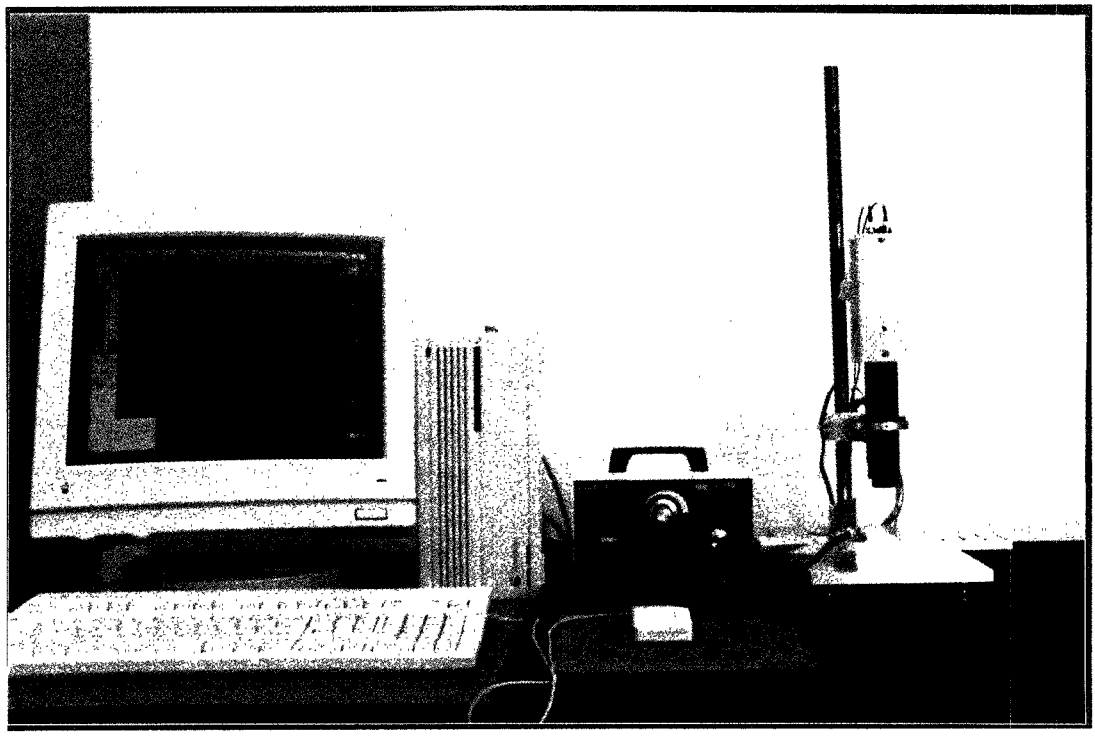

Figure 3.2 – Photograph of prototype vision system

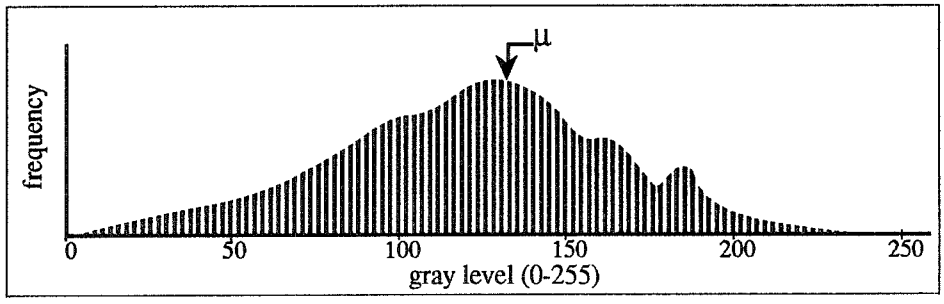

Figure 3.3 – Typical gray-level histogram of illuminated rough surface

The histogram allows the distribution of gray-levels in an image to be quantitatively described in terms of basic statistical properties. It will be shown that the

histograms of rough surfaces are often close to being normally distributed, so that the distribution can be described in terms of the mean and standard deviation of the histogram. Equation 3.1 provides two forms for calculating m and s. The first form is appropriate when working directly from the histogram, while the second form is convenient when working from the brightness levels of the individual pixels in the image.

$$\mu = \frac{1}{n}\sum_{i=0}^{255} F_i b_i \qquad \text{or} \qquad \mu = \frac{1}{n}\sum_{i=1}^{n} x_i$$

$$\sigma = \sqrt{\frac{1}{n}\sum_{i=0}^{255} F_i (b_i - \mu)^2} \qquad \text{or} \qquad \sigma = \sqrt{\frac{1}{n}\sum_{i=1}^{n} (x_i - \mu)^2} \qquad (3.1)$$

More typically, the distribution is bounded at the low (less bright) end, while the upper (brighter) end trails off towards zero more gradually. In this case, the distribution can be better modeled by a two-parameter gamma distribution of the form

$$f(x) = \frac{\xi^{\eta} x^{\eta-1} e^{-\xi x}}{\Gamma(\eta)} \qquad \text{where:}$$

$$\Gamma(\eta) = \int_0^{\infty} x^{\eta-1} e^{-x} dx$$

$$\eta = \text{shape factor} \qquad \eta > 0$$

$$\xi = \text{scale factor} \qquad \xi > 0 \qquad (3.2)$$

which is more suitable for distributions which are bounded at one end. In practice, it seems that most histogram distributions are close enough to the normal distribution that the extra computational overhead involved with the gamma distribution is unnecessary. The optical roughness parameter (Ω), can be determined directly from the statistical properties of the histogram's distribution, using whatever distribution model best fits the histogram.

3.2. Application of Scattering Theory to Vision System Operation

The theoretical basis for the operation of the vision system involves the combination of scattering theory and a more basic geometric interpretation of incoherent light reflection. While scattering theory can be directly applied to single-point measurement systems (see Section 2.4. Survey of Current Measurement Systems Based on Light Scattering), it does not lend itself directly to area-based optical measurement.

A surface is normally characterized by parameters such as roughness, average slope, and waviness (where roughness and waviness are defined with respect to some chosen cutoff frequency). Alternately, we can imagine a model which describes the surface in terms of a series of multi-angled, flat facets. These facets are interconnected to form the overall surface topography. Instead of the smooth facets described in the Surface Facet Model discussed in Section 2.3.2., the model can be further enhanced by considering each facet to have a 'local roughness'. In a concept similar to the cutoff frequency, which defines the boundary between surface roughness and waviness, the boundary between 'facet geometry roughness' and 'local roughness' must be defined. This issue will be addressed further in a later section.

Consider a small 'ray cluster' of light directed at a single facet in this model. Some of the radiation is reflected in the specular direction, defined by the incident angle and the global orientation of the facet. In addition, due to the local roughness of the facet, some of the incident radiation is scattered away from the specular direction as defined by Eqn.. 2.4. In a surface composed of a large number of individual facets, the reflected intensity field of light directed in any particular direction is comprised of the individual reflections in that direction from each facet of the surface. As a two-dimensional case, consider a quarter circle illuminated by a distant light source as in

Figure 3.4. As an individual light ray hits the surface of the circular object, much of the incident radiation is reflected away from the surface along the specular direction, which is defined by an angle equal to the incident angle as measured from the surface normal at the point of incidence (via Snell's law). A lens collects any reflected light which is directed upwards, and projects it onto an imaging array that displays the intensity of light reaching it. For the sake of clarity, three vectors are shown in the figure for each light ray: incident direction, specular direction, and the upward-directed component of

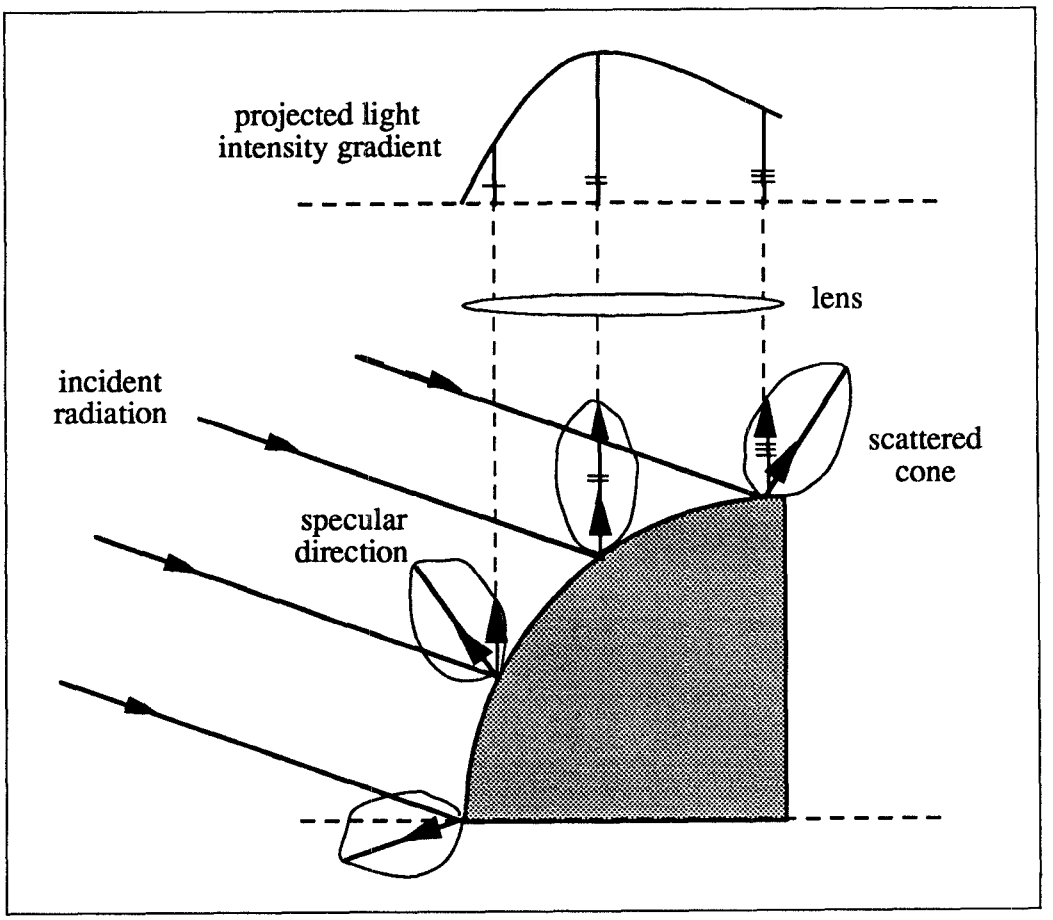

Figure 3.4 – Projected light intensity gradient from a quarter-circle

the scattered field. As shown in the figure, the projected light intensity gradient does not provide a faithful reconstruction of the actual surface. The maximum in the projected light intensity gradient occurs at the point where the specular direction is coincident with

the upward-directed component of the scattered field, rather than at the top of the circle, while the minimum in the projected light intensity gradient coincides with the bottom point of the circle as expected.

The simplified two-dimensional case shown in fig 3.4 demonstrates that the scattered light intensity does not necessarily correlate directly to the geometry of the illuminated surface. While it would be ideal if a direct correlation did exist, the lack of such a proportional relationship does not invalidate the potential effectiveness of the optical system. Although it is clear that the scattered field in a given direction over an area of a surface is not proportional to the height variation across the illuminated area, there is a unique relationship between the surface geometry and the scattered field. This relationship clearly must take into account the slopes of the 'roughness elements' across the surface. In order to quantify this relationship, the integrated scattering/surface facet reflection model can be combined with knowledge of the facet orientations (and thus facet slopes) to provide a mathematical model of the scattered light field.

Figure 3.5 depicts a two-dimensional continuous surface which can be modeled as a series of discrete surface facets, each with some given local roughness. One such facet, magnified from the continuous surface, shows the local roughness and the geometrical parameters which define the facet orientation. The surface normal, N, is shown with respect to the mean level of the facet's surface height variation. The incident and observation vectors, I and O, are shown at angles θ_1 and θ_2 from N. The direction of O is dictated by the location of the receiver in the vision system (in this case directed in the +Z direction). In addition, the global angle of incidence, γ, indicates the orientation of I with respect to the global horizontal. Given a fixed incident angle, the geometric parameters θ_1 and θ_2 are defined with knowledge of the surface facet's

normal vector. Extending the figure into three dimensions, knowledge of the facet's normal vector would provide the parameters θ_1, θ_2, and θ_3 ,where θ_3 describes the tilt of the observation vector in the third dimension, just as θ_2 describes the tilt in the second dimension depicted in Fig. 3.5. Referring to the scattering equation, Eqn.. 2.4, we see that the intensity of the scattered field in the known direction of observation can be determined given θ_1, θ_2, and θ_3 in addition to information about the local surface roughness of the facet. Thus, if the surface normal vector is provided for a given facet, and the local roughness and correlation distance of the facet is also known, then the mean scattered power towards the overhead vision system can be calculated for each individual facet of the surface.

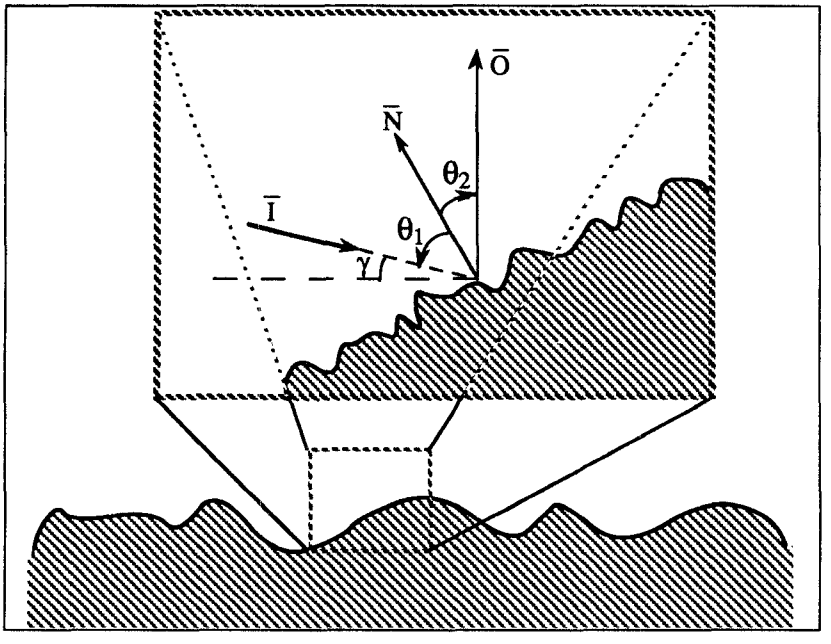

Figure 3.5 – two-dimensional reflection under combined scattering/facet model

In order to determine the mean scattered power from a particular facet, the scattering due to each wavelength of incident radiation must be calculated, and the resulting scattered field determined by the superposition of the scattering due to each wavelength. To do so, a new term must be provided to describe the relative

contribution of each wavelength to the overall incident radiation power, since the light source used to illuminate the surface does not have constant power across the visual spectrum. The function $C(\lambda)$ is introduced to represent the ratio of the power from a particular wavelength to the total spectral power of the incident radiation, as shown in equations 3.3 and 3.4.

$$C(\lambda_n) = \frac{P(\lambda_n)}{\int_{\lambda_{min}}^{\lambda_{max}} P(\lambda)\,d\lambda} \tag{3.3}$$

$$\int_{\lambda_{min}}^{\lambda_{max}} C(\lambda)\,d\lambda = 1 \tag{3.4}$$

The scattering equation can be integrated over the incident spectral range, resulting in

$$\Psi_{i,j,\frac{\pi}{2}} = \int_{\lambda_{min}}^{\lambda_{max}} \left\{ C(\lambda)\exp\left(-g_{i,j}(\lambda)\right)\left[\rho_{0_{i,j}}(\lambda) + \frac{\pi F T^2}{A}\sum_{m=1}^{\infty}\frac{g_{i,j}(\lambda)}{m!m}\exp\left(\frac{-v_{xy}^2 T^2}{4m}\right)\right]\right\} d\lambda \tag{3.5}$$

where λ_{min} and λ_{max} are the lower and upper limits of the spectrum to which the optical receiver is sensitive. Note that Eqn.. 3.5 assumes that the global incident angle (γ) is constant over the full illuminated area of the surface, which is not entirely true for the vision system at hand, since the light source is not distant enough from the surface for the incident light rays to be considered entirely parallel. However, this fact can be overlooked for the current approximation to the scattered field.

Equation 3.5 dictates the scattered power in the observation direction for a given facet defined by the i, j subscripts. This assumes that the facets can be identified in terms of a two-dimensional nxm grid, where i and j are integers such that $1 \le i \le n$, and $1 \le j \le m$. This notation is convenient, as will be shown in the following discussion of

appropriate surface facet dimensions. The parameters which appear in Eqn.. 3.5 are calculated with θ_2 and θ_3 defined with the observation angle towards the vision system's CCD camera, and θ_1 defined with respect to the local x-y plane.

In order to apply Eqn.. 3.5, appropriate dimensions for the facets must be chosen such that the continuous surface can be accurately modeled. For the present application, there is a relatively simple choice for facet dimensions. The CCD camera used in the vision system has a resolution of 510 x 492, with each pixel in the camera receiving an amount of light reflected into the camera from a small area of the surface. It is reasonable, then, to model the surface as a 510 x 492 grid of interconnected facets, with each facet scattering the light incident on the facet into a corresponding pixel in the CCD camera. This is reasonable so long as the surface area covered by each facet is small enough compared to the global roughness of the surface. That is, the camera magnification and resolution must be sufficient so that the area of the surface which scatters light into an individual CCD pixel is smaller than about 1/2 the lower cutoff period of the global surface roughness. Using this 1/2 period criterion assures that the upper cutoff frequency of the continuous surface is modeled by the facets. In summary, the result given by Eqn. 3.5 rests on these assumptions:

- The global incident angle is approximately constant over the full area of the surface under inspection.
- The camera magnification and resolution are high enough so that the surface facet dimensions are smaller than 1/2 the lower cutoff period of the global surface roughness. This criterion must hold in both the x and y directions.

- The facet dimensions are large relative to the wavelengths in the spectrum of incident radiation.

3.3. Phenomena Affecting Vision System Performance

There are several considerations which must be taken into account before light scattering theory can be applied to the task of roughness measurement, two of which are considered in this thesis. The first consideration is that if the angle of incidence is too small for a given surface roughness, some of the valleys on the surface will be shadowed by the higher peaks. The second consideration is the phenomenon of multiple scattering, which occurs when light scattered from one region of the surface strikes a second region , where it is scattered once again. Both of these phenomena affect the measurement accuracy of the vision system.

Shadowing:

Shadowing occurs when the angle of incidence is too small for a given surface topography, so that some of the valleys on the surface will be shadowed by the higher peaks. This effect does not depend on the roughness of a surface per se, but rather on the slopes of the roughness elements on the surface. If the slopes are steeper than the incident angle, then shadowing will occur, as shown in Figure 3.6. In this figure, the incident light hits the surface with an incident angle λ. The surface is

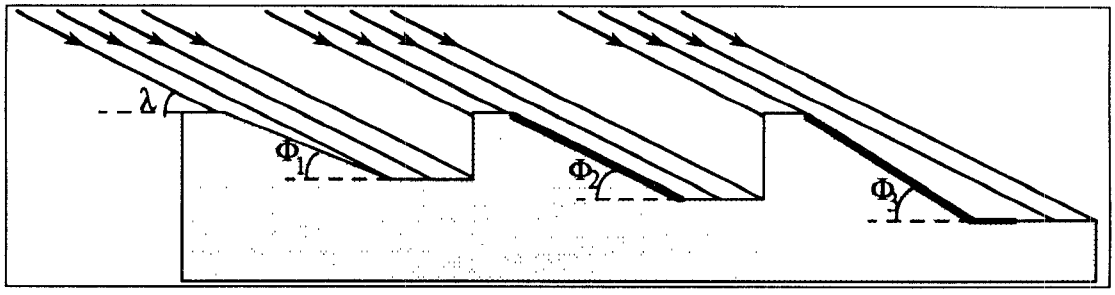

Figure 3.6 – Shadowing effects

characterized by three distinct slopes of angles $\Phi_1 < \lambda$, $\Phi_2 = \lambda$, and $\Phi_3 > \lambda$. The areas of the surface indicated with the heavy lines are shadowed. As evidenced by Fig. 3.6, shadowing occurs when the surface slope is larger than the incident angle, with $\Phi = \lambda$ being a critical angle where shadowing is initiated.

One result of shadowing is that the gray-level histogram on the surface may become bi-modal. that is, the shadowed areas of the surface will create a hump at the low (less bright) end of the histogram, while the standard normal distribution hump will also be in evidence. This bi-modal nature of the histogram will affect the measurement of both the mean and standard deviation of the histogram, and thus will have a strong effect on the optical roughness parameter. For this reason, the incident angle used in the system should be large enough to avoid significant shadowing effects.

Multiple Scattering:

Multiple scattering occurs when the incident light is reflected from one section of the surface, and the reflected light strikes a second region of the surface where it is scattered again, and so on, as shown in Figure 3.7. Multiple scattering is most likely to occur when the surface slopes are relatively large, since the scattered radiation is more

likely to be reflected away from the surface when the surface slopes are small, thus limiting the effects of multiple scattering. Since it is extremely complex to describe the scattered field reflected from a surface under multiple scattering, the effects of this phenomenon can best be determined through empirical observation rather than from a mathematical description.

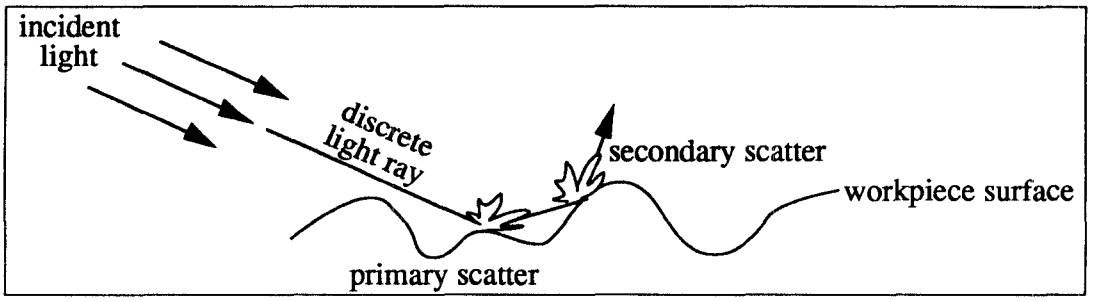

Figure 3.7 – Multiple scattering

CHAPTER 4
EXPERIMENTAL PROCEDURE AND RESULTS

4.1. Preliminary Study

While Chapter 3 is concerned with a theoretical treatment of vision system operation, the present chapter is concerned with developing empirical models of the system output which are required to perform actual roughness measurements. Before entering into a detailed investigation of how to apply the scattering theory to an optical surface roughness measurement system, a preliminary study is presented to examine some of the basic attributes of the proposed system.

4.4.1. Sample Preparation and Measurement Apparatus

The experimental study began with the preparation of samples of machined surfaces as illustrated in Figure 4.1. Four samples of aluminum, labeled A through D, were prepared under four different machining parameter settings to produce different surface roughnesses.

Each sample was photographed with a Nikon camera using high resolution black and white Kodak film. A high magnification lens system, capable of filling a standard 3 1/2" x 5" photograph with a 2.0cm x 1.4 cm image of the sample, was employed. Direct lighting was achieved using a 3.6W white light bulb to produce three sets of images of each sample. The lighting arrangement for each set is depicted in Figure 4.2.

A set of photographs was also made under diffuse conditions, produced using a 150W light projected located behind the samples onto a white, granular mat designed to produce diffuse lighting conditions. Baseline conditions between different samples for a given lighting setup were maintained by simply swapping the samples without altering either the lighting or camera setup. An additional photograph was made of a sheet of precision graph paper placed at the same focal point used for the sample photographs. This photograph was used to determine the scale of the samples. The photographs produced under diffuse lighting conditions are shown in Figure 4.3.

Each of the pictures resulting from the photo-optical apparatus was scanned into a Macintosh II microcomputer using an 8-bit (256 gray level) scanner, and the resulting gray-scale images were loaded into an image manipulation program for processing (*NIH Image* * running on a Macintosh II microcomputer was used for this purpose). Using a variety of histogram analysis tools for *NIH Image*, several macros were written to determine three image parameters: standard deviation (σ), arithmetical average deviation (AAD), and RMS values based on the brightness level histogram over a 12.5 mm^2 region of each image. These parameters are defined as follows:

$$\mu = \frac{1}{n}\sum_{i=0}^{255} F_i b_i \tag{4.1}$$

$$\sigma = \sqrt{\frac{1}{n-1}\sum_{i=0}^{255} F_i (b_i - \mu)^2} \tag{4.2}$$

$$RMS = \sqrt{\frac{1}{n}\sum_{i=0}^{255} F_i^2} \tag{4.3}$$

* NIH Image is a public domain image processing software package developed and supported by researchers at the National Institute of Health. It is available through the Internet via anonymous FTP to zippy.nih.gov.

$$AAD = \frac{1}{n}\sum_{i=1}^{n}|x_i - \mu| \tag{4.4}$$

where n = # of pixels in the image, μ = mean gray (brightness) level of all pixels in the image, b_i = i^{th} brightness level ($0 \le i \le 255$), x_i = brightness level of the ith pixel ($0 \le i \le n$), and F_i = frequency count of pixels in the image at i^{th} brightness level. The parameter values calculated for each sample are listed in Table 4.1.

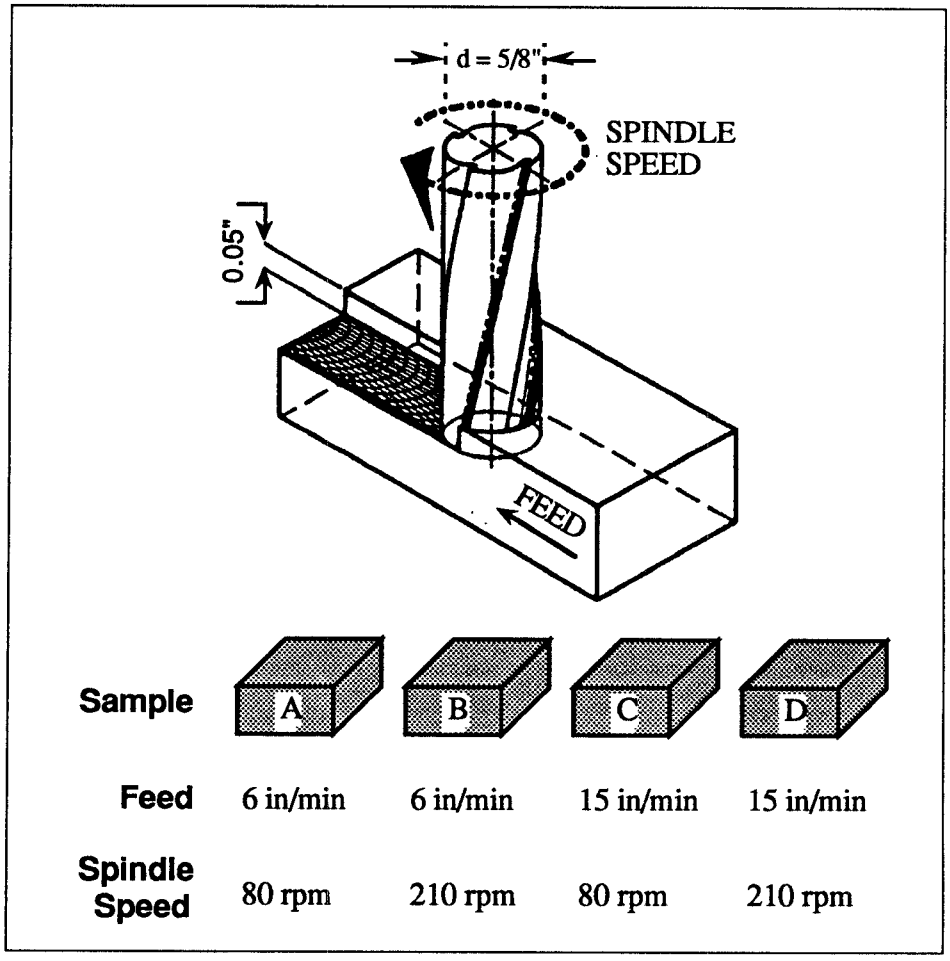

Figure 4.1 – Machining parameter settings used to produce preliminary samples

With the image parameters determined, calibration data was required to produce the desired correlation curves. Facilities at the Metrology Division of the National

Institute of Standards and Technology (NIST) were used to measure the sample surface roughnesses. A Perthometer stylus device was used to calculate the average roughness index, R_a, for each sample averaged over multiple measurement trials. In addition to these stylus measurements, a series of 151 parallel traces were taken on the samples using a custom stylus-based apparatus developed at NIST. This device was designed for the purpose of producing a 3-dimensional reconstruction of the surface topography over a region of a surface. Figure 4.4 presents surface profiles traced from each of the four samples. The average R_a values are listed in Table 4.1.

Table 4.1 - Optical and Stylus Parameters

	(NIST)	*(Optically*	*Derived*	*Parameters)*
Sample	**R_a**	**AAD**	**RMS**	**SD**
A	2.9	18.109	134.909	12.872
B	0.9	85.578	96.362	45.808
C	4.9	33.037	119.993	28.453
D	4.0	51.892	107.737	33.639

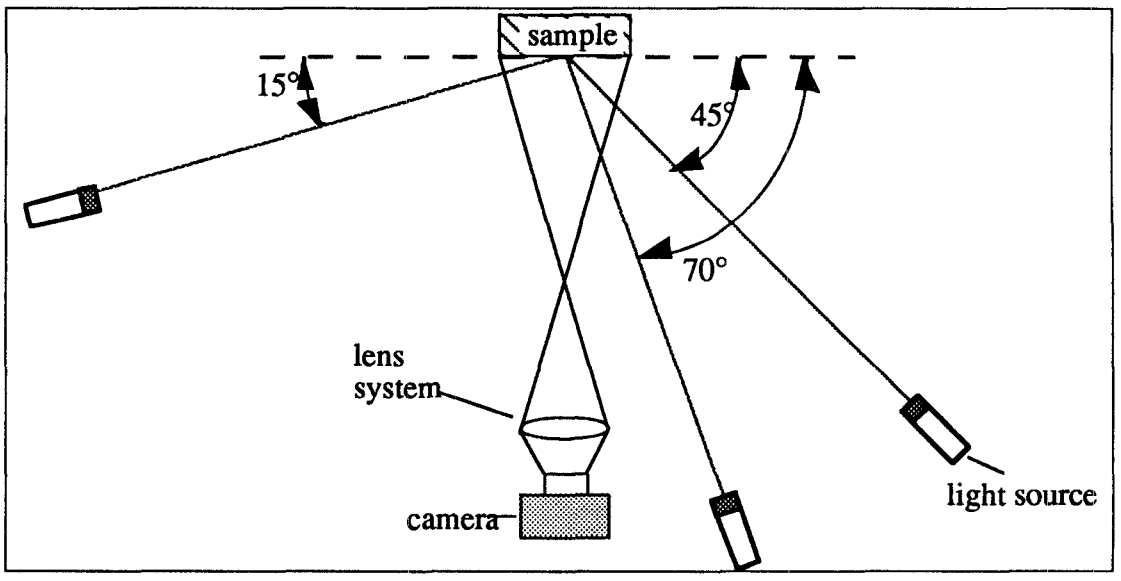

Figure 4.2 – Lighting system

Numerical data obtained from both the stylus measurement and optical inspection methods are listed in Table 4.1. However, variations of both R_a and optical

parameter values were observed across individual samples. These variations are due to the nature of the machining process employed to produce the samples. Therefore, the R_a data listed in Table 4.1 represents the mean level of R_a for the given sample. The variation of R_a across

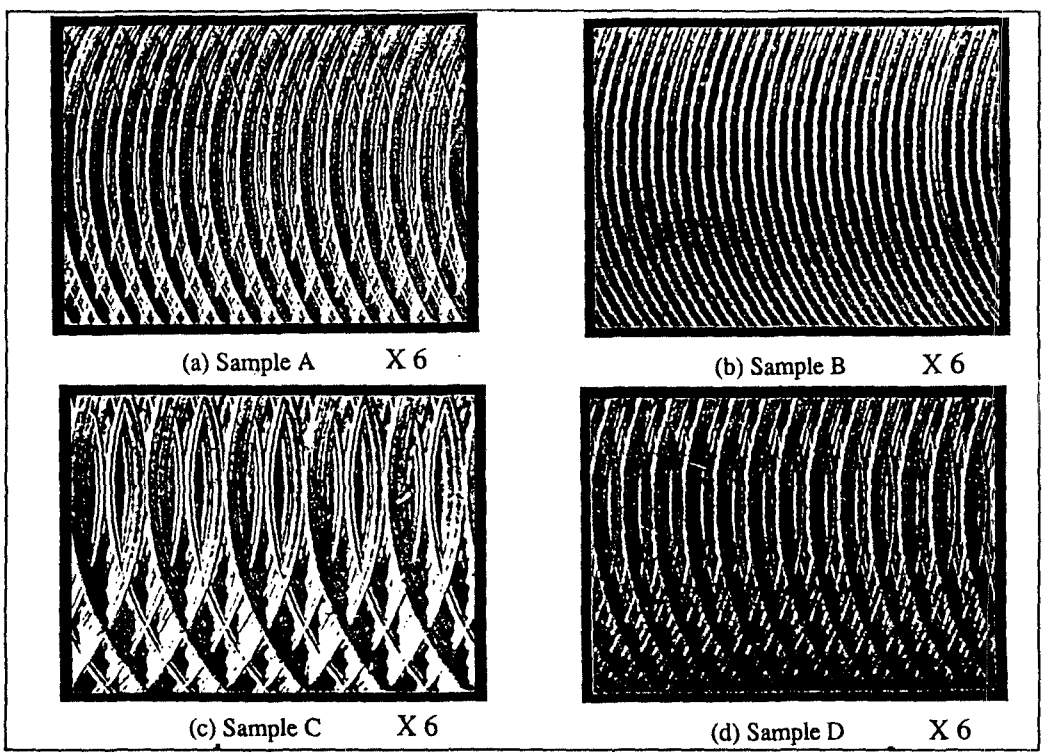

Figure 4.3 – Images of aluminum samples

each sample can be observed qualitatively in the 3-dimensional reconstructions of the sample surfaces produced using *NIH Image*. These images, shown in Figure 4.5, were created by plotting the brightness level of the scanned image along the z-axis, with the sample's spatial coordinates in the x-y plane.

Examining these four topographic reconstructions, it is evident that the irregularities displayed in the topographic reconstruction from sample C, which has the

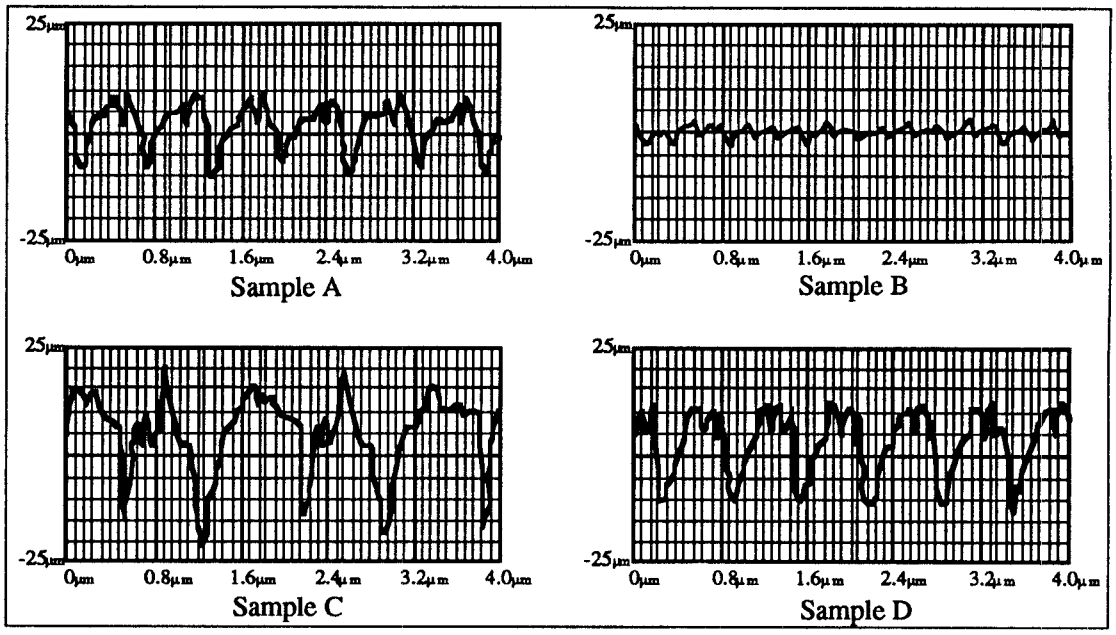

Figure 4.4 – Surface profiles of each sample

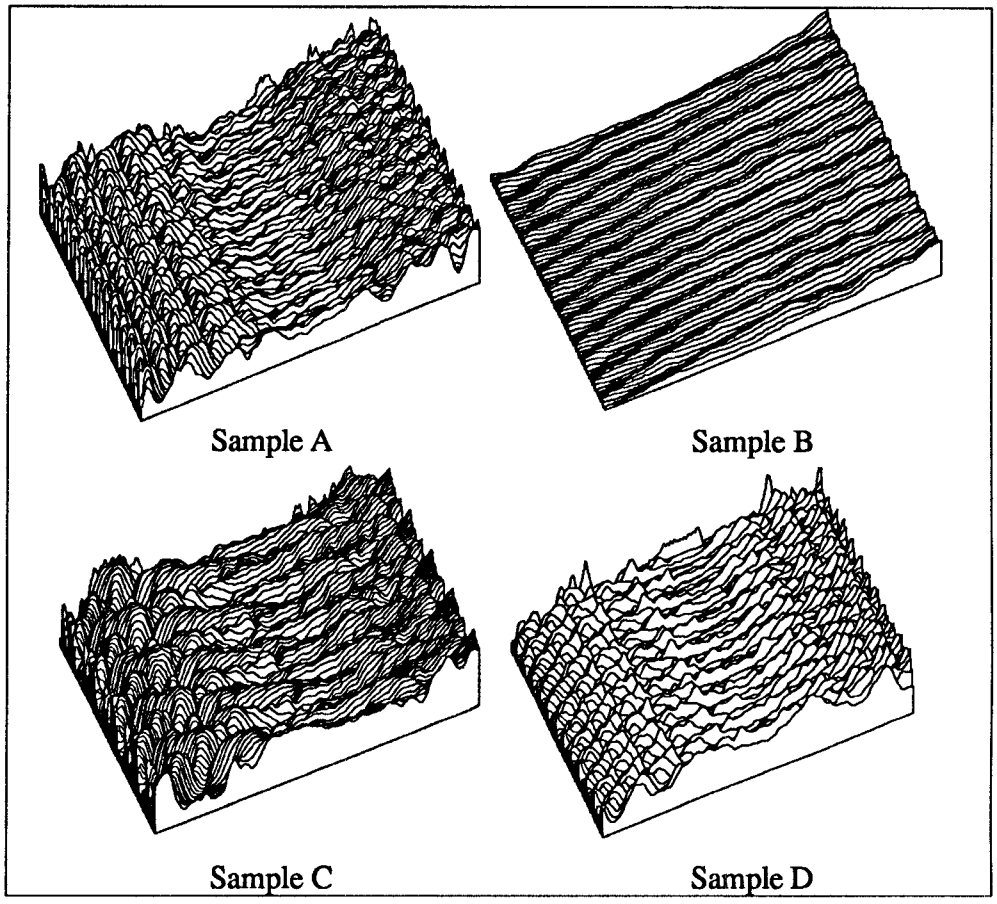

Figure 4.5 – 3-dimensional reconstructions of surface topography

largest R_a value, are much larger than those displayed in the reconstruction of sample B, which has the smallest R_a value. This observation confirms that the optical inspection method has the capability to distinguish between different patterns of surface roughness. Figure 4.6 shows the surface topography reconstructed from the surface roughness profilometer measurements. Similarity in appearance can be observed between the two methods of reconstruction. This also confirms the validity of applying the optical inspection method to surface roughness assessment. It should be noted that the profilometer-based topographic reconstruction required over 150 individual stylus traces, and significant time investment, whereas the optical measurement method produced similar results for considerably less effort.

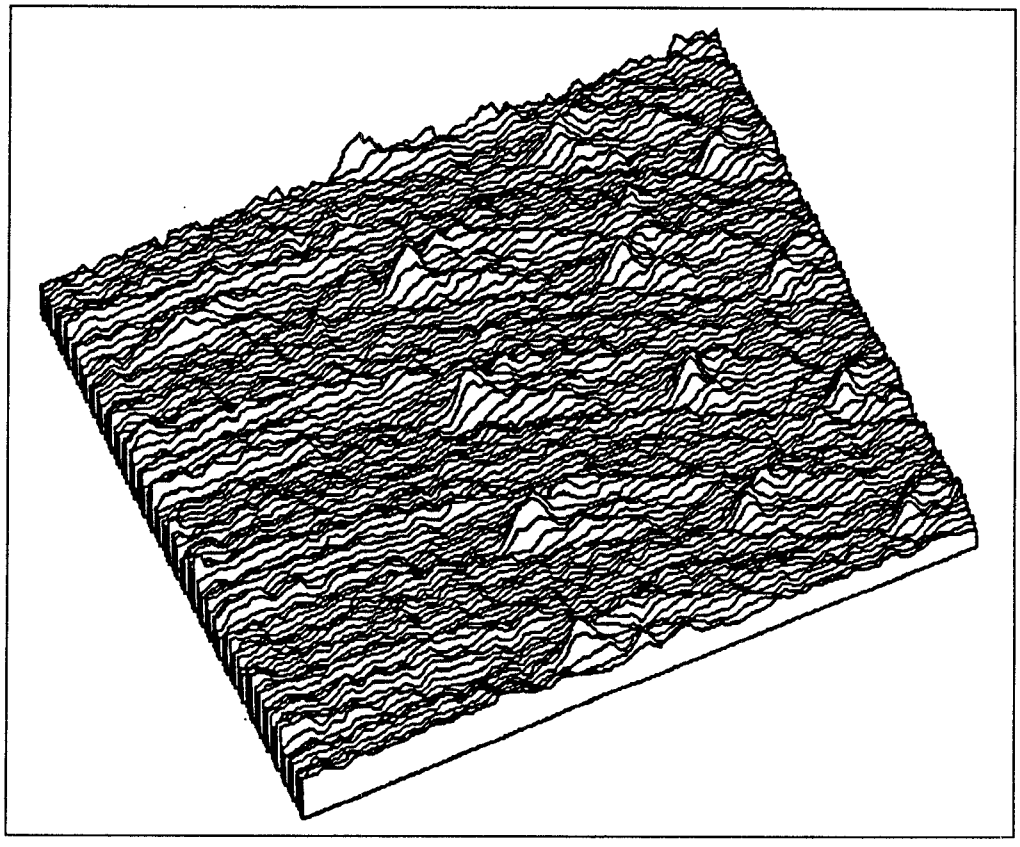

Figure 4.6 – 3-dimensional reconstruction of surface topography (sample D) using stylus instrument at NIST

4.1.2. Logarithmic Regression Analysis

Figures 4.7a through 4.7c show graphs of each of the three optically-derived parameters (RMS, AAD, and SD) plotted against the known R_a values determined using the calibrated stylus measurement system at NIST. A logarithmic curve was found to achieve a good fit through the data, and these curves are shown in each of the graphs. For example, the logarithmic fit to the SD data results in the relationship $SD = 14.8(R_a^{0.659})$, with a good correlation coefficient ($R^2 = 0.852$. Since the exponential power of R_a represents the slope of the curve in log-space, a higher value for this exponent indicates increased sensitivity of the SD parameter to changes in R_a.

Examination of the curve fits obtained by logarithmic regression in Figs. 4.7a through 4.7c shows that the curve fit to the *RMS* parameter data has the largest exponential value for R_a, indicating that this parameter is most sensitive to small variations in R_a. However, the logarithmic fit through the *standard deviation* data provides the best correlation between the curve and data (an R^2 value of 0.852 for *standard deviation* , as opposed to 0.666 for *RMS* and 0.637 for *AAD*), suggesting that this parameter may yield more accurate estimations of the average surface roughness than either of the other parameters. Since only four data points were used for this investigation, it is difficult to make broad claims regarding the accuracy and sensitivity of the optical parameters, but these preliminary values suggest that both the *RMS* and *standard deviation* optical parameters are most useful in producing the desired correlation curves, while the *AAD* parameter is less than ideal. In the experimental study which follows this preliminary investigation, it will be shown that the *standard*

deviation parameter, coupled with the mean value of the histogram brightness, are especially useful for determining the surface roughness.

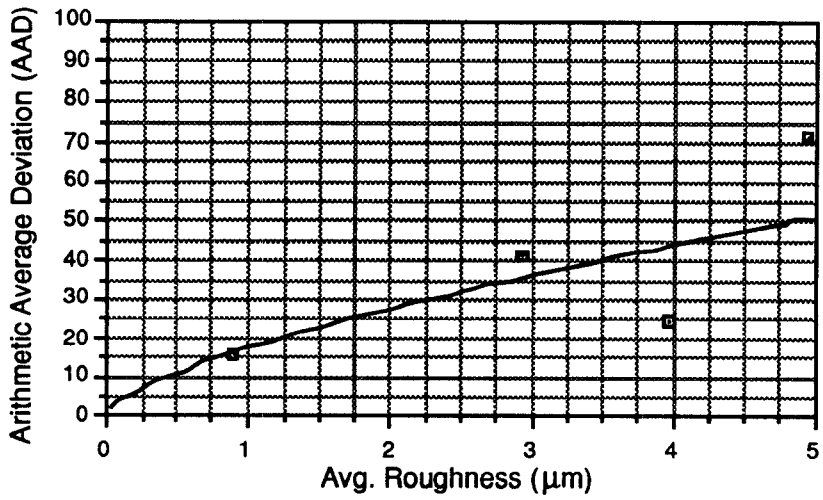

Figure 4.7a - Relationship between arithmetic average deviation determined using optical inspection method and average roughness values determined using stylus device. The logarithmic curve fit through the data has the relationship AAD = $16.5(R_a^{0.693})$, and a correlation coefficient of $R^2 = 0.595$

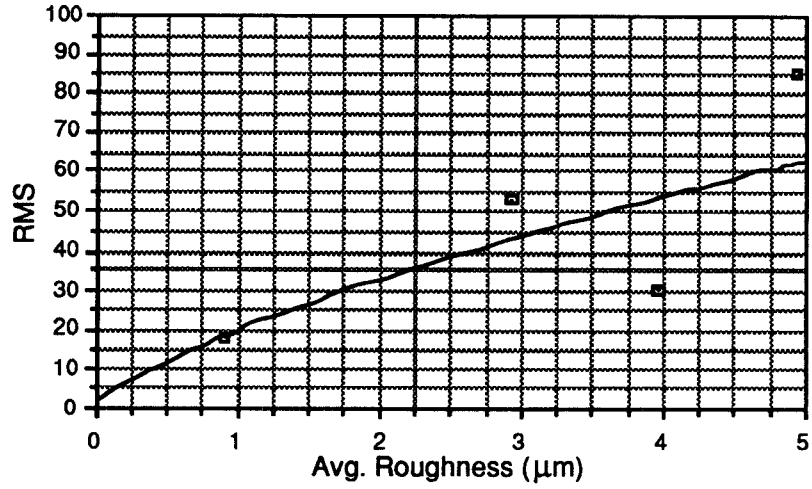

Figure 4.7b - Relationship between RMS values determined using optical inspection method and average roughness values determined using stylus device. The logarithmic curve fit through the data has the relationship RMS = $19.3(R_a^{0.732})$, and a correlation coefficient of $R^2 = 0.666$

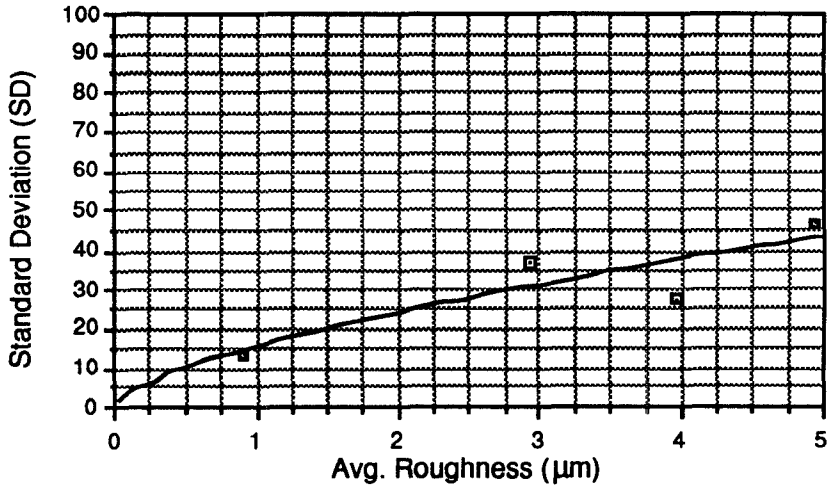

Figure 4.7c - Relationship between standard deviation values determined using optical inspection method and average roughness values determined using stylus device. The logarithmic curve fit through the data has the relationship $SD = 14.8(R_a^{0.659})$, and a correlation coefficient of $R^2 = 0.852$

4.2. Specimen Preparation

Fifty aluminum specimens were machined to R_a values ranging from 0.15 µm to 0.60 µm using a four-flute 3/4" diameter end mill. The samples were machined on a Matsuura CNC Milling Center. The specimens were machined out of 2" wide blocks using a 0.05" depth of cut. Each of the samples was measured using a calibrated stylus profilometer at the National Institute of Standards and Technology (NIST) to determine the average roughness (R_a) of the surfaces. Since the surface roughness of samples machined using a milling process varies over the machined path, the roughness of each sample was determined from the average of five stylus traces over the full width of the milled path. This variation in roughness over the milled path highlights the need for profilometry techniques capable of area-based measurements, since point or line measurement techniques cannot provide roughness information from such a large region of a surface. The measured roughness values are listed in Appendix A1.

4.3. Vision System Measurements

4.3.1. Histogram Variation

It has been established that the amount of light scattered into the overhead camera used in the vision system depends on the roughness of the surface, with Eqn. 3.5 dictating the amount of light received by an individual CCD element in the camera. Since from Eqn. 3.5 we know that the light received by each of the CCD elements depends directly upon the local roughness and orientation of the surface facets which comprise the surface, The activation levels of all CCD elements in the camera will depend upon the overall global roughness of the surface.

Figure 4.8 shows the variation of the histogram measured from three different surfaces with roughnesses ranging from 0.2 μm - 0.5 μm. Photographs of the three surfaces are shown along with three-dimensional reconstructions of the surfaces, to provide a sense of the variation in surface topography between the surfaces. The three-dimensional reconstructions are produced by plotting the brightness level of the digital images of each surface along the z-axis. From Fig. 4.8, it is clear that as the roughness increases, both the mean (σ) and standard deviation (μ) increase as well. This demonstrates that by measuring the values of σ and μ for a given histogram, the roughness of the surface from which the histogram was measured can be predicted. For this reason, it has been proposed that a non-dimensional index be used for the optical roughness parameter (Ω_1) which depends on both σ and μ:

$$\Omega_1 = \mu/\sigma \qquad (4.5)$$

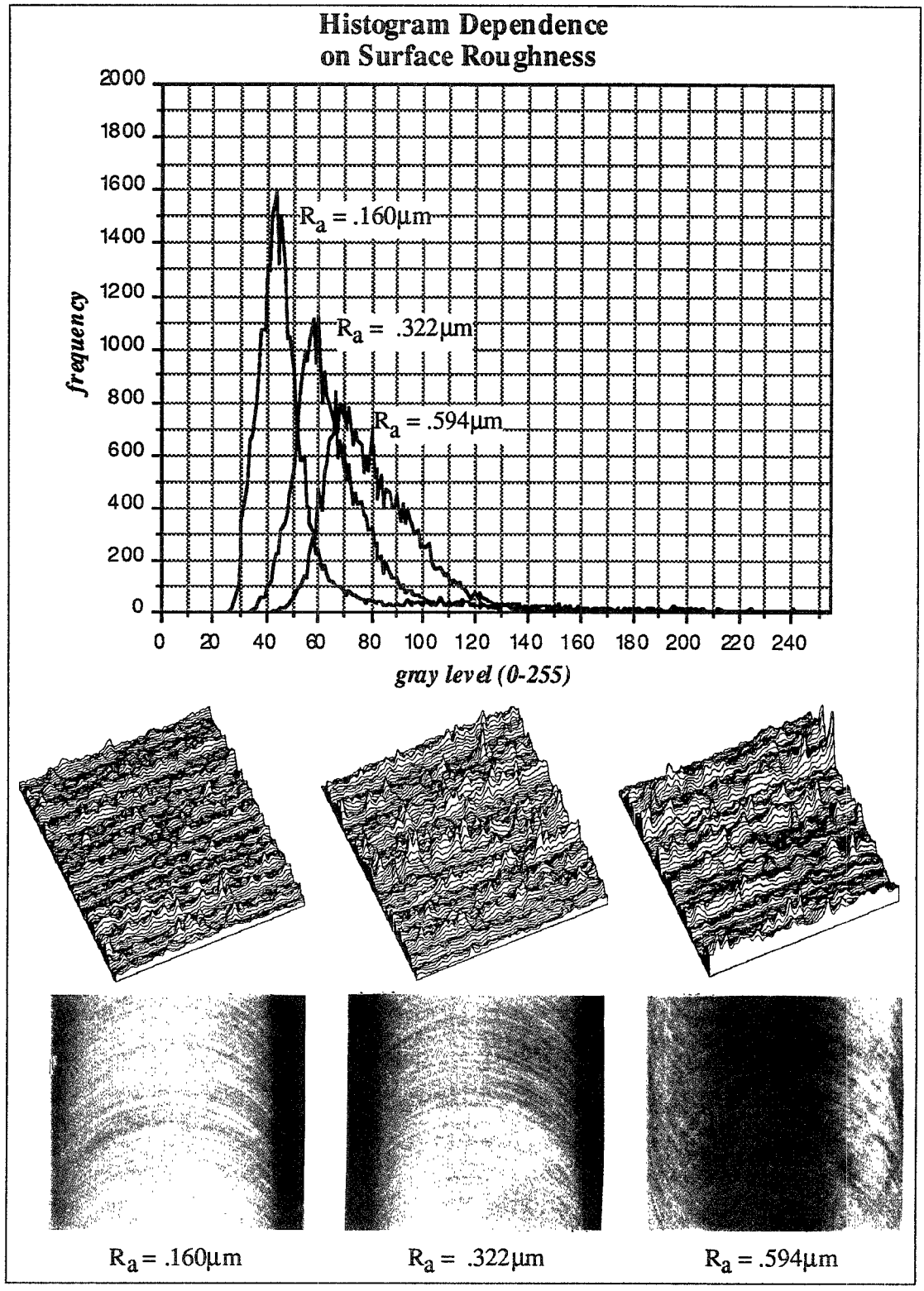

Figure 4.8 – Variation of gray-level histogram with increasing surface roughness

The experimental results from this work as well as from other investigations (Luk 1989, DeVoe 1992) indicate that the definition for the optical parameter provided by Eqn. 4.5 can be successfully correlated to the average roughness of the surface. In addition, certain higher order surface statistics such as the autocorrelation distance and kurtosis can be determined from the 3-dimensional reconstructions shown in Fig. 4.8.

Note that from a theoretical standpoint, the optical roughness parameter can be determined using the mean scattered power given by Eqn. 3.5, combined with Eqn. 3.1 calculating the mean and standard deviation necessary to determine the optical parameter. To perform such a calculation, the mean power scattered into a given CCD element must be translated into the brightness level output by that element. This transformation may be performed by

$$x_i = \varepsilon \Psi_i \tag{4.6}$$

where ε is a 'brightness coefficient' which relates the mean scattered power received by the ith CCD element in the camera to the brightness level output by the element. The brightness coefficient depends on the camera gain, CCD voltage limits and sensitivity, and other factors which are specific to the camera used in the vision system. The three subscripts on Ψ given in Eqn. 3.5 (i, j, $\pi/2$) have been discarded in favor of a single subscript which refers to the ith surface facet. This approach is less tedious than referring to the surface facets in terms of their Cartesian coordinates as proposed earlier.

4.3.2. Incident Angle

According to the light scattering theory, the sensitivity of the system depends greatly on the grazing angle used by the light source, with increased sensitivity for

incident angles close to grazing incidence, and decreased sensitivity for incident angles further from grazing incidence. To validate this effect, three roughness specimens were chosen, and the optical roughness parameter was measured for each specimen at different incident angles.

Table 4.2 – Optical measurements at three incident angles

R_a	Ω_2 (10°)	Ω_2 (15°)	Ω_2 (20°)
0.178 μm	6.745	5.372	5.942
0.402 μm	4.466	4.221	4.373
0.594 μm	3.592	3.667	3.586

Figure 4.9 shows the measurements performed at each incident angle. Note that as the incident angle increases, the slope of the roughness curve decreases. This indicates that using a small incident angle provides a large slope for the roughness curve, and hence better discrimination between surfaces of varying roughness, i.e. better sensitivity.

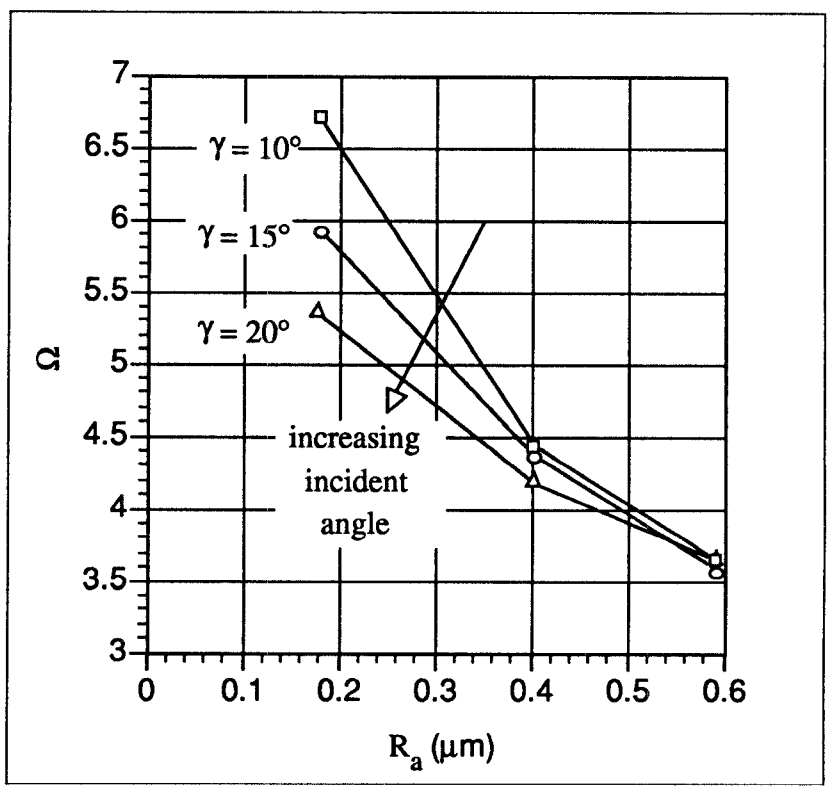

Figure 4.9 – Effect of incident angle on system sensitivity

4.3.3. Baseline Calibration

In order for the vision system to provide consistent results, particularly after disturbances in the system configuration, a procedure for calibrating the system needs to be developed. For the measurements performed in this work, the calibration procedure involves measuring a 'standard' roughness specimen which is known to yield a given value of the optical roughness parameter, denoted here by Ω_c. The standard specimen is measured, and the system configuration is adjusted until the vision system yields the known value of the optical parameter ($\Omega = \Omega_c$).

An aluminum roughness specimen of $R_a = 0.45$ μm was chosen as the standard calibration surface. The value of Ω_c ,which the system must be calibrated to, depends entirely on the chosen configuration of the system (magnification, light intensity, grazing angle, etc.). Since the optimum configuration of the vision system remains to be determined, Ω_c was chosen for each configuration used in this work by fixing the system in the given base configuration, and averaging five consecutive measurements. Whenever the system was disturbed from this configuration, the system was reset by returning to the base configuration, performing a measurement of Ω, and comparing it to the known value of Ω_c. Adjustments to the configuration were then performed until $\Omega = \Omega_c$. The adjustments were made by first manipulating the camera focus, followed by light intensity. Adjustment of these two parameters alone proved sufficient in all cases to bring the system into calibration. Note that the light intensity often required slight adjustment due to changes in the light input to the CCD camera over a period of

several hours, possibly due to fluctuations in the light source power line, or gradual changes in the response of the CCD elements in the camera.

4.3.4. Roughness Correlation

After determining the R_a value of the aluminum samples, the optical roughness parameter of each specimen was measured using the vision system, with $\lambda = 10°$ and $\alpha = 45°$. The resulting values of Ω were plotted against the known roughness values

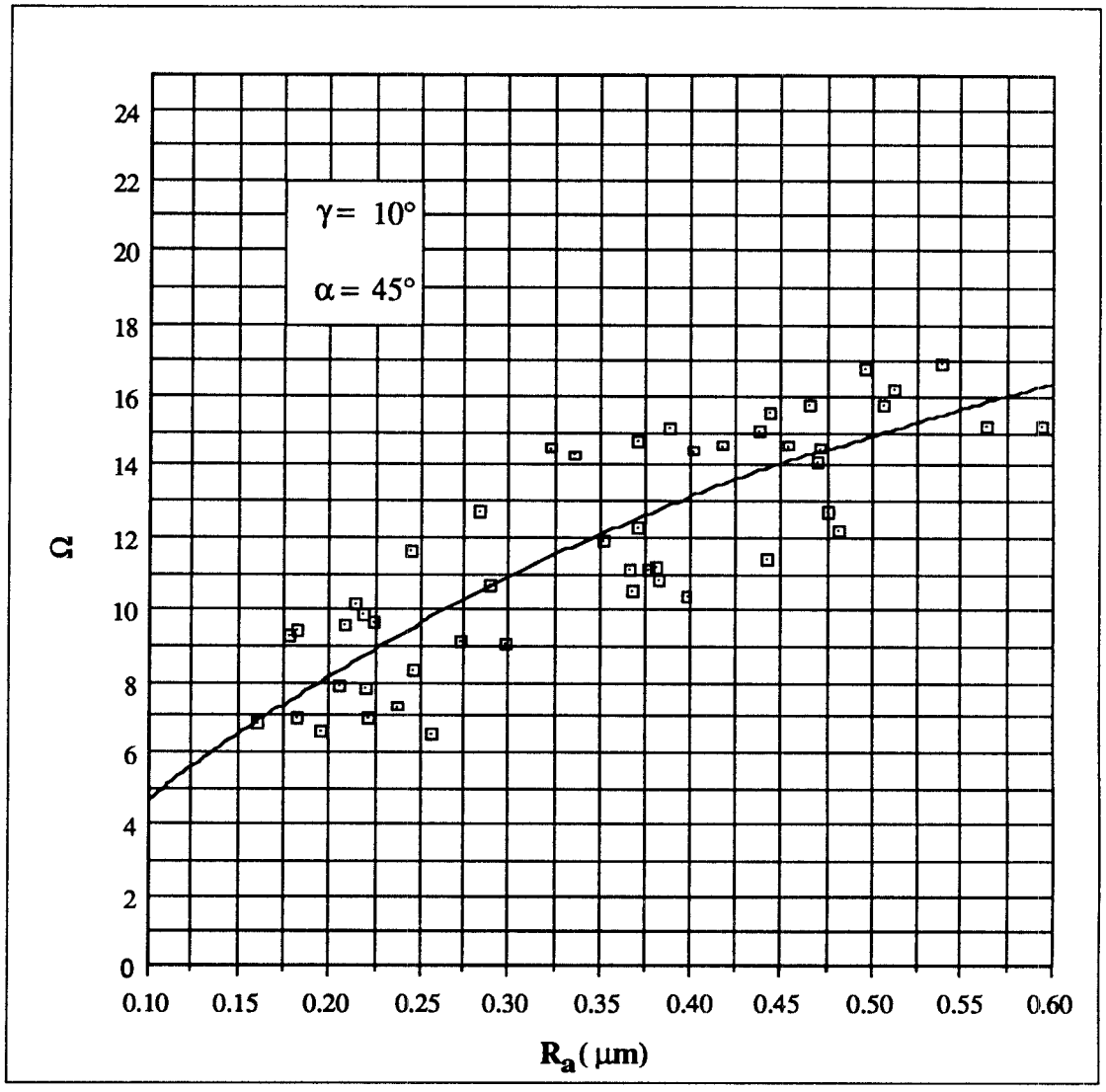

Figure 4.10 – Optical Calibration Curve for Aluminum

determined at NIST, and a curve fit was performed through the data as shown in Figure 4.10. A third degree polynomial curve was found to provide the best fit to the experimental data, with a correlation coefficient of $R^2 = 0.78$. The equation of this empirical relationship is given by

$$\Omega_1 = 22.497R^3_a - 48.762R^2_a + 47.944R_a + 0.316 \qquad (4.7)$$

The resulting calibration curve can be used to determine the roughness of an aluminum workpiece simply by measuring the optical roughness parameter, and finding the corresponding R_a value by solving Eqn. 4.7.

4.4. Sensitivity Analysis

The performance of the vision system is affected by a broad variety of factors, ranging from environmental conditions (vibration, ambient lighting, etc.) to the repeatability of the system setup. In order to discuss the viability of utilizing the system in an industrial setting, the sensitivity of the system to these various factors must be determined. If it is found that the system is especially sensitive to factors which cannot be easily measured or controlled in a machining environment, then it cannot provide accurate surface quality measurements. In order to determine the feasibility of using the system in a machining environment, the six most important factors for system performance were identified, and a full 2^6 factorial design was developed and instituted

on the prototype vision system. The significance of the various factors was then estimated to determine the degree to which each factor affects the system performance .

4.4.1. Parameters Affecting Systems Performance

The factors which are most likely to affect system performance were determined to be as follows:

1. environmental vibration
2. ambient lighting
3. grazing angle
4. light source brightness
5. horizontal orientation of light source
6. camera magnification

The effects on system performance associated with each of these factors can be guessed at based on prior knowledge of the system and the basic light-scattering theory. Environmental vibration will affect the system by causing relative motion between the vision system and the workpiece under observation, thus producing a blurring effect on the resulting image. Ambient lighting is expected to affect the measurement accuracy by shifting the mean histogram brightness level and altering the histogram's standard deviation due to the addition of secondary incident angle. According to the light scattering theory, altering the grazing angle will have a predictable effect on the optical roughness parameter, but it remains to be seen if this effect is significant enough so that a slight variation in the system setup will cause a severe change in the measurement

repeatability. The light source brightness is expected to have an effect on the mean histogram level, and the degree of sensitivity to this effect must be determined. Adjusting the horizontal orientation of the vision system's camera may have a significant effect for milled surfaces, since there is a defined orientation in the lay of the surface machining marks; directing the light from different angles relative to the machining direction may produce significantly different measurement results. Moderate changes in camera magnification may also produce large variations in system performance, although this factor is expected to be of secondary importance compared to the other five factors.

4.4.2. Factorial Design

A full 2^6 factorial design was applied in order to determine the main effects for each of the six factors, as well as the second and third degree interaction effects. Effects due to higher order interactions were assumed to be negligible and were thus ignored in this analysis. Two levels for each factor were chosen for use in the factorial analysis. The levels were chosen to provide small to moderate variations about the normal levels of the factors. The levels were fixed as shown in Table 4.3:

Table 4.3 — Factorial design levels

factor	high level	low level
environmental vibration	minimal	moderate
ambient lighting	none	normal
grazing angle	20°	10°
light source brightness	100%	80%
horizontal orientation of light source	55°	45°
camera magnification	20x	30x

Environmental vibration was produced via a mechanical shaker which produced a sinusoidal excitation with a frequency of 20Hz. The shaker device was strapped to the workpiece holder during measurements, and a noticeable blurring of the captured images resulted. Ambient lighting was produced by eight 34W florescent bulbs placed between 1.5m and 3m overhead of the experimental arrangement. For the case of no ambient lighting, the only light source used to illuminate the workpiece was the fiber optic lighting integrated with the vision system. In both cases, no natural light (sunlight) was allowed to reach the workpiece. The light source brightness was measured using a simple calibrated photoresistor circuit placed at the workpiece surface in order to determine the energy incident on the surface, rather than the energy leaving the fiber optic cable, since much of the light from the cable is not directed onto the surface. The high level lighting was produced with the light source at the maximum setting (100%), and the low level was produced by reducing the light source brightness to 80% of the maximum brightness.

The factorial design employed for this investigation is shown in Table 4.4. Here, the six main factors are designated by a number code (1-6), and the two- and three-factor interactions are designated by the combination of two or three main factor codes (i.e. the two-factor interaction between horizontal orientation and ambient light is designated as '14' in the table). The table was constructed by performing 64 individual measurements; one measurement for each unique combination of the six factors used in the analysis. The optical roughness parameter (Ω_1) was the measured value.

Table 4.4 – Factorial design grid

ambient lighting	grazing angle	light intensity	horizontal orientation	camera magnification	environment vibration	12	13	14	15	16	23	24	25	26	34	35	36	45	46	56	123	124	125	126	134	135	136	145	146	156	234	235	236	245	246	256	345	346	356	456	W
1	2	3	4	5	6																																				
+	+	+	+	+	+	+	+	+	+	+	+	+	+	+	+	+	+	+	+	+	+	+	+	+	+	+	+	+	+	+	+	+	+	+	+	+	+	+	+	+	4.21943
+	+	+	+	+	−	+	+	+	+	−	+	+	+	−	+	+	−	+	−	−	+	+	−	+	+	+	−	+	−	−	+	+	−	+	−	−	+	−	−	−	4.51719
+	+	+	+	−	+	+	+	+	−	+	+	+	−	+	+	−	+	−	+	−	+	+	−	+	+	−	+	−	+	−	+	−	+	−	+	−	−	+	−	−	4.75078
+	+	+	+	−	−	+	+	+	−	−	+	+	−	−	+	−	−	+	−	+	+	+	+	−	+	+	−	−	−	+	+	−	−	−	−	+	−	−	−	+	+	5.20376
+	+	+	−	+	+	+	+	−	+	+	+	−	+	+	−	+	+	−	−	+	+	−	+	+	−	+	+	−	−	+	−	+	+	−	−	+	−	−	+	−	−	3.25811
+	+	+	−	+	−	+	+	−	−	−	+	−	+	−	−	+	−	+	−	−	+	−	+	−	−	+	−	+	+	−	−	−	−	+	+	−	−	+	−	−	+	3.30182
+	+	+	−	−	+	+	+	+	+	+	+	+	+	+	−	−	+	+	+	+	+	+	+	+	−	−	+	+	−	−	−	−	+	+	−	+	+	+	+	+	+	3.29628
+	+	+	−	−	−	+	+	+	+	+	+	+	+	+	+	+	+	+	+	+	+	+	+	+	+	+	+	+	+	+	+	+	+	+	+	+	+	+	+	+	+	3.30985
+	+	−	+	+	+	+	+	−	+	+	+	+	+	+	+	+	+	+	+	+	+	+	+	+	+	+	+	+	+	+	+	+	+	+	+	+	+	+	+	+	+	4.12669
+	+	−	+	+	−	+	+	+	+	−	+	+	+	+	+	+	+	+	+	+	+	+	+	+	+	+	+	+	+	+	+	+	+	+	+	+	+	+	+	+	+	4.17959
+	+	−	+	−	+	+	+	−	+	+	+	+	+	+	+	+	+	+	+	+	+	+	+	+	+	+	+	+	+	+	+	+	+	+	+	+	+	+	+	+	+	4.67032
+	+	−	+	−	−	+	+	+	+	+	+	+	+	+	+	+	+	+	+	+	+	+	+	+	+	+	+	+	+	+	+	+	+	+	+	+	+	+	+	+	+	4.93973
+	+	−	−	+	+	+	+	−	+	+	+	+	+	+	+	+	+	+	+	+	+	+	+	+	+	+	+	+	+	+	+	+	+	+	+	+	+	+	+	+	+	3.19982
+	+	−	−	+	−	+	+	−	+	+	+	+	+	+	+	+	+	+	+	+	+	+	+	+	+	+	+	+	+	+	+	+	+	+	+	+	+	+	+	+	+	3.2418
+	+	−	−	−	+	+	+	+	+	+	+	+	+	+	+	+	+	+	+	+	+	+	+	+	+	+	+	+	+	+	+	+	+	+	+	+	+	+	+	+	+	2.44888
+	+	−	−	−	−	+	+	+	+	+	+	+	+	+	+	+	+	+	+	+	+	+	+	+	+	+	+	+	+	+	+	+	+	+	+	+	+	+	+	+	+	2.4483
+	+	−	+	+	+	+	+	+	+	+	+	+	+	+	+	+	+	+	+	+	+	+	+	+	+	+	+	+	+	+	+	+	+	+	+	+	+	+	+	+	+	3.6732
+	−	+	+	+	−	+	+	+	+	+	+	+	+	+	+	+	+	+	+	+	+	+	+	+	+	+	+	+	+	+	+	+	+	+	+	+	+	+	+	+	+	3.69914
+	−	+	+	+	−	+	+	+	+	+	+	+	+	+	+	+	+	+	+	+	+	+	+	+	+	+	+	+	+	+	+	+	+	+	+	+	+	+	+	+	+	4.10484
+	−	+	+	−	+	+	+	+	−	+	+	+	+	+	+	+	+	+	+	+	+	+	+	+	+	+	+	+	+	+	+	+	+	+	+	+	+	+	+	+	+	4.16768
+	−	+	+	−	−	+	+	+	+	+	+	+	+	+	+	+	+	+	+	+	+	+	+	+	+	+	+	+	+	+	+	+	+	+	+	+	+	+	+	+	+	3.31662
+	−	+	−	+	+	+	+	−	+	+	+	+	+	+	+	+	+	+	+	+	+	+	+	+	+	+	+	+	+	+	+	+	+	+	+	+	+	+	+	+	+	3.58842
+	−	+	−	+	−	+	+	+	+	+	+	+	+	+	+	+	+	+	+	+	+	+	+	+	+	+	+	+	+	+	+	+	+	+	+	+	+	+	+	+	+	3.03567
+	−	+	−	−	+	+	+	−	+	+	+	+	+	+	+	+	+	+	+	+	+	+	+	+	+	+	+	+	+	+	+	+	+	+	+	+	+	+	+	+	+	3.14898
+	−	+	−	−	−	+	+	+	+	+	+	+	+	+	+	+	+	+	+	+	+	+	+	+	+	+	+	+	+	+	+	+	+	+	+	+	+	+	+	+	+	3.21814
+	−	−	+	+	+	+	+	+	+	+	+	+	+	+	+	+	+	+	+	+	+	+	+	+	+	+	+	+	+	+	+	+	+	+	+	+	+	+	+	+	+	3.26059
+	−	−	+	+	−	+	+	+	+	+	+	+	+	+	+	+	+	+	+	+	+	+	+	+	+	+	+	+	+	+	+	+	+	+	+	+	+	+	+	+	+	3.73819
+	−	−	+	−	+	+	+	+	+	+	+	+	+	+	+	+	+	+	+	+	+	+	+	+	+	+	+	+	+	+	+	+	+	+	+	+	+	+	+	+	+	3.82615
+	−	−	+	−	−	+	+	+	+	+	+	+	+	+	+	+	+	+	+	+	+	+	+	+	+	+	+	+	+	+	+	+	+	+	+	+	+	+	+	+	+	3.04484
+	−	−	−	+	+	+	+	+	+	+	+	+	+	+	+	+	+	+	+	+	+	+	+	+	+	+	+	+	+	+	+	+	+	+	+	+	+	+	+	+	+	3.08445
+	−	−	−	+	−	+	+	+	+	+	+	+	+	+	+	+	+	+	+	+	+	+	+	+	+	+	+	+	+	+	+	+	+	+	+	+	+	+	+	+	+	3.02071
+	−	−	−	−	+	+	+	+	+	+	+	+	+	+	+	+	+	+	+	+	+	+	+	+	+	+	+	+	+	+	+	+	+	+	+	+	+	+	+	+	+	3.04555
+	−	−	−	−	−	+	+	+	+	+	+	+	+	+	+	+	+	+	+	+	+	+	+	+	+	+	+	+	+	+	+	+	+	+	+	+	+	+	+	+	+	4.66901
−	+	+	+	+	+	+	+	+	+	+	+	+	+	+	+	+	+	+	+	+	+	+	+	+	+	+	+	+	+	+	+	+	+	+	+	+	+	+	+	+	+	4.66001
−	+	+	+	+	−	+	+	+	+	+	+	+	+	+	+	+	+	+	+	+	+	+	+	+	+	+	+	+	+	+	+	+	+	+	+	+	+	+	+	+	+	5.1334
−	+	+	+	−	+	+	+	+	+	+	+	+	+	+	+	+	+	+	+	+	+	+	+	+	+	+	+	+	+	+	+	+	+	+	+	+	+	+	+	+	+	5.09832
−	+	+	+	−	−	+	+	+	+	+	+	+	+	+	+	+	+	+	+	+	+	+	+	+	+	+	+	+	+	+	+	+	+	+	+	+	+	+	+	+	+	3.995
−	+	+	−	+	+	+	+	+	+	+	+	+	+	+	+	+	+	+	+	+	+	+	+	+	+	+	+	+	+	+	+	+	+	+	+	+	+	+	+	+	+	3.95724
−	+	+	−	+	−	+	+	+	+	+	+	+	+	+	+	+	+	+	+	+	+	+	+	+	+	+	+	+	+	+	+	+	+	+	+	+	+	+	+	+	+	3.92146
−	+	+	−	−	+	+	+	+	+	+	+	+	+	+	+	+	+	+	+	+	+	+	+	+	+	+	+	+	+	+	+	+	+	+	+	+	+	+	+	+	+	3.91798
−	+	+	+	−	−	+	+	+	+	+	+	+	+	+	+	+	+	+	+	+	+	+	+	+	+	+	+	+	+	+	+	+	+	+	+	+	+	+	+	+	+	5.45806
−	+	−	+	+	+	+	+	−	+	+	+	+	+	+	+	+	+	+	+	+	+	+	+	+	+	+	+	+	+	+	+	+	+	+	+	+	+	+	+	+	+	5.5182
−	+	−	+	+	−	+	+	+	+	+	+	+	+	+	+	+	+	+	+	+	+	+	+	+	+	+	+	+	+	+	+	+	+	+	+	+	+	+	+	+	+	5.57793
−	+	−	+	−	+	+	+	−	+	+	+	+	+	+	+	+	+	+	+	+	+	+	+	+	+	+	+	+	+	+	+	+	+	+	+	+	+	+	+	+	+	5.69517
−	+	−	+	−	−	+	+	+	+	+	+	+	+	+	+	+	+	+	+	+	+	+	+	+	+	+	+	+	+	+	+	+	+	+	+	+	+	+	+	+	+	4.46835
−	+	−	−	+	+	+	+	+	−	+	+	+	+	+	+	+	+	+	+	+	+	+	+	+	+	+	+	+	+	+	+	+	+	+	+	+	+	+	+	+	+	4.47651
−	+	−	−	+	−	+	+	+	+	+	+	+	+	+	+	+	+	+	+	+	+	+	+	+	+	+	+	+	+	+	+	+	+	+	+	+	+	+	+	+	+	4.264
−	+	−	−	−	+	+	+	+	+	+	+	+	+	+	+	+	+	+	+	+	+	+	+	+	+	+	+	+	+	+	+	+	+	+	+	+	+	+	+	+	+	4.15244
−	+	−	−	−	−	+	+	+	+	+	+	+	+	+	+	+	+	+	+	+	+	+	+	+	+	+	+	+	+	+	+	+	+	+	+	+	+	+	+	+	+	4.66683
−	−	+	+	+	+	+	−	−	−	−	−	−	−	−	+	+	+	+	+	+	+	+	+	+	−	−	−	−	−	−	−	−	−	−	−	−	+	+	+	+	+	4.58351
−	−	+	+	+	−	+	+	−	+	+	−	−	−	+	+	+	+	+	+	+	+	+	+	+	+	+	+	+	+	+	+	+	+	+	+	+	+	+	+	+	+	5.05181
−	−	+	+	−	+	+	+	−	+	+	+	+	+	+	+	+	+	+	+	+	+	+	+	+	+	+	+	+	+	+	+	+	+	+	+	+	+	+	+	+	+	5.0065
−	−	+	+	−	−	+	+	+	+	+	+	+	+	+	+	+	+	+	+	+	+	+	+	+	+	+	+	+	+	+	+	+	+	+	+	+	+	+	+	+	+	4.16567
−	−	+	−	+	+	+	+	−	+	+	+	+	+	+	+	+	+	+	+	+	+	+	+	+	+	+	+	+	+	+	+	+	+	+	+	+	+	+	+	+	+	4.24223
−	−	+	−	+	−	+	+	+	+	+	+	+	+	+	+	+	+	+	+	+	+	+	+	+	+	+	+	+	+	+	+	+	+	+	+	+	+	+	+	+	+	4.03406
−	−	+	−	−	+	+	+	+	+	+	+	+	+	+	+	+	+	+	+	+	+	+	+	+	+	+	+	+	+	+	+	+	+	+	+	+	+	+	+	+	+	4.01158
−	−	+	−	−	−	+	+	+	+	+	+	+	+	+	+	+	+	+	+	+	+	+	+	+	+	+	+	+	+	+	+	+	+	+	+	+	+	+	+	+	+	4.46774
−	−	−	+	+	+	+	+	+	+	+	+	+	+	+	+	+	+	+	+	+	+	+	+	+	+	+	+	+	+	+	+	+	+	+	+	+	+	+	+	+	+	4.42465
−	−	−	+	+	−	+	+	+	+	+	+	+	+	+	+	+	+	+	+	+	+	+	+	+	+	+	+	+	+	+	+	+	+	+	+	+	+	+	+	+	+	5.21283
−	−	−	+	−	+	+	+	+	+	+	+	+	+	+	+	+	+	+	+	+	+	+	+	+	+	+	+	+	+	+	+	+	+	+	+	+	+	+	+	+	+	5.08917
−	−	−	+	−	−	+	+	+	+	+	+	+	+	+	+	+	+	+	+	+	+	+	+	+	+	+	+	+	+	+	+	+	+	+	+	+	+	+	+	+	+	3.93838
−	−	−	−	+	+	+	+	+	+	+	+	+	+	+	+	+	+	+	+	+	+	+	+	+	+	+	+	+	+	+	+	+	+	+	+	+	+	+	+	+	+	3.80933
−	−	−	−	+	−	+	+	+	+	+	+	+	+	+	+	+	+	+	+	+	+	+	+	+	+	+	+	+	+	+	+	+	+	+	+	+	+	+	+	+	+	4.13929
−	−	−	−	−	+	+	+	+	+	+	+	+	+	+	+	+	+	+	+	+	+	+	+	+	+	+	+	+	+	+	+	+	+	+	+	+	+	+	+	+	+	4.08143
divisor:	32	32	32	32	32	32	32	32	32	32	32	32	32	32	32	32	32	32	32	32	32	32	32	32	32	32	32	32	32	32	32	32	32	32	32	32	32	32	32	1	
effects:	-0.90313152	0.3182586	0.045318	0.97726704	-0.1588585	-0.0446849	0.066	0.794	0.056	0.022	-0.072	-0.148	0.322	0.062	-0.03	-0.056	-0.007	-0.027	-0.335	-0.027	0.002	0.155	0.161	-0.047	-0.004	0.037	-0.033	-0.02	-0.089	-0.02	0.01	-0.078	-0.149	0.008	-0.031	-0.052	0.012	0.025	0.013	-0.006	0.024	4.092354

levels:

	ambient lighting	grazing angle	light intensity	horizontal orientation	camera magnification	environment vibration
high (1):	none	15°	high	45°	3x	none
low (-1):	normal	10°	low	39°	2x	vibration

4.4.3. Significance of Effects

In order to evaluate the significance of each effect, it is necessary to estimate the experimental variation under a constant set of measurement conditions. To determine this variation, ten measurements were performed under the 'high level' conditions used in the design. The standard deviation of these ten measurements was calculated, and the effects determined under the factorial design were compared against the natural standard deviation using a 2-sigma significance test. Those effects which are smaller than twice the standard deviation are assumed to be caused by natural variation in the measurements, and thus they do not represent true effects in the measurement process and may be ignored. Table 4.5 shows the results of the 10 measurements, the calculation of Ω_1 for each measurement, and the resulting standard deviation, which we take as our natural variation in system measurements.

Table 4.5 – Calculation of natural variation for factorial design

Measurement	Histogram Mean (μ)	Histogram Std. Dev. (σ)	Ω_1 ($=\mu/\sigma$)
1	111.04	25.84	4.29
2	111.63	26.96	4.14
3	93.7	22.79	4.11
4	108.34	25.93	4.17
5	108.8	25.68	4.23
6	106.47	25.15	4.23
7	107.2	25.32	4.23
8	107.5	25.82	4.16
9	108.89	25.79	4.22
10	108.6	24.91	4.35
		Std Dev (σ_C):	0.0738

The significance of the 6 main effects, 15 second order effects (two-factor interactions), and 20 third order effects (three-factor interactions) were determined, using the estimated experimental variation to decide which effects were significant. Of the 41 total effects, only 11 were found to be significant compared to the measured natural variation in the measurements. The factorial design yields a mathematical model of the relationship between system performance and the various effects given by

$$\begin{aligned}\Omega_1 = \text{mean} &+ k_1[1] + k_2[2] + k_4[4] + k_5[5] + k_{13}[1][3] \\ &+ k_{23}[2][3] + k_{24}[2][4] + k_{45}[4][5] + k_{123}[1][2][3] \\ &+ k_{124}[1][2][4] + k_{235}[2][3][5] \qquad (4.8)\end{aligned}$$

Each of the coefficients presented in Eqn. 4.9 was calculated from half of the difference between the system output under two different sets of conditions. As a preliminary examination of the empirical model given by Equation 4.9, each of the main effects will be discussed individually. Although the importance of examining the second and third order interaction effects is recognized, these higher order effects will be excluded from this investigation.

mean (4.094) – The mean level in the factorial design indicates the value of Ω_1 which the vision system would output with each of the six factors in the design fixed at their median, or zero, level.

[1] *Ambient Lighting* (k_1 = -0.931) – With a main effect of -0.931 when ambient lighting is reduced from normal room lighting to no lighting, it is clear that changes in ambient light has a large affect on the system performance. This presents a problem since fluctuations in ambient lighting are expected in a manufacturing environment, thus jeopardizing the accuracy of system measurements. One solution to

this problem is to use the system only in an environment where the ambient lighting can be maintained at a constant level, which may not be practical in many situations. Another option is to isolate the surface being measured from all ambient light. For certain machining operations, this option may provide a reasonable solution for eliminating the effect of ambient lighting.

[2] *Grazing Angle* ($k_2 = 0.318$) – As predicted by Beckmann's scattering theory, the grazing angle used in the system has a strong affect on the system performance, with a small increase in grazing angle resulting in moderate increase in the optical roughness parameter. Since the grazing angle is controllable, this effect does not present a problem for achieving consistent system performance. However, this effect implies that accuracy of the system's initial setup is critical, since a small error in the grazing angle will produce a measurable error in Ω_1.

[3] *Light Source Brightness* ($k_3 = 0$) – In spite of the original prediction that the brightness of the fiber optic light source would have a significant affect on measurement of the optical roughness parameter, the factorial design suggests that this is not the case. While it is clear that increased brightness produces an increase in the mean histogram level, the factorial design data indicates that the standard deviation of the gray-level histogram also increases by a proportional amount, thereby leaving the optical parameter unchanged.

[4] *Horizontal Orientation* ($k_4 = 0.977$) – There is a strong relationship between the horizontal orientation of the light source relative to the machining direction (α) and the system performance. This is unfortunate, since it implies that α must be held constant in order to assure repeatable system performance. This effect is suggested by light scattering theory, since milled surfaces are essentially one-dimensionally rough, or at best the superposition of several one-dimensionally rough surfaces. In a one-dimensionally rough surface, the correlation distance changes significantly with the horizontal angle at which the surface is observed. Thus, the pattern and intensity of the light scattered from the surface will vary with the horizontal orientation of the light source.

[5] *Camera Magnification* ($k_5 = -0.159$) – As the camera magnification is increased a moderate amount, the optical roughness parameter is decreased a moderate amount. This may occurs because as the magnification is increased, the amount of light scattered into the CCD camera is decreased due to the smaller area of the surface under observation, so that μ is decreased. At the same time, σ remains unchanged, resulting in a decrease in Ω_1. Since the camera magnification can be held constant, this effect is controllable.

[6] *Environmental Vibration* ($k_6 = 0$) – The vibration employed during the factorial design caused a visually observable blurring of the digital image. Since a blurred image is in some senses similar to an image with reduced resolution, it was expected that measurements

performed under vibration would yield decreased measurement accuracy. Surprisingly, the vibration was found to have no significant affect on the system performance.

Second- and Third-order interaction effects:

Each of the higher-order effects contains at least one element which can be held constant in the vision system, and so they do not introduce any uncontrollable effects which must be contended with in order to achieve consistent system performance. The contribution of each effect is indicated below.

[13] *Ambient Lighting + Light Source Intensity* ($k_{13} = 0.274$)

[23] *Grazing Angle + Light Intensity* ($k_{23} = -0.148$)

[24] *Grazing Angle + Horizontal Orientation* ($k_{24} = 0.322$)

[45] *Horizontal orientation + Camera Magnification* ($k_{45} = -0.335$)

[123] *Ambient Lighting + Grazing Angle + Light Intensity* ($k_{123} = 0.155$)

[124] *Ambient Lighting + Grazing Angle + Horizontal Orientation* ($k_{124} = 0.161$)

[235] *Grazing Angle + Light Intensity + Camera Magnification* ($k_{235} = -0.149$)

The sensitivity analysis brings to light several of the positive and negative aspects of the vision system, as discussed below:

positive aspects:

- The vision system is immune to the effects of environmental vibration. Clearly, this is important attribute for any measurement system used in a manufacturing environment.

- Changes in the brightness of the light source used to illuminate the surface do not affect the system performance. This indicates that a consumer quality light source can be used in the system, with no requirement for expensive voltage regulation for powering the light source.

negative aspects:

- Changes in ambient lighting can have a moderate affect on the system performance. this effect can perhaps be eliminated in most situations by maintaining the ambient lighting at a constant level, or by isolating the CCD camera and machined surface from ambient lighting entirely.
- Slight changes in the grazing angle of incident light can produce measurable errors in the optical parameter. While the grazing angle is held constant in the system operation, initial setup errors in the lighting geometry must be avoided.
- Changes in the horizontal orientation of the light source relative to the machined surface causes moderate changes in the measured optical parameter. This presents a significant problem when measuring milled surfaces, since it is difficult to maintain a constant value of α in such a machining operation. This effect occurs because of the anisotropic nature of milled surfaces.
- The system performance is moderately affected by changes in camera magnification. As with the grazing angle, the camera magnification must be carefully maintained during system setup in order to assure consistent system performance.

4.5. Comparison of Alternate Optical Parameters

The optical roughness parameter, $\Omega_1 = \mu/\sigma$ as defined by equation 4.2, has been shown to be a useful parameter for correlating the statistical properties of a surface's gray-level histogram to the known average roughness of the surface. This claim is supported by the optical correlation curve shown in Fig. 4.10, which provides a functional equation which relates the optical parameter to an aluminum surface's R_a value. However, this definition is not unique, and any number of alternate definitions based on σ and μ can be devised. In the following discussion, an alternative definition for the optical parameter based on the product of σ and μ will be explored.

It was shown in Section 4.3 that both the mean (μ) and standard deviation (σ) of a surface's histogram increase as the surface roughness increases. Using this information, Ω should be defined to yield a parameter with optimal sensitivity to changes in surface roughness. To achieve this goal, an alternate optical roughness parameter is suggested here as

$$\Omega_2 = \sigma\mu/1000 \qquad (4.9)$$

rather than the original definition given by $\Omega_1 = \mu/\sigma$. Note that the original optical parameter was dimensionless, while the new definition for the optical roughness parameter has dimensions of $\Omega_2 = [b]^2$, where 'b' is a unit which denotes the brightness difference between two adjacent gray levels in a histogram. The dimensions of this newly defined parameter, however, are not of particular concern for the present application.

Defining the optical parameter as the product of the mean and standard deviation provides better sensitivity than the previous definition, since an increase in surface roughness leads to an increase in both σ and μ, resulting in a steeper increase in Ω_2 than would have been observed using Ω_1 as the optical parameter. This effect is displayed by the correlation curve shown in Figure 4.11. As with the original correlation curve, a third order polynomial curve provided the best fit through the data, with an equation defined by

$$R_a = .021\Omega^3 - .139\Omega^2 + 0.396\Omega + 0.004 \qquad (4.10)$$

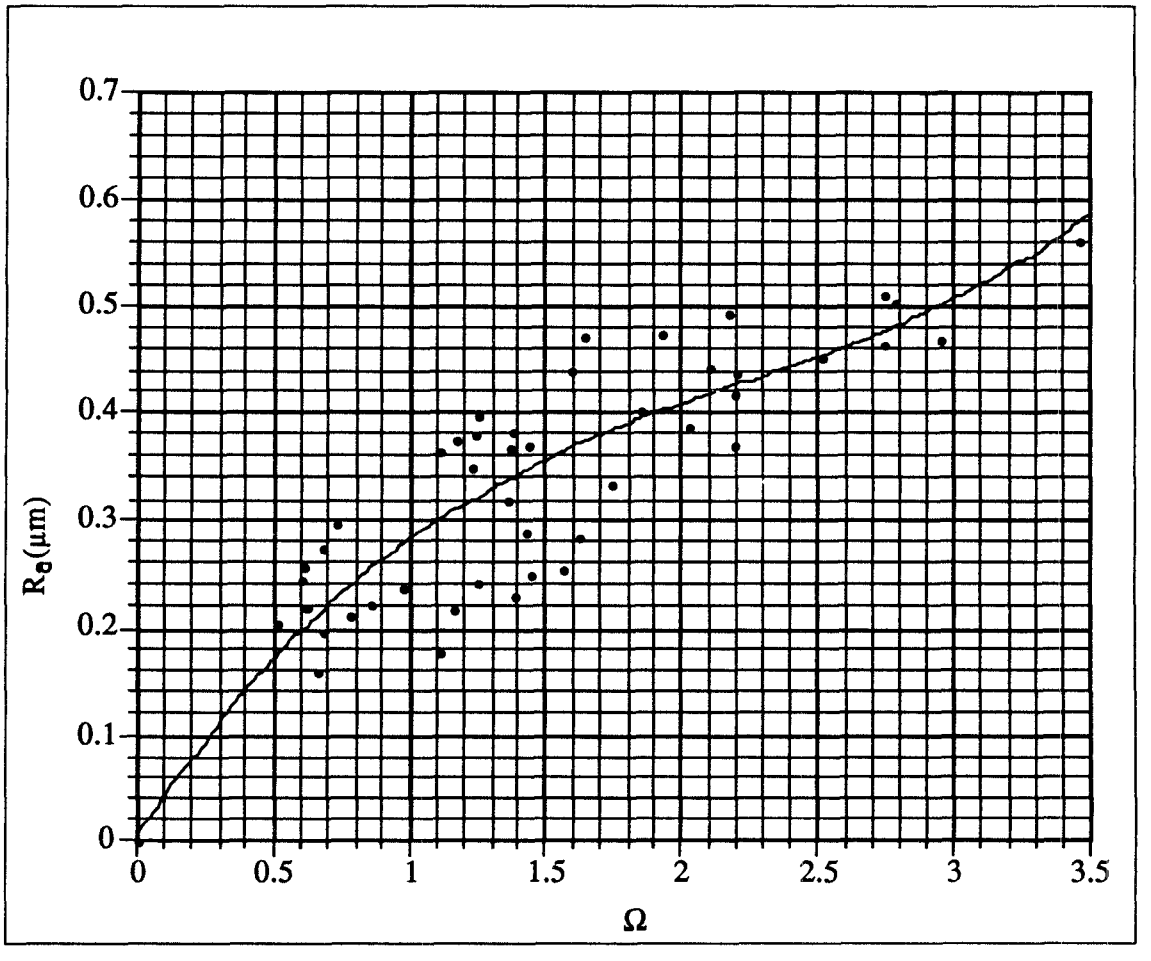

Figure 4.11 – Optical correlation curve using $\Omega_2 = \mu*\sigma/1000$

Comparing the optical correlation curve presented in Fig. 4.10 to the curve of Fig.4.11, it is clear that the sensitivity of Ω_2 to surface roughness is improved over the sensitivity of the previous definition for the optical roughness parameter. However, using Ω_2 as an optical parameter may not be advantageous when significant noise appears in the video image, since this parameter can be more sensitive to noise than Ω_1. This is the case since the error in Ω_2 comes from the product of the errors in σ and μ, while the error in Ω_1 is produced by the ratio of the errors in σ and μ. Both the original definition of the optical roughness parameter (Ω_1), as suggested by Luk (1989) and used in this work and by DeVoe (1992), and the new definition given by Eqn. 4.9 can be useful, and the choice of using one rather than the other depends on the degree of roughness and noise sensitivity required for a given application.

CHAPTER 5
INTEGRATION OF VISION SYSTEM AND CNC MACHINE

To ascertain whether the vision system proposed in this work is applicable for active control in a manufacturing environment, an apparatus was constructed to attach a modified vision system to a Matsuura CNC milling center. In this chapter, the effects of several attributes of a machining environment on the system are considered, and the overall performance of the system in this environment is analyzed.

5.1. Design Considerations

In order to apply the proposed vision system to the in-process control of a machining process, there are several considerations which must be addressed. The primary question which must be answered is whether the vision system can operate reliably and accurately in a true machining environment. There are many aspects of a machining environment which make vision system measurements considerably more difficult to perform than similar measurements in a controlled experimental environment, such as:

- cutting fluid / coolant
- camera vibration
- dynamic movement of camera
- reflections from machine tool surfaces

For instance, coolant may obscure the surface from the camera, thus preventing reliable measurements. Additionally, coolant must be prevented from fouling the camera lens.

Due to relative motion between the camera and workpiece, there may be a limit to feed rates beyond which digitized images will be excessively blurred. Reflections of the light source off of the machine tool surfaces may affect the sensitivity of the system, and excessive vibrations may also have an adverse affect on the system.

In order to examine the effects of these factors on the vision system, a prototype apparatus was designed and constructed to mount the vision system on a CNC milling machine. The new system differs from the original experimental apparatus primarily in the type of camera employed. The new system uses a 'micro-CCD' camera, which is significantly smaller than the original CCD camera used in the previous experimental study. The original camera, while excellent for investigating the overall potential of the measurement technique due to its excellent resolution, proved to be unsuitable for use as an in-process sensor due to its large size. The micro-CCD camera is capable of focusing on an area of the workpiece quite close to the machining zone (the tool-workpiece interface), while the original camera would be forced to focus on a more distant region of the workpiece.

The new apparatus, depicted in schematic form in Figure 5.1 and photographed in Figure 5.2, consists of a base ring which mounts onto the spindle stock of the machine tool, a connecting brace which supports the camera, and a bracket which mounts the light source onto the camera body. All components of the apparatus are adjustable to examine the effects of various mounting configurations. The apparatus mounts directly to the spindle stock of the milling machine so that the camera will move with the spindle, thus ensuring that the camera is always focused on the machined region of the workpiece. A miniature CCD camera with an integrated lens system was used in the apparatus since the low weight and small size of the camera allowed for

considerable flexibility in mounting configurations, and since the size of the camera allowed the imaging element to be placed quite close to the tool-workpiece interface. Due to cost considerations, the camera employed in the apparatus uses an imaging element with lower resolution than the camera used in the earlier experimental study. While the original camera has a resolution of 510 (horizontal) x 492 (vertical), the miniature CCD camera uses an imaging element with a resolution of 324 x 246.

As indicated by the sensitivity analysis described in Chapter 4, the reduced resolution of the camera used in the system should not severely affect the sensitivity of the system, so long as the resolution is sufficient based on the roughness criterion suggested in Section 3.2 (see the discussion on the 1/2 cutoff period criterion). In this case, the area of the surface under observation is 4 cm^2 , and the camera resolution is 324 pixels per 2 cm. If we consider typical cutting conditions using a single-point tool on a milling machine (assume a feed rate of 10 in/min, and a spindle speed of 800 rpm), then the tool will trace out a series of 'grooves' in the workpiece , with a spacing between grooves of 317.5 μm. Thus, a reasonable cutoff wavelength for roughness calculations of such a typical surface would equal this spacing between grooves. That is, any variation in surface height with a wavelength greater than this cutoff frequency is assumed to be due to waviness in the surface, and does not contribute to the roughness of the surface. Using the above information, the 1/2 cutoff period criterion can be applied: Each pixel in the captured image represents a section of the surface with sides of length 61.7 μm, and since this distance is well below 158.8 μm (1/2 the cutoff wavelength) the selected micro-CCD camera should perform acceptably for surfaces machined under typical cutting conditions.

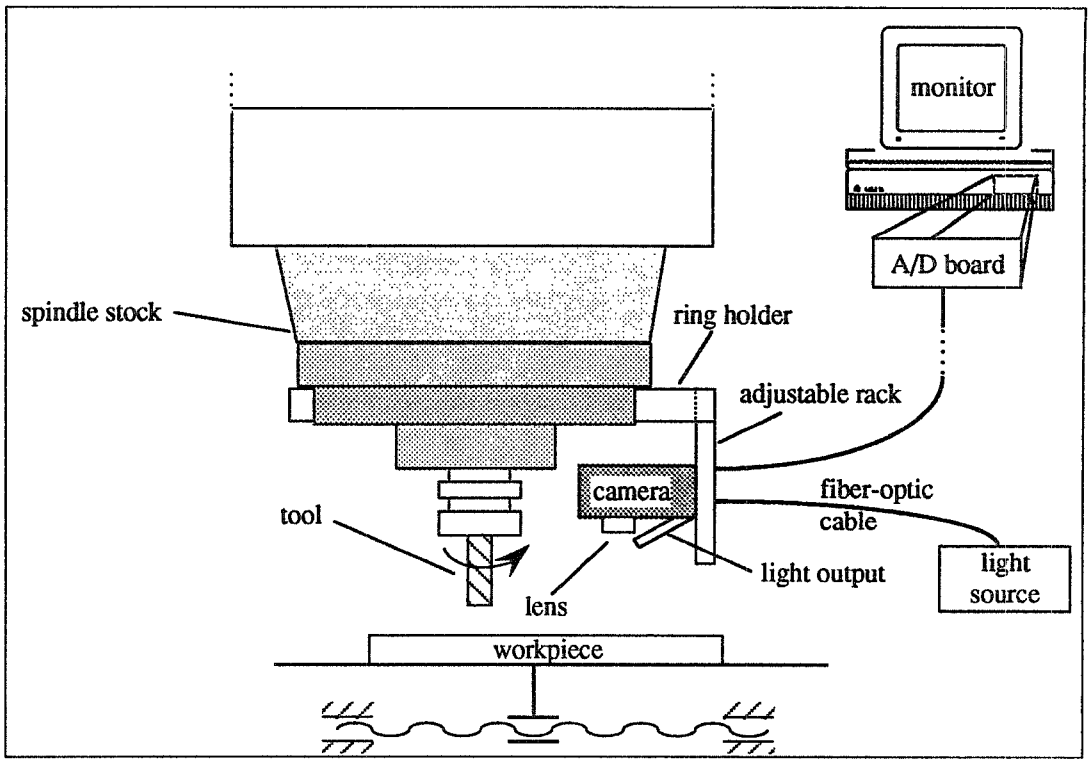

Figure 5.1 – Schematic of vision apparatus used with CNC milling machine

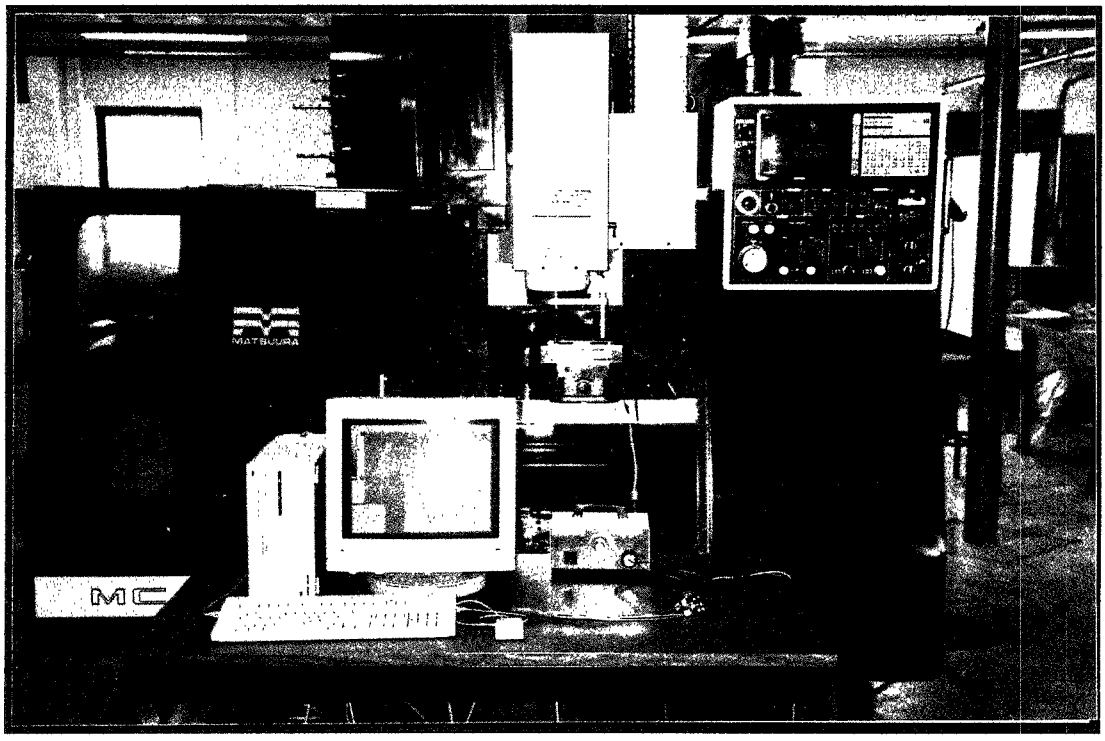

Figure 5.2 – Photograph of vision apparatus mounted onto Matsuura 510 Milling Center

Using the vision system in a dry cutting environment is relatively uncomplicated, with the primary difficulty arising from the existence of cutting chips in the measurement area. Performing measurements in a wet machining environment, however, presents a greater challenge, since both cutting chips and cutting fluid may be present in the measurement area. In order to reduce the problems associated with cutting fluid obscuring the camera, a flexible protector was placed around the lens to prevent stray coolant from reaching the camera optics. Another problem associated with the use of cutting fluid is that any fluid which remains on the surface during the measurement process will interact differently with the incident light than the interaction predicted by scattering theory. Because of this, it is imperative that the measurement area be cleared of any residual cutting fluid before measurements are performed, or that an alternate calibration curve be developed with a film of cutting fluid present on the surface of the workpiece. The latter solution to the problem is not ideal, since it is extremely difficult to predict how thick of a layer of fluid will be present at any given time, the concentration and size of air bubbles present in the fluid, the nature of miscellaneous impurities in the fluid, and any number of other factors which will affect results. For this reason, the former solution will be taken into consideration here, and the development of an alternate 'wet' calibration curve will not be pursued in this work.

The centerline of the camera lens is located approximately 53 mm from the cutting tool, and 16 mm above the workpiece surface (the working distance dictated by the lens optics and observable surface area). These dimensions are shown on the photograph of the vision system in Figure 5.3. Due to the proximity of the lens to the workpiece surface, the potential for reflections from the camera body onto the workpiece is high. In order to minimize there reflections, which can reduce the

sensitivity of the vision system, the camera case and lens mounting were coated with a flat black enamel paint. However, no such modifications were made to the surrounding parts of the machine tool, since in a true production environment modifications of this sort may not be reasonable. Thus, reflections from these surfaces present a real problem which may affect the system performance.

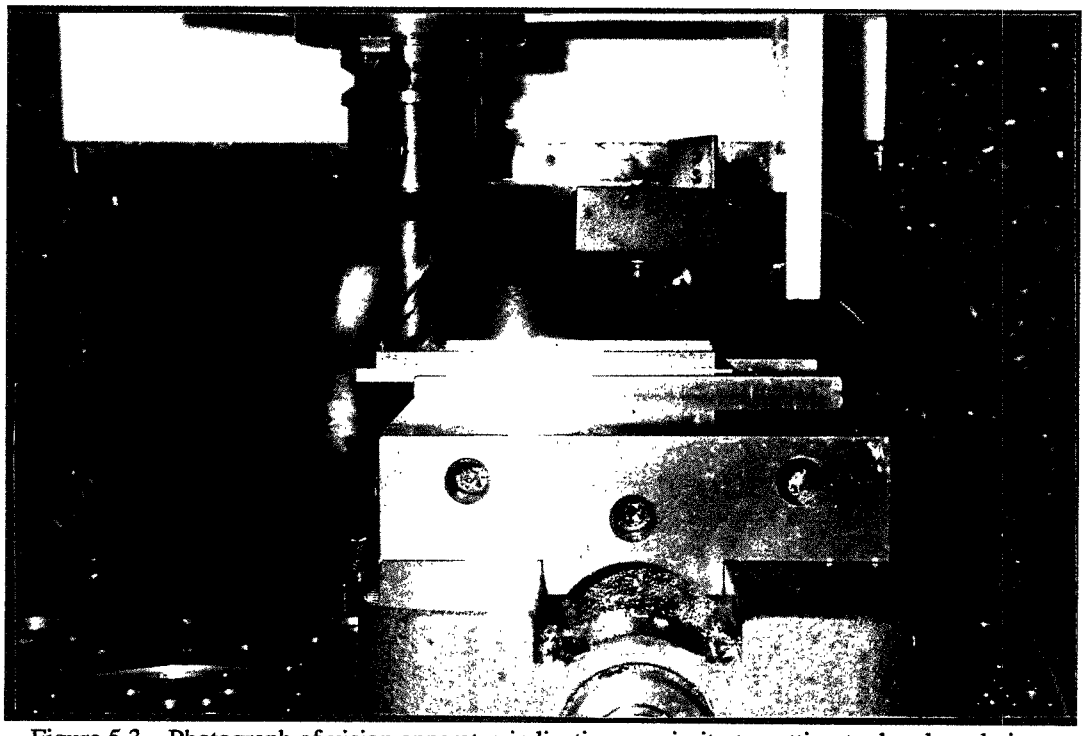

Figure 5.3 – Photograph of vision apparatus indicating proximity to cutting tool and workpiece

Another concern with mounting the vision system on the machine tool is the often severe vibration which exists in a machining environment. Such vibration could cause significant problems for the vision system, in terms of performance degradation and mechanical failure. From the factorial design performed in Chapter 3, it is clear that vibration should not adversely affect the performance of the system to a significant degree. Indeed, the factorial design indicates that the effects of vibration on the system are essentially negligible, and so vibration can be eliminated as a source of sensitivity degradation. However, the effects of vibration on the mechanical performance of the

system is as yet unknown. In order to reduce any problems which may occur, the camera holder used in the apparatus was made highly rigid in order to reduce the amplitude of vibration experienced by the camera and lens system.

The effects of dynamic motion of the camera on system performance are unknown. The primary question which must be asked is: what is the limiting speed at which the camera can be moved while providing acceptable output? This is vital since if the system cannot provide accurate measurements at relatively low feed rates, then it is not suitable for use in a machining environment. This issue will be addressed in a later section.

5.2. Calibration of Integrated Vision System

Before any measurements can be performed using the new vision system and mounting apparatus, the system must be properly calibrated by producing a optical correlation curve (see Chapter 4). The camera and mounting apparatus were placed on a Matsuura 510 Milling Center as indicated in Figs. 5.1 and 5.2, and the 50 aluminum samples used in the preliminary experimental investigation were examined by the vision system. For this calibration, the system used the following settings:

Table 5.1 – Vision system settings used for integrated system

factor	setting
ambient lighting	normal
light source grazing angle	10°
light source brightness	40%
light source horizontal orientation	45°
magnified area	4 cm^2

The horizontal orientation of the light source indicated in Table 5.1 is defined with respect to the x-axis of the milling table. For the experimental work performed here, the only table motion permitted was along this axis, so that the light source could remain at a constant orientation with respect to the cutting direction. This is necessary, since the factorial design of Chapter 4 indicates that changing the horizontal orientation has a strong affect on system performance. Obviously, this limits the usefulness of the system, since the system can perform accurate measurements only along a single axis. In order to eliminate this limitation, it would be necessary to construct a rotary actuator which could maintain the orientation of the light source with respect to the cutting direction. Such a modification is feasible, but beyond the scope of this work.

The mounted camera system was found to yield images which suffered from secondary light reflection from the camera lens. That is, a circular ghost-like picture of the lens support appeared in the center of each of the images captured by the system due to the reflection of light from the sample surface onto the lens body. A portion of this reflected light is directed back onto the surface, where it again reflects into the lens to

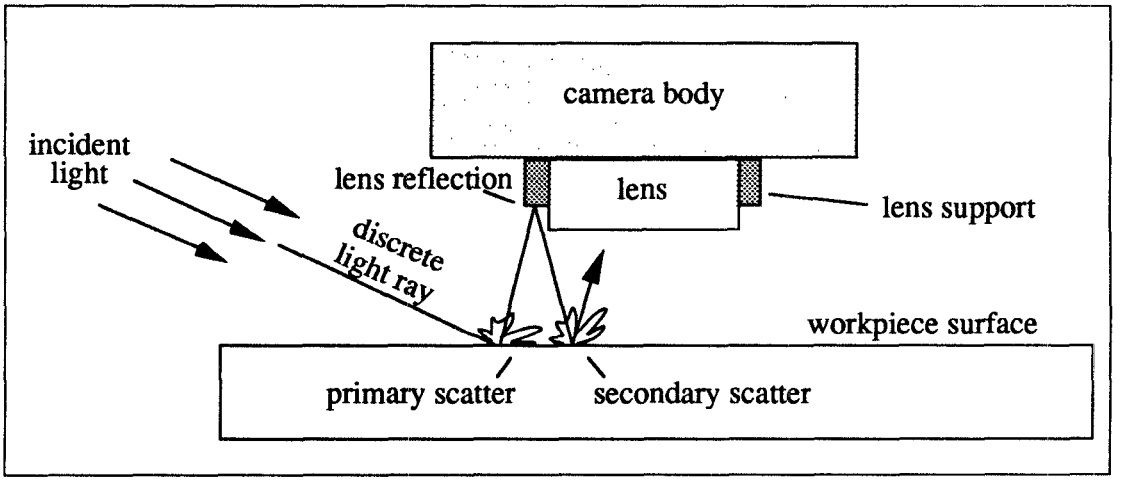

Figure 5.4 – Secondary light reflection from camera lens

form a hazy image of the lens support superimposed over the image of the surface. The mechanics of this effect are illustrated in Figure 5.4. This effect was not observed in the initial experimental investigation since the lens and camera system was significantly farther from the workpiece surface than in the present case (approximately 5 times as far), so a smaller amount of light was reflected onto the lens body, and an essentially negligible amount is re-directed onto the workpiece from the lens. This situation presents a problem, since the light reflected from the lens body acts as a secondary light source with a 90° incident angle, and scattering theory suggests that the majority of this light will be reflected directly upwards into the vision system as glare. This glare will affect the sensitivity of the system, since the intensity of the glare will not depend as greatly on the surface roughness as the intensity of the scattered light from the primary light source. In addition, the gray-level histogram exhibits a tendency to become bi-modal under these conditions, since the secondary light from the glare is scattered about a mean level which is independent from the mean level of the scattered field from the primary light source. This problem was overcome by 'editing out' the section of the image affected by the glare, and calculating the optical parameter using this edited image. This approach is only possible because the glare from the lens body

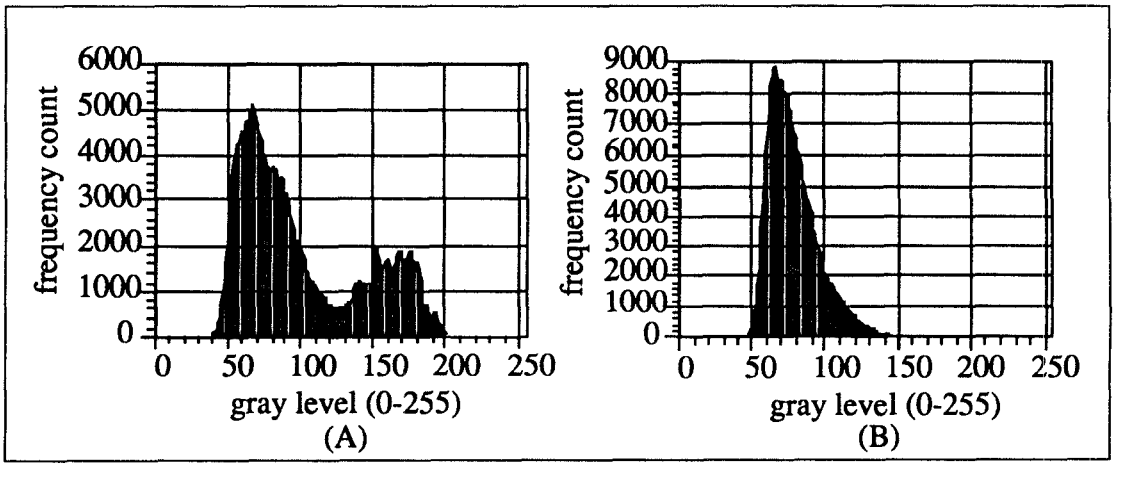

Figure 5.5 – Effect on histogram due to elimination of glare

always occurs in the same section of the image, so that a consistent editing method could be employed. To demonstrate the effectiveness of approach, Figure 5.5 depicts two histogram from a single image. Histogram A is produced from the entire image, while histogram B is produced from the same image with the glare from the lens body edited out. Note the bi-modal nature of the first histogram, while the second is quite close to obeying the desired normal distribution. The process of editing out the glare was performed by adding code to the *NIH Image* macro which automatically created a custom "region of interest" (the term used by *NIH Image* for a measurement area) that excluded the regions of the image affected by the glare.

Measurements of the 50 aluminum samples produced the optical calibration curve shown in Figure 5.6. Ω_2 was used as the optical parameter in the curve due to its increased sensitivity to roughness compared to Ω_1.

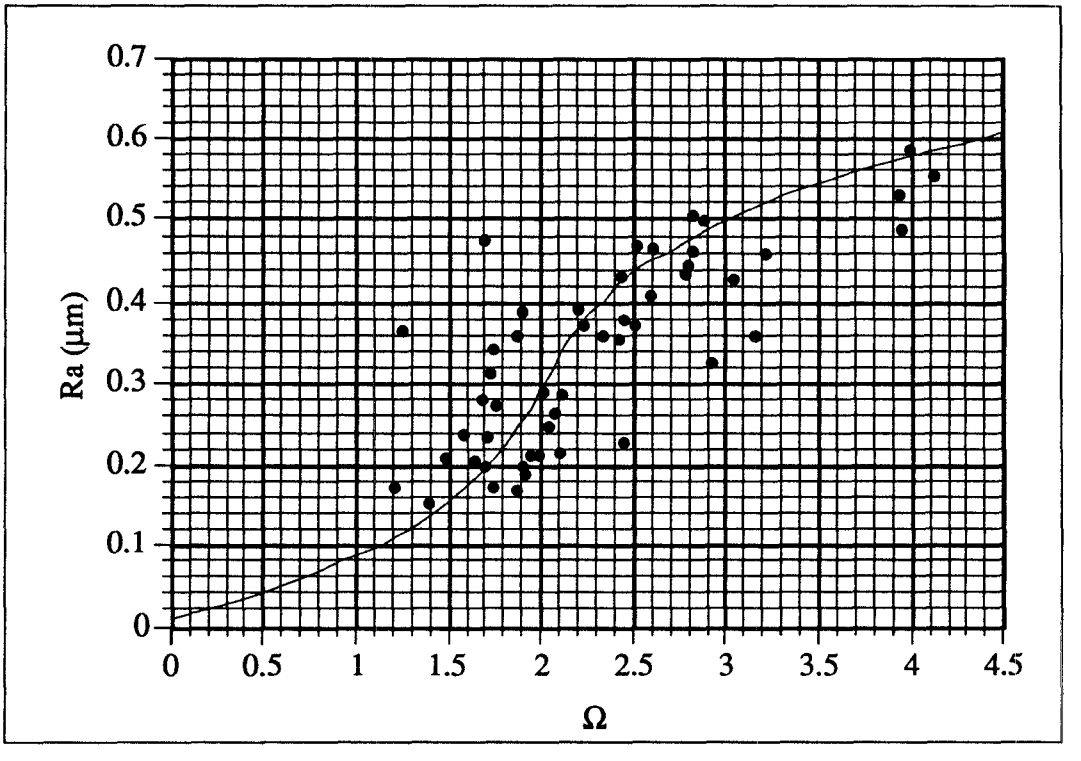

Figure 5.6 – Optical calibration curve for integrated system using Ω_2

The equation of the calibration curve is

$$\Omega_2 = 55.02R_a^3 + 48.01R_a^2 - 16.51R_a + 0.008 \qquad (5.1)$$

In order to reduce the noise in the images used to produce Fig. 5.6, each image was processed by applying a smoothing filter. The filter used in this case was a 3 x 3 spatial convolution which utilized the following convolution matrix:

$$\begin{matrix} 1 & 1 & 1 \\ 1 & 4 & 1 \\ 1 & 1 & 1 \end{matrix}$$

This filter was implemented by replacing each pixel in the image with the weighted average of its 3 x 3 neighborhood, with the weighting performed by the convolution matrix. The effect of this filtering operation is to reduce the noise present in the image while slightly sacrificing image crispness. It was found that for images with minimal noise, applying the smoothing filter did not affect the measurements, while measurements on noisy images were often affected as much as 5% by removing the noise.

The calibration curve given in Fig. 5.6 compares favorably with the calibration curve of Fig. 4.11, produced with the original experimental apparatus, although the current data exhibits more scatter from the correlation curve than the data in Fig. 4.11. This is expected, since the camera used for the on-line system is of somewhat lower quality than the original experimental camera, and the effects of ambient lighting (which could not be eliminated from the experimental conditions) are likely to reduce the sensitivity of the system (see Chapter 3).

5.3. System Performance Under Motion

In order to examine the output of the system under motion, the camera/lighting apparatus was placed on the milling machine, and a CNC program was written to move the workpiece being observed by the camera at varying rates of speed. The workpiece used in this experiment was a block of aluminum with a 1" wide path milled across a 4" length, using a 1" diameter end mill. During the process of moving the workpiece, the vision system performed three measurements for each feed rate used in the experiment. In order to eliminate the effect of the natural roughness variation along the length of the milled surface, the CNC code and the software controlling the vision system were synchronized so that the same section of the workpiece was measured for each feed rate. The variation between the roughness measurements performed by the vision system were then examined to determine the effect of workpiece motion on system performance.

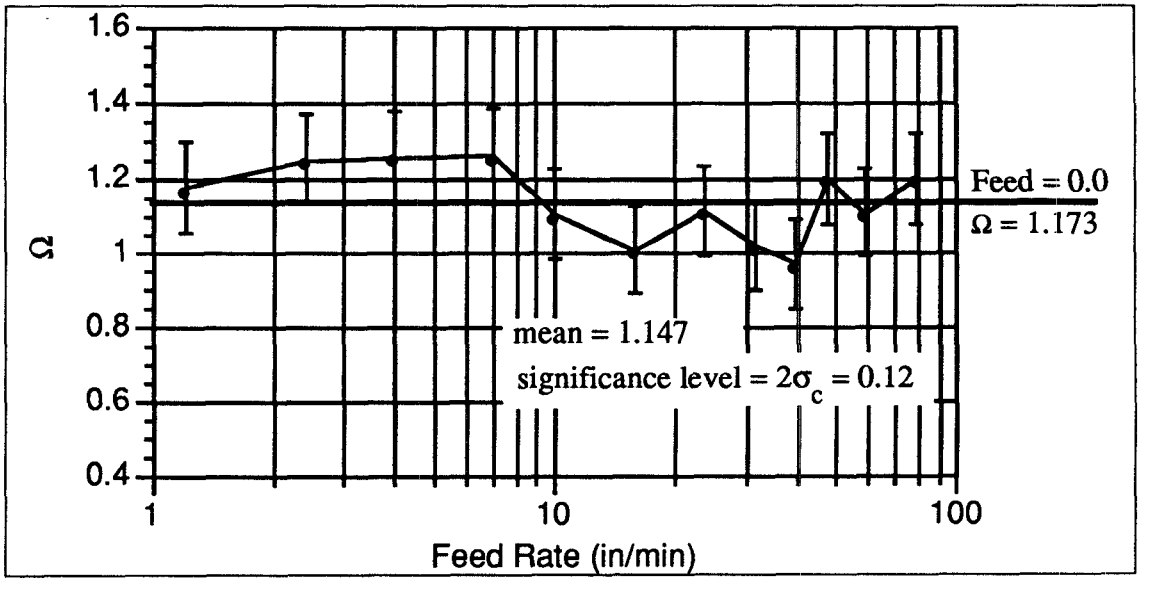

Figure 5.7 – Dependence of Ω_2 on feed rate

Feed rate ranging from 0 to 79 in/min were programmed into the milling machine, and the resulting optical roughness parameters measured during the experiment are plotted in Figure 5.7. In order to determine the significance of the variation in Ω_2 shown in this plot, the standard error was determined from the standard deviation of ten measurements on the same roughness specimen measured in Fig. 5.7. The workpiece table was held stationary during these measurements. The measurement data and resulting standard deviation are shown in Table 5.2. Figure 5.7 indicates this natural variation in the system measurements by error bars around each data point in the graph, using a significance level of twice the measured standard deviation. In addition to error bars, the system output for the stationary workpiece (the zero value) is shown as a straight line through the data to help illustrate the deviation of measurements under motion from the stationary measurement.

Table 5.2 — Calculation of natural variation of Ω_2

Measurement	μ	σ	Ω_1	Ω_2
1	91.27	10.43	8.751	0.952
2	88.75	10.27	8.642	0.911
3	88.61	9.95	8.906	0.882
4	89.86	10.91	8.236	0.980
5	90.02	10.81	8.327	0.973
6	91.13	11.68	7.802	1.064
7	91.56	11.30	8.103	1.035
8	92.70	11.06	8.382	1.025
9	93.23	11.32	8.236	1.055
10	93.21	10.47	8.903	0.976
		Average:	8.429	0.985
		Std Dev (σ_c):	0.363	0.060
		% of average:	4.3%	6.1%

It is clear from Fig. 5.7 that the variation in Ω_2 due to changes in feed rate cannot be accounted for purely by the natural variation in the measurements, since not all data is within the confidence interval. The conclusion is that the feed rate used in the

milling machine does have a significant affect on the performance of the vision system. Examination of the data (Table A3) and Fig. 5.7 indicates that for feed rates greater than about 10 in/min, the system measurements leave the bounds defined by the confidence interval. Since typical milling conditions require feed rates as high as 40 in/min, the cause of this restriction on feed rates deserves close investigation.

Figure 5.8 shows four images captured by the vision system for a range of feed rates, from stationary to 118 in/min. The feed direction is oriented in the north-south direction in these images. The clarity of the images progressively deteriorates as the feed rate increases. The stationary image clearly shows the individual machining marks caused by the combined rotation and translation of the end mill, with a strong differentiation between the hills and valleys on the surface. The image produced under a feed rate of 7.0 in/min is essentially unchanged from the stationary image, although the clarity of the image is impaired. In the third image, captured while moving at a feed rate of 23.6 in/min, the machining marks are no longer discernible as individual tracks in the surface, and the overall clarity of the image is significantly reduced from that of the stationary image. The final image was produced with a feed rate of 118 in/min, resulting in a severely blurred and indistinct picture which exhibits a 'double image' effect. This is apparent in the repeating pattern of small white regions in the image. While a feed rate of 118 in/min is well beyond the usable range of feed rates useful in a milling operation, the problems with the image resulting from this extreme feed rate illustrates the difficulties of performing optical measurements on a moving workpiece.

Figure 5.9 shows two- and three-dimensional reconstructions of the images presented in Fig. 5.8, produced by plotting the gray level of the images on the z-axis, and the spacial dimensions in the x-y plane. The two dimensional 'traces' are each

shown with different scales to emphasize the form of the traces rather than the relative amplitudes. Clearly, the first and second sets of reconstructions (feed = 0.0 and 7.0 in/min) are quite similar in form, keeping in mind that the reconstructions are not produced from exactly the same location on the workpiece surface. For both cases, the reconstructed surfaces exhibit very similar patterns with well defined topographical frequencies. In the third reconstruction, produced from the image captured at 23.6 in/min, the smooth surface topography apparent in the first two reconstructions has given way to a lower frequency topography, with a higher frequency component. This topography is quite dissimilar to the topography produced from the stationary workpiece. This same behavior is evident in the last set of reconstruction, produced at a feed rate of 118 in/min. Somewhere between the feed rates of 7.0 and 23.6 in/min, the ability of the vision system to accurately reproduce the form of the actual surface topography is lost (judging from the data presented in Fig. 5.7 and Table A3, the crossover point occurs between the feed rates of 10 and 15.7 in/min). This behavior can be explained in part by the specifications of the frame grabber board used in the system to capture images from the CCD camera (see Appendix C). The board receives an NTSC video signal from the CCD camera, which it samples 30 times each second. NTSC video is composed of two sets of raster groups, where each group is offset from the other by one scan line. Thus, the CCD image is captured by sampling every other scan line of the image, from top to bottom, and then repeating the same sampling process offset by one scan line to 'fill in' the remaining scan lines omitted during the first raster group. Because of this process, two adjacent scan lines in the image are not sampled at adjacent moments in time, but rather are separated by half of the time required to scan the entire image. Thus, two adjacent scan lines are sampled in half of the 1/30 s required to capture a full image. This effect is a feature called *interlace video*, which is used by the NTSC (National Television Standards Committee) video standard

to reduce eye strain on video monitors with low persistence phosphor screens. In short, interlacing is a format where a field of odd image lines is displayed, followed by a second field of even image lines. The two fields are then combined to produce the overall image, displayed as a single frame.

Consider a workpiece examined by the vision system while moving at a feed rate of 1 in/min. Due to a combination of the time lag between capturing adjacent scan lines and the motion of the workpiece, any two adjacent scan lines will show sections of the surface which are separated by a distance of:

$$\left(\frac{1}{2}\cdot\frac{1}{30}\text{sec}\right)\left(1\frac{\text{in}}{\text{min}}\right)\left(\frac{1\text{min}}{60\text{sec}}\right)=0.00028\text{in}$$

Thus, in the case of a workpiece moving at 118 in/min, the distance between adjacent scan lines will be 118 * 0.00028 in = 0.0333 in. The actual separation distance can be measured from the image in Fig. 5.8 produced at a feed rate of 118 in/min. The images in this figure are produced from sections of the surface 0.265" in length, and the ratio between the separation of the 'double images' in the figure to the total length of the figure is 0.125. Using this information, the actual separation between the 'double images' under a feed rate of 118 in/min is found to be:

$$0.125 \cdot 0.265 \text{ in} = 0.0331 \text{ in}$$

This result agrees with the theoretical separation distance of 0.0333 in, suggesting that interlace video is the cause of the double image blurring which occurs at high feed rates. The difficulty in producing a clean image at high feed rates, then, is not a function of the quality of camera or frame grabber used in the vision system, but rather it is due to an inherent property of NTSC video.

It should be noted here that measurements using high feed rates are similar to measurements performed while the system is subject to vibration. In the case of feed rates, the effect on system performance is a function of the workpiece velocity, i.e. the feed rate. In the case of vibration, the performance of the system will depend on the instantaneous relative velocity between the camera and workpiece. Assuming a sinusoidal vibration of the form $x(t) = A\cos(\omega t)$, the maximum instantaneous velocity has a magnitude of $v_{max} = A\omega$. Since the amplitude of vibration can be reduced by increasing the stiffness of the camera mounting assembly, the instantaneous velocity can be maintained below the critical level to ensure good system performance regardless of the frequency of vibration.

Feed = 0.0 in/min

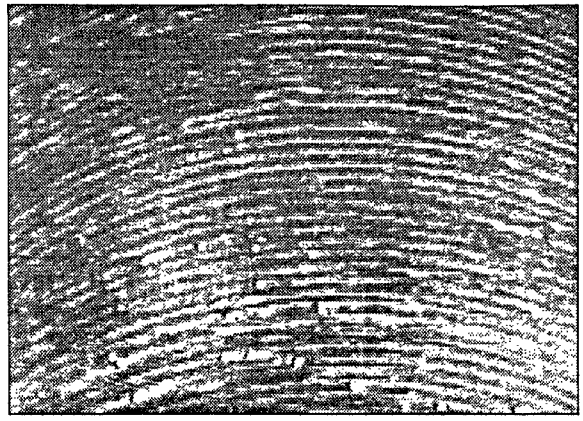

Feed = 7.0 in/min

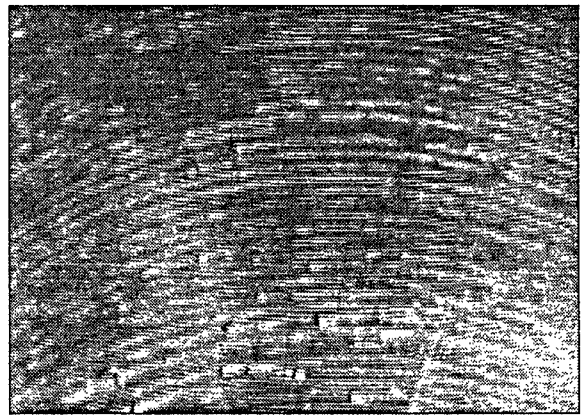

Feed = 23.6 in/min

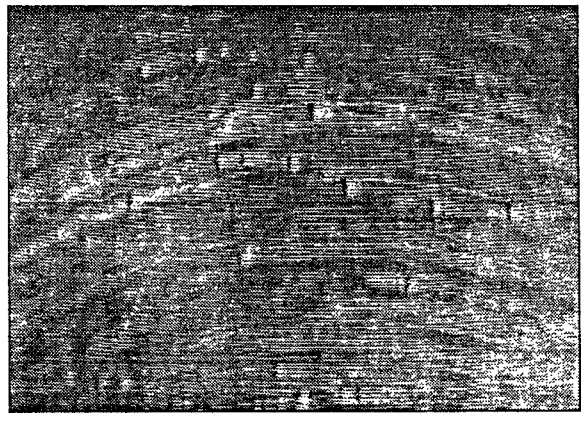

Feed = 118.0 in/min

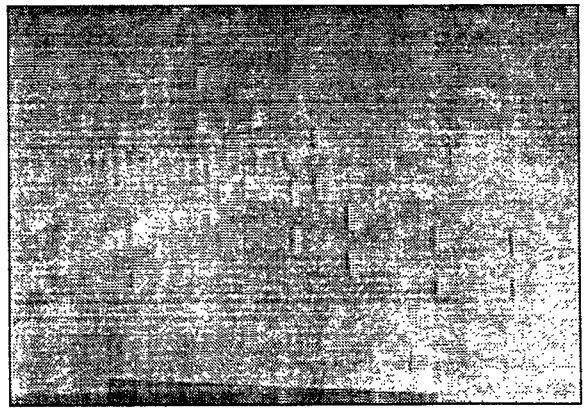

Figure 5.8 – Surface images captured under four different feed rates

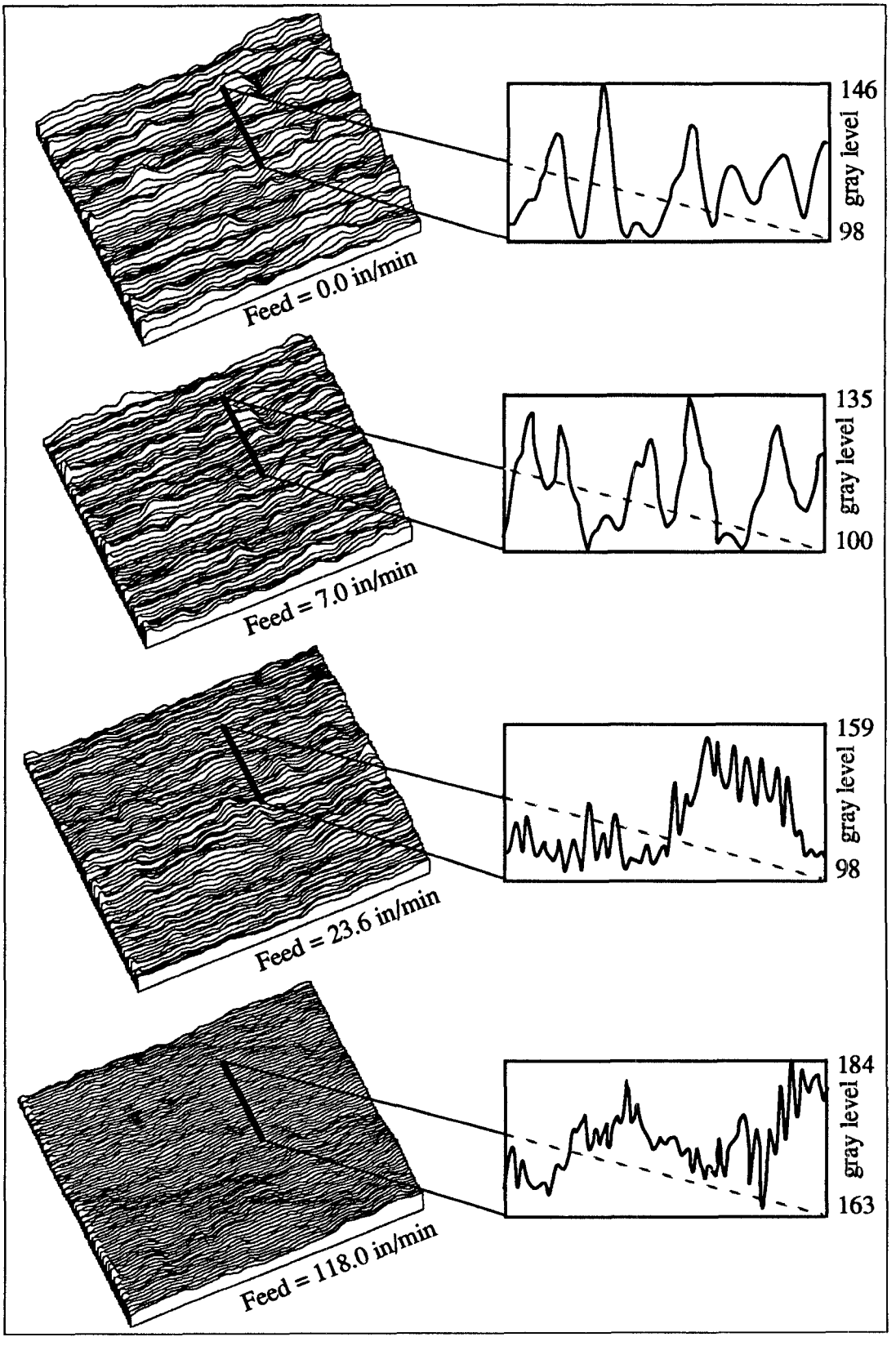

Figure 5.9 – Distortion of surface reconstructions due to feed rates

5.4. System Performance During Machining Operation

To test the overall viability of using the vision system in a machining environment, the system output was examined during an actual machining operation. The test was performed under the cutting conditions indicated in Table 5.3.

Table 5.3 – Settings used during machining operation

condition	setting
ambient lighting	normal
light source grazing angle	10°
light source brightness	80%
light source horizontal orientation	45°
magnified area	4 cm^2
tool	1" diameter end mill
depth of cut	0.05"
feed rate	7 in/min
cutting fluid	maximum flow rate
spindle speed (1)	500 rpm
(2)	700
(3)	900
workpiece surface roughness (1)	0.21 μm
(2)	0.33
(3)	0.40

Three workpieces of varying roughnesses were used during the test. The roughness was manipulated by using varying spindle speeds during the combined machining/measurement process, while holding the feed rate constant. During each machining operation, the cutting fluid was free to flow into the cutting region, and a directed stream of compressed air was used to clear the measurement area of as much excess fluid as possible.

Table 5.4 lists the optical measurements performed under the given machining conditions. The optical roughness parameter is given for each workpiece, in addition to the actual R_a value of the machined surface (measured using facilities at NIST), and the R_a value as determined using the measured value Ω_2 and the optical correlation curve given in Fig. 5.6. The error between the actual and measured roughness values is also provided. The maximum error is only 0.07 μm, which is quite good considering the conditions in which the measurements were taken: heavy vibration, moving workpieces, coolant obscuring workpiece surfaces, etc. Although this study is limited primarily by the small number of surface measurements performed, the results demonstrate the effectiveness of the system under the adverse conditions found in a machining environment.

Table 5.4 – Roughness measurements during milling process

Sample #	Ω_2	R_a (actual)	R_a (curve)	Error
1	2.02	0.21μm	.26μm	.05μm
2	2.45	0.33μm	.40μm	.07μm
3	2.53	0.40μm	.44μm	.04μm

In performing the measurements listed in Table 5.4, great care was taken to ensure that (a) the measured surface was sufficiently clear of coolant to ensure an accurate measurement, and (b) the camera lens remained free of coolant splashed from the surface , so that the image would not be obscured. The first issue was solved by directing a constant stream of compressed air onto the surface, so that any coolant in the region of the surface directly below the camera lens is forced away. The latter issue, however, presents a more difficult problem to solve for the optical apparatus presented in this work. Since the working distance of the camera is 16mm, a significant amount of cutting fluid will be splashed onto the lens unless measures are taken to deflect the

fluid away from the camera. In the present system, this was accomplished by directing the same compressed air stream used to clear the workpiece surface of coolant such that the air also forced any coolant splashed towards the lens back onto the workpiece. While this method proved sufficient for the three measurements performed in this work under wet machining conditions, it does not provide a workable solution for use on a real-world measurement system. The primary cause for the difficulty is the small working distance of the lens used in the system. A lens with a larger working distance would allow the camera to be mounted further from the workpiece surface, and gravity would do much of the necessary work in isolating the camera and lens from stray cutting fluid. An additional measure which would alleviate the problem is presented in Figure 5.10. In this diagram, the lens is surrounded by a cylindrical tube which extends towards the workpiece surface. The tube is baffled, so that any fluid which entered through the uncapped end near the workpiece would not progress up the tube towards the lens. Two hoses supply compressed air to the interior of the tube, in order to maintain positive pressure between the lens and the workpiece.

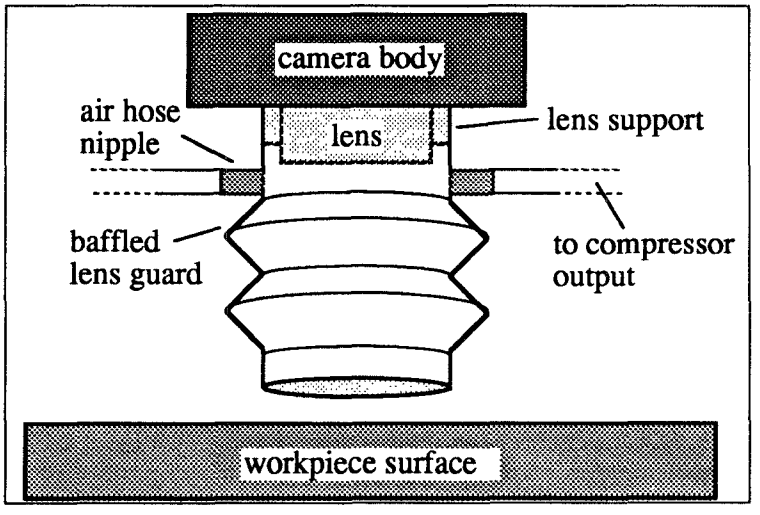

Figure 5.10 – Proposed technique for repelling coolant from lens

CHAPTER 6
CONCLUSIONS AND RECOMMENDATIONS

In this research, a true area-based surface roughness measurement system is considered in terms of its theoretical background, experimental performance, and potential use for on-line monitoring in a real world CIM environment. The system is capable of measuring both the average roughness from a large region of a surface, and determining certain higher order surface statistics. The combination of these two capabilities differentiates the proposed system from other surface roughness assessment methods. The measurement technique employs an optical approach whose theoretical foundations are based on the principles of electromagnetic wave scattering. The theoretical basis for the behavior of the system is developed as an extension of traditional models of electromagnetic wave scattering, and justification for system performance is presented based on this theory. The developed theory, which dictates the pattern of light scattered into the vision system's receiver as a function of parameters which define the surface topography, provides a starting point for understanding the operation of the system.

A prototype vision system is designed and constructed to examine the capabilities of the measurement technique off-line. Using this prototype system, two definitions for an optical roughness parameter are developed by examining the statistical behavior of the system output for varying surface roughness. The results of measurements performed using the prototype vision system on milled aluminum surfaces clearly demonstrate the effectiveness of the measurement technique by providing a functional calibration curve, which relates the known roughness of a surface to the optical roughness parameter derived from a digitized image of the illuminated

surface. A sensitivity analysis is performed to demonstrate the effects of various environmental factors on the performance of the system. As indicated by the results of the sensitivity analysis, the system output is unaffected by vibration, which is an important characteristic for in-process sensors that is lacking from traditional contact-based profilometry techniques. The sensitivity analysis also points out the importance of baseline calibration to ensure consistent system performance, and the potential difficulties when measuring anisotropic surfaces due to a strong dependence on horizontal light orientation.

In order to study the potential for using the proposed vision system in a true machining environment, a second system using a miniature CCD camera was designed, constructed, and mounted directly to the spindle of a CNC milling machine. The on-line performance of the system during a dry end-milling operation was considered, and the results demonstrate the generally strong performance of the system even under the extreme conditions of a machining environment. A study of the system performance under wet machining conditions was also undertaken. The results indicate the potential for integrating such a device into an active control system to maintain surface quality during a machining operation.

The vision system is found to be insensitive to moderate motion of the workpiece while performing on-line measurements, while feed rates above 10 in/min impair the system output. The cause of this problem is identified as an inherent attribute of the NTSC video used by the camera. While current cost considerations prevent the elimination of this problem, it is recognized that such difficulties can be avoided by using hardware capable of digitizing video images at higher frame rates than the equipment used in this thesis work (30 frames/sec). Another possible alternative is the

use of a frame grabber capable of digitizing only one field of scan lines while ignoring the other field. Such an approach would relieve the effects of interlacing at the expense of reducing the effective resolution of the system. In any case, the limitation imposed by interlacing and relatively low frame rates does not reflect on the effectiveness of the proposed measurement method, but rather on the particular implementation considered in this thesis.

The results of this work clearly indicate the potential for using an area-based vision system for the measurement of surface roughness during a machining operation by applying the basic principles of light scattering, especially for precision machining where feed rates are maintained within a limited range. However, there are a number of issues which have not been addressed in this work which deserve consideration. A list of the important issues as seen by the author are as follows:

(1) Examine effects of multiple scattering by using surfaces with varying slopes.
(2) Use of calibrated roughness specimens for system calibration.
(3) Develop calibration curves for other common engineering materials.
(4) Study the performance of the system for extremely smooth and extremely rough surfaces, i.e. determine the applicable range of the system.
(5) Define the optical parameter from the distribution skewness rather than the mean and standard deviaion .
(6) Develop alternate calibration curve for measurements with cutting fluid.

Each of these issues will be briefly discussed.

(1) As noted in Section 3.3, multiple scattering is a phenomenon which can adversely affect the performance of the vision system when the slopes of the surface under observation are relatively large. As noted in Section 3.3, it is extremely complex to describe the scattered field reflected from a surface under multiple scattering, and so the effects of this phenomenon can best be determined through empirical observation rather than from a mathematical description. To this end, the extent to which this phenomenon affects the system can be studied by examining a series of surfaces with equivalent roughnesses, but varying surface slopes.

(2) Measurements should be performed using calibrated roughness specimens to provide a known base level from which the performance of the system can be determined. In this work, the experimental samples were prepared using a milling process which produced surfaces with varying roughness across the width of the machined path. While this approach has the advantage of producing samples which represent actual surfaces produced by a machining process, it may be more appropriate to perform baseline measurements using surfaces with constant roughness across the entire area of the surface.

(3) Throughout this work, all experimental samples have been aluminum. Since other engineering material have different optical absorption and reflection spectra, the optical calibration curves produced using aluminum are not applicable for other materials. In order to apply the vision system in a flexible machining system, calibration curves for a full range of typical engineering materials must be developed.

(4) The range of roughness considered here has been $0.15\mu m < R_a < 0.60\mu m$. Since many precision engineered surfaces require surface roughnesses below $0.15\mu m$, a

complete study should be performed using samples with $R_a < 0.15\mu m$ to determine the useful roughness range of the vision system. Additionally, the upper bound of the system ($R_a > 0.60\mu m$) should also be determined.

(5) Two optical parameters have been used in this work: $\Omega_1 = \mu/\sigma$, and $\Omega_2 = \mu\sigma/1000$. Both of these parameters have been defined under the assumption that the gray-level distribution of the captured surface image is normally distributed. While this is a reasonable approximation, the distribution is in fact slightly skewed (see Section 3.1), and a gamma distribution is more appropriate. The disadvantage of using the gamma distribution is the increased computational power required to calculate the shape factor (η) and the scale factor (λ), which are the defining parameters of the gamma distribution (just as σ and μ are the defining parameters of the normal distribution). Because the computational load imposed by the gamma distribution was excessive for the real-time calculation of Ω_2, given the hardware being used, it was not considered for this work. With faster hardware and improved algorithms, however, the use of the gamma distribution is well worth considering as a way of improving the sensitivity of the system.

(6) Since dry-machining processes are in the minority, it is critical that the vision system be capable of performing measurements under wet-machining conditions. As pointed out in Section 5.1, any cutting fluid which remains on the surface during the measurement process will interact differently with the incident light than the interaction predicted by scattering theory. Therefore, it is imperative that the measurement area be cleared of any residual cutting fluid before measurements are performed, or that an alternate calibration curve be developed with a film of cutting fluid present on the surface of the workpiece. The former solution to the problem was utilized in this work,

while the latter solution was avoided due to the difficulty of predicting how many air bubbles will be present in the fluid, what other impurities in the fluid will affect results, etc. While the first solution is the most promising, there is still a need to develop alternative optical correlation curves for surfaces coated with a film of cutting fluid, since even a thin film will affect the optical properties of the surface. This approach should be considered for a serious investigation of how to utilize the vision system in a wet-machining environment.

Appendix A – Experimental Data

This appendix contains a variety of experimental data which was either inappropriate or excessively lengthy for inclusion into the main body of this work.

Table A1 – Stylus measurement results for experimental samples

Cutting Speed (rpm)	Feed Rate (in/min)	R_a (μm) trial 1	R_a (μm) trial 2	R_a (μm) trial 3	R_a (μm) trial 4	R_a (μm) trial 5	R_a (μm) AVG
500	1.0	0.21	0.25	0.27	0.24	0.25	**0.244**
	1.2	0.35	0.37	0.36	0.35	0.33	**0.352**
	1.4	0.49	0.48	0.49	0.50	0.45	**0.482**
	1.6	0.43	0.39	0.38	0.41	0.38	**0.398**
	1.8	0.37	0.37	0.36	0.38	0.35	**0.366**
	2.0	0.42	0.45	0.52	0.63	0.67	**0.538**
	2.2	0.48	0.46	0.42	0.41	0.44	**0.442**
	2.4	0.44	0.47	0.49	0.48	0.50	**0.476**
	2.6	0.42	0.41	0.41	0.38	0.39	**0.402**
	2.8	0.46	0.47	0.48	0.48	0.47	**0.472**
	3.0	0.30	0.28	0.31	0.34	0.38	**0.322**
	3.2	0.32	0.32	0.39	0.31	0.34	**0.336**
	3.4	0.38	0.35	0.37	0.39	0.45	**0.388**
	3.6	0.37	0.39	0.39	0.46	0.48	**0.418**
	3.8	0.37	0.42	0.44	0.48	0.56	**0.454**
	4.0	0.44	0.46	0.50	0.43	0.52	**0.470**
	4.2	0.44	0.45	0.45	0.51	0.48	**0.466**
	4.4	0.44	0.47	0.52	0.57	0.56	**0.512**
	4.6	0.54	0.61	0.62	0.58	0.62	**0.594**
	4.8	0.41	0.40	0.44	0.43	0.51	**0.438**
700	1.0	0.35	0.38	0.40	0.39	0.36	**0.376**
	1.5	0.30	0.28	0.29	0.29	0.29	**0.290**
	2.0	0.38	0.36	0.39	0.40	0.37	**0.380**
	2.5	0.38	0.38	0.36	0.38	0.41	**0.382**
	3.0	0.37	0.35	0.36	0.38	0.38	**0.368**
	3.5	0.33	0.35	0.39	0.42	0.36	**0.370**
	4.0	0.47	0.53	0.53	0.59	0.70	**0.564**
	4.5	0.39	0.47	0.48	0.56	0.63	**0.506**
	5.0	0.44	0.42	0.39	0.44	0.53	**0.444**
	5.5	0.46	0.43	0.46	0.54	0.59	**0.496**
	1.0	0.17	0.17	0.19	0.18	0.18	**0.178**
	1.2	0.17	0.18	0.18	0.19	0.19	**0.182**

900	1.4	0.15	0.16	0.16	0.17	0.16	**0.160**
	1.6	0.18	0.19	0.20	0.20	0.21	**0.196**
	1.8	0.21	0.21	0.23	0.23	0.23	**0.222**
	2.0	0.22	0.22	0.22	0.21	0.23	**0.220**
	2.2	0.18	0.21	0.19	0.23	0.22	**0.206**
	2.4	0.25	0.27	0.26	0.26	0.25	**0.258**
	2.6	0.26	0.27	0.26	0.27	0.31	**0.274**
	2.8	0.23	0.29	0.37			**0.297**
1100	1.0	0.22	0.22	0.22	0.22	0.21	**0.218**
	1.2	0.21	0.22	0.23	0.23	0.23	**0.224**
	1.4	0.25	0.24	0.25	0.25	0.24	**0.246**
	1.6	0.23	0.23	0.23	0.24	0.26	**0.238**
	1.8	0.29	0.27	0.29	0.31	0.33	**0.298**
	2.0	0.17	0.18	0.18	0.19	0.19	**0.182**
	2.2	0.20	0.20	0.21	0.22	0.24	**0.214**
	2.4	0.21	0.19	0.21	0.22	0.21	**0.208**
	2.6	0.23	0.21	0.28	0.33	0.37	**0.284**
	2.8	0.37	0.35	0.32	0.40	0.41	**0.370**

Table A2 – Optical data from integrated system calibration experiment

Speed (rpm)	Feed Rate (in/min)	μ	σ	R_a	Ω_1 (μ/σ)	Ω_2 $\mu\sigma/1000$
500	1	**79.14**	**15.8**	0.244	5.01	1.25
	1.2	**72.37**	**16.95**	0.352	4.27	1.23
	1.4	**67.84**	**17.29**	0.482	3.92	1.17
	1.6	**70.36**	**17.76**	0.398	3.96	1.25
	1.8	**64.79**	**17.07**	0.366	3.80	1.11
	2	**63.89**	**19.82**	0.538	3.22	1.27
	2.2	**68.41**	**23.18**	0.442	2.95	1.59
	2.4	**79.51**	**24.28**	0.476	3.27	1.93
	2.6	**72.16**	**25.65**	0.402	2.81	1.85
	2.8	**71.65**	**22.83**	0.472	3.14	1.64
	3	**59.5**	**22.79**	0.322	2.61	1.36
	3.2	**66.27**	**26.21**	0.336	2.53	1.74
	3.4	**70.43**	**28.77**	0.388	2.45	2.03
	3.6	**74.99**	**29.21**	0.418	2.57	2.19
	3.8	**83.31**	**30.2**	0.454	2.76	2.52
	4	**92.68**	**31.83**	0.47	2.91	2.95
	4.2	**95.3**	**28.78**	0.466	3.31	2.74
	4.4	**86.49**	**31.69**	0.512	2.73	2.74
	4.6	**73.85**	**30.19**	0.594	2.45	2.23
	4.8	**81.03**	**27.15**	0.438	2.98	2.20

700	1.0	81.69	14.28	0.376	5.72	1.17
	1.5	83.07	17.17	0.29	4.84	1.43
	2.0	75.27	16.53	0.38	4.55	1.24
	2.5	70.58	19.5	0.382	3.62	1.38
	3.0	67.01	20.46	0.368	3.28	1.37
	3.5	79.29	27.61	0.37	2.87	2.19
	4.0	100.61	34.39	0.564	2.93	3.46
	4.5	85.79	32.45	0.506	2.64	2.78
	5.0	69.38	30.22	0.444	2.30	2.10
	5.5	80.53	26.96	0.496	2.99	2.17
900	1	74.31	14.92	0.178	4.98	1.11
	1.2	71.72	19.37	0.182	3.70	1.39
	1.4	57.22	11.46	0.16	4.99	0.66
	1.6	56.85	11.92	0.196	4.77	0.68
	1.8	54.14	11.26	0.222	4.81	0.61
	2	50.04	12.44	0.22	4.02	0.62
	2.2	47.76	10.69	0.206	4.47	0.51
	2.4	50.18	12.14	0.258	4.13	0.61
	2.6	50	13.55	0.274	3.69	0.68
	2.8	79.3	18.82	0.296	4.21	1.49
1100	1	70.65	16.39	0.218	4.31	1.16
	1.2	63.11	13.59	0.224	4.64	0.86
	1.4	53.03	11.39	0.246	4.66	0.60
	1.6	59.08	16.58	0.238	3.56	0.98
	1.8	55.03	13.26	0.298	4.15	0.73
	2	70.94	20.42	0.182	3.47	1.45
	2.2	53.62	14.43	0.214	3.72	0.77
	2.4	70.97	21.96	0.208	3.23	1.56
	2.6	66.62	24.36	0.284	2.73	1.62
	2.8	77.35	18.61	0.37	4.16	1.44

Table A3 – Optical data for feed rate experiment using integrated vision system

Feed rate (in/min)	μ	σ	Ω_1	Ω_2
0	89.76	13.07	6.868	1.173
1.2	89.85	13.13	6.843	1.179
2.4	89.37	14.03	6.370	1.253
4	89.34	14.12	6.327	1.261
7	89.21	14.17	6.296	1.264
10	90.87	12.19	7.454	1.107
15.7	90.39	11.20	8.071	1.012
23.6	90.76	12.32	7.367	1.118
31.5	90.95	11.22	8.106	1.020
39.4	93.79	10.36	9.053	0.971
47.3	95.81	12.55	7.634	1.202
59	95.65	11.63	8.224	1.112
78.7	95.82	12.54	7.641	1.201
118	95.94	12.56	7.639	1.205

Appendix B – Surface Roughness Characterization Parameters

This appendix presents an overview of some of the important terminology used in this work. Definitions related to surface roughness characterization follow:

Texture – Although texture and roughness are often used interchangeably in reference to surface topography, texture is more properly defined as the characteristics which define the overall surface topography. Thus, texture includes all other surface properties, such as roughness, waviness, lay, and flaws.

Roughness – As defined by the ANSI/ASME B46.1-1985 standard, *roughness* refers to the fine irregularities present on a machined surface as a result of the action of the production process used to produce the surface, including traverse feed marks and other irregularities. The 'fineness' of the irregularities considered to be part of the surface roughness must be defined in terms of a roughness sampling length, or cutoff wavelength.

Waviness – Waviness is a more widely spaced (longer wavelength) component of the surface texture. Waviness includes any irregularities with a wavelength greater than the roughness cutoff wavelength, but less than the waviness sampling cutoff wavelength. Typically, the waviness cutoff wavelength is defined by surface irregularities caused by machine tool deflections, vibration, chatter, or heating effects.

Form Error – A form error is any surface irregularity which is not included with the surface texture. Form errors may be caused by tool misalignment, improper workpiece mounting, or similar errors.

Lay – The dominant direction in the surface striations, typically directed along the dominant motion of the cutting tool used in the machining operation. For instance, in a milling operation the lay is directed along the radial motion of the milling bit, rather than along the feed direction.

Center Line – The line about which the surface roughness is measured. The center line (also called the graphical center line) is measured parallel to the measured profile direction, and is defined within the limits of the roughness cutoff frequency. The center line is found such that the areas between the center line and the roughness height level are equal on each side of the center line.

Figure B1 graphically shows the differences between roughness, waviness, and form error.

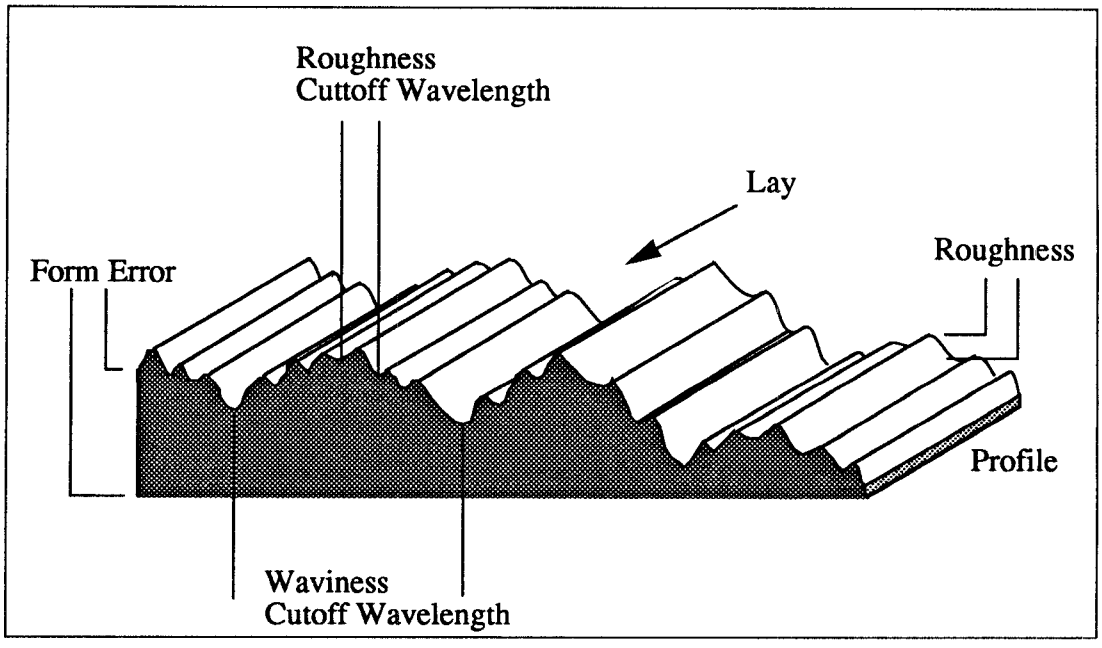

Figure B1 – Graphical comparison of texture components

Roughness Parameters – While there are many parameters used to describe the roughness of a surface, the only parameter used in this work is the 'average roughness,' or R_a value. The average roughness is defined as the average deviation of the roughness profile from the center line of the surface. This definition is applied through Equation B1.

$$R_a = \frac{1}{L}\int_0^L |q(s)|ds \cong \frac{1}{N}\sum_{i=1}^{N}|q_i| \qquad \text{(B1)}$$

where:

L = trace length

s = distance along length from origin

q(s) = surface height at distance x

N = number of discrete data points used to digitize the surface heights

q_i = surface height at the ith data point

Appendix C – Hardware Specifications

The specifications of three commercially available pieces of hardware used in the vision system are described here: (1) CCD camera used in initial experimental study, (2) CCD camera integrated with CNC machine, and (3) frame grabber used for both experimental studies. For each device, only the applicable hardware specifications are provided.

(1)	Manufacturer:	Sony
	Model #:	SSC-M350 monochrome CCD video camera
	Pickup device:	1/2" Inter-line transfer type monochrome CCD
	Effective pixels:	510 (horizontal) x 492 (vertical)
	Automatic gain control:	switched off
	Video out:	NTSC
(2)	Manufacturer:	Supercircuits
	Model #:	PC-3 microvideo camera
	Pickup device:	1/3" MOS monochrome CCD
	Effective pixels:	324 (horizontal) x 246 (vertical)
	Automatic gain control:	none
	Video out:	NTSC
(3)	Manufacturer:	Data Translations
	Model #:	QuickCapture frame grabber board
	Video input:	NTSC, monochrome
	Video Format:	interlaced

Resolution:	640 (horizontal) x 480 (vertical)
Frame grab speed:	1/30 sec.
Aspect ratio:	1:1 (square pixels)

References

Beckman P, Spizzichino A., "The Scattering of Electromagnetic Waves From Rough Surfaces," Oxford:Pergamon, 1963.

Bennett J. M., Dancey J. H., *Stylus Profiling Instruments for Measuring Statistical Properties of Smooth Optical Surfaces*, Appl. Opt. 20, p 1785, 1981

Bennett J. M., Mattson L., *Introduction to Surface Roughness Scattering*, Optical Society of America, 1989

Blessing G. V., Eitzen D. G., Surface Roughness Sensed by Ultrasound, Journal of Topography 1, 2, 253-267, 1988.

Brodman R., Gerstorfer O., Thurn G., *Optical Roughness Measuring Instrument for Fine Machined Surfaces*, Opt. Eng. 24, 408, 1985

Church E. L., *The Measurement of Surface Texture and Topography by Differential Light Scattering*, Wear, 57, 93-105, 1979.

Church E. L., Vorburger T. V., Wyant J. C., *Direct Comparison of Mechanical and Optical Measurements of the Finish of Precision machined Optical Surfaces*, Opt. Eng. 24, p 388, 1985

Detrio J. A., Miner S. M., "Standardized Total Integrated Scatter Measurements of Optical Surfaces," Opt. Eng. 24, 419, 1985.

DeVoe D., Knox L., Zhang G., *Research on Surface Roughness Measurement Techniques for On-Line Machining Process Monitoring*, SRC Technical Report U.G.92-1, Systems Research Center (1991).

DeVoe L., Duong L., Knox L., Wen J., *An Experimental Study of Surface Roughness Assessment Using Image Processing*, SRC Technical Report T.R.92-28, Systems Research Center (1992).

DeVoe D., Knox L., Zhang G., *Active Control of Machining Processes Using Image Reconstruction and Processing*, Proceedings of the 30th Annual Allerton Conference on Communication Control and Computing, 742-750, 1992.

Dornfeld D. A., Fei R. Y., *In Process Surface Finish Characterization*, ASME, Prod. Eng., Division PED 20, 191-204, 1986

Garbini J. L., Koh S.-P., Jorgensen J. E., Ramulu M., *Surface Profile measurement During Turning Using Fringe-Field Capacitive Profilometry*, J. of Dynamic Sys., Meas., and Control, 114, 235-43, 1992.

Hahn G. J. and Shapiro S. S., "Statistical Models in Engineering," John Wiley and Sons, Inc., New York, 1967.

Huynh V. M., Peticca G., *An Optical Technique for Roughness Measurement of Printing Papers*, Journal of Imaging Technology 16, 22-26, 1990.

Kerr D. E., *The Propagation of Short Radio Waves*, MIT Radiation Laboratory Series No. 13, McGraw-Hill, New York 1951.

Lieberman A.G., Vorburger T. V., Giaugue C. H. W., Risko D. G., Rathbun K. R., *Capacitance vs. Stylus Measurements of Surface Roughness*, Journal of Topography, 1, 3, 315-330, 1988.

Luk F., Huynh V., North W., *Measurement of Surface Roughness by a Machine Vision System,* Journal of Physics E: Scientific Instruments 22, 977-80, 1989.

Rice S. O., *Reflection of Electromagnetic Waves From Slightly Rough Surfaces*, Comm. Pure Appl. Math. **4**, 351-378, 1951.

Saya T., *Surface Finish in Metal Cutting*, Annals of CIRP 12, 190-197, 1964

Saya T., Moritada K., *On the Forming of Surface Roughness in Finished Processing*, Bull. the Japan Soc. of Prec. Eng. 1, 4, 287-293, 1966

Sayles R. S., "Rough Surfaces," T. R. Thoma, Ed., Longman, London, 1982

Song J. F., "Surface Texture and Measurements," NIST Report, 1993

Song J. F., Vorburger T. V., "Surface Texture," Metals handbook 18 reprint, 1992

Spurgeon D., Slater R., *In-Process Indication of Surface Roughness Using a Fibre-Optics Transducer*, Machine Tool Design and Research, England, 339-347, 1974.

Thomas T. R., Ed., "Rough Surfaces," Longman, London, p 189, 1982

Twersky V., *On the Scattering and Reflection of Electromagnetic Waves by Rough Surfaces*, Trans. I.R.E. AP-5, 81-90, 1957.

Vorburger T., Raja J., "Surface Finish Metrology," NISTIR-4088, U. S. Dept. of Commerce, 1990.

Zimmerman J. H., Vorburger T. V., Moncarz H. T., "Automated Optical Roughness Inspection," Optical Testing and Metrology II, Proc. SPIE 954, 252, 1989

"Instruments for the Measurement of Surface Roughness by the Profile Method – Vocabulary," ISO 1879/1981, International Organization for Standardization, 1981

"Surface Roughness — Terminology — Part 1: Surface and Its Parameters," ISO 4287/1, International Organization for Standardization, 1984

"Surface Texture (Surface Roughness, Waviness, and Lay)," ANSI/ASME B46.1-1985, American Society of Mechanical Engineers, 1985

Index

active control 3
ambient light 56
ambient lighting 53, 54, 56, 73
angle of incidence 15, 22
angle of reflection 22
arithmetical average deviation 38
average roughness 101
calibration 51
calibration curve 53, 71, 76
camera magnification 54, 55
CCD camera 68
center line 100
CIM 3
CNC program 78
coherent 14
confidence interval 80
convolution matrix 77
coolant 67, 87
correlation coefficient 53
correlation curve 64, 65
correlation distance 18, 31
correlation function 15
cutoff frequency 28
cutoff wavelength 69
cutting fluid 71, 86
DALLAS 10
diffuse reflection 13, 17
diffuse scattering 17
dimensional accuracy 2, 3
dimensionality 15
effective roughness 15
electromagnetic radiation 13
facet 31
facet geometry roughness 28
factorial design 53, 55, 56, 72
feed rate 68, 81, 82
form error 100
gamma distribution 27
Gaussian 15
glare 75, 76
grazing angle 49, 54, 73
histogram 26, 35, 38, 47, 64, 76
horizontal orientation 54, 55, 56, 73
incident angle 20, 50, 54
incoherent 14
interaction effects 55
interferometry 8
interlacing 82
lay 55, 100
light ray 22

linear diode array 4
local roughness 20, 28
logarithmic regression 44
mean 47, 64
mean scattered power 20, 31
milling center 67
milling machine 68
multiple scattering 34, 35
NIH Image 41, 76
NIST 46, 53
noise 77
normal distribution 27
NTSC 81, 102
optical roughness parameter 24, 27, 47, 51, 53, 54, 56, 64
passive control 3
periodicity 15
phase cancellation 16
power density 14
profilometer 2, 4
profilometry 5
Raleigh criterion 15, 17
Rayleigh Criterion 16
repeatability 53
RMS 38
roughness 1, 6, 28, 100
scattered field 32
scattering 14
sensitivity 53
Shadowing 34, 35
smoothing filter 77
Snell's law 29
spatial convolution 77
spectral power 32
specular direction 14, 16
specular reflection 13, 17
spindle speed 86
standard deviation 15, 38, 47, 54, 58, 64, 79
standard error 79
stylus 4, 5, 40
sunlight 56
surface facet model 23
surface finish 2, 3
surface normal 30
texture 1
TIS 9, 10
tool wear 3
Total Integrated Scatter (TIS) 8
vibration 53, 54, 72
waviness 1, 28, 100